Fall 12-4-2019

Elucidation of the Factors Affecting the Production and Properties of Novel Wood Composites Made Using Renewable Nanomaterials as a Binder

Ezatollah Amini
University of Maine, ezatollah.amini@maine.edu

ELUCIDATION OF THE FACTORS AFFECTING THE PRODUCTION AND PROPERTIES OF NOVEL WOOD COMPOSITES MADE USING RENEWABLE NANOMATERIALS AS A BINDER

By

Ezatollah Amini

B.S. Amirkabir University of Technology, 2011

M.S. Amirkabir University of Technology, 2014

A DISSERTATION

Submitted in Partial Fulfillment of

the Requirements for the Degree of

Doctor of Philosophy

(in Forest Resources: Bioproducts Engineering)

The Graduate School

The University of Maine

December 2019

Advisory Committee:

Mehdi Tajvidi, Associate Professor of Renewable Nanomaterials, Advisor

Douglas J. Gardner, Professor of Forest Operations, Bioproducts, & Bioenergy

Douglas W. Bousfield, Professor of Chemical and Biomedical Engineering

William M. Gramlich, Associate Professor of Chemistry

Stephen M. Shaler, Professor & Director of School of Forest Resources

ELUCIDATION OF THE FACTORS AFFECTING THE PRODUCTION AND PROPERTIES OF NOVEL WOOD COMPOSITES MADE USING RENEWABLE NANOMATERIALS AS A BINDER

By Ezatollah Amini

Thesis Advisor: Dr. Mehdi Tajvidi

An Abstract of the Dissertation Presented
in Partial Fulfillment of the Requirements for the
Degree of Doctor of Philosophy
(Forest Resources)
December 2019

A novel application of cellulose nanofibrils (CNF) as a binding agent is proposed. In this work the utilization of CNF as a complete replacement for the conventional resin-adhesives in the formulation of particleboard (PB) was evaluated. PB panels with varying CNF contents and target densities were produced using a two-step (i.e. cold and hot) pressing process. For initial evaluation, the mechanical and physical properties of the manufactured panels were determined. The need to remove a considerable amount of water from the wood particle (WP)-CNF mixture during cold pressing, motivated the study of the furnish dewatering behavior. Dewatering was assessed through pressure filtration tests, centrifugation, and characterization of hard-to-remove (HR) water. Expressions to predict the dewatering behavior were compared to the results. In search of a cost-effective alternative to the highly refined (90% fines) CNF for the particleboard manufacture, lignin-containing CNF (LCNF) was produced at different fines fractions ranging from 50% to 100%, from recycled old corrugated containers (OCC) as a low-

cost precursor. Comparisons of morphology, surface characteristics, turbidity, transparency, tensile and binding properties of the produced LCNF to the CNF at different levels of fines% were made. To investigate the feasibility of producing PB panels with LCNF, a selection of LCNF materials with various fines contents (i.e. 50, 70, 80, and 90%) were used to make the PB panels with the same processing parameters employed to make CNF-bonded PB panels and the physico-mechanical properties of the resulting LCNF-bonded panels were determined. It was found that LCNF 70% is the optimal binder formulation for PB manufacture both technically and economically.

DEDICATION

- This dissertation is affectionately dedicated to my parents for always being supportive of me and my decisions, and for encouraging me to go on every adventure, especially this one.
- I would also like to dedicate this thesis to my loving wife, Shokoofeh Ghasemi, for always being there for me.

ACKNOWLEDGEMENTS

- I would like to thank my advisor, Dr. Mehdi Tajvidi, for his continuous support, patience, and enthusiasm during my PhD studies.
- I would also like to express my gratitude to other members of my advisory committee, Dr. Douglas J. Gardner, Dr. Douglas W. Bousfield, Dr. Stephen M. Shaler, and Dr. William M. Gramlich, for their great suggestions and comments on my research work.
- Special thanks to the U.S. Endowment for Forestry and Communities Inc. (P3Nano), USDA National Institute of Food and Agriculture McIntire-Stennis, and USDA Agricultural Research Service for all the financial support generously provided to this project.
- I gratefully acknowledge the contributions of the staff and graduate students at UMaine's School of Forest Resources, Advanced Structures and Composites Center (ASCC), Process Development Center (PDC), and Forest Bioproducts Research Institute (FBRI), who have kindly helped me throughout my doctoral research.
- Last but certainly not least, I want to thank the wonderful and kind-hearted people at the Office of International Programs (OIP), especially Mireille Le Gal and Sarah Joughin, for all the great help and advice during these years.

TABLE OF CONTENTS

LIST OF TABLES

LIST OF FIGURES

CHAPTER 1

INTRODUCTION

Nanocellulose, better called cellulose nanomaterials (CN), is a general term that refers to all kinds of nano-structured cellulose. CN is generating significant interest because of possessing exceptionally outstanding characteristics such as large specific surface area, low density, mechanical robustness, renewability and biodegradability that make it a fascinating building block for functional materials and end products [1,2]. Cellulose nanomaterials are mainly classified into three groups including cellulose nanofibrils (CNF), cellulose nanocrystals (CNC), and bacterial cellulose (BC). CNF (fiber-like structure) and CNC (needle-like particles) are produced through top-down methods involving mechanical, chemical, or combination of the two to isolate nano-scale elements from wood or agricultural/forest residues, whereas BC (ribbon-shaped nanofibers) is produced in a bottom-up process by bacteria and microorganisms [3,4]. Electrospinning is another way to produce cellulose fibers with diameters as small as several nanometers [5]. CNF has been one of the most commonly produced and commercialized types of cellulose nanomaterials to date. It is mostly produced in the form of a low-consistency (less than 4 wt.%) aqueous suspension of nano-scale cellulose fibers suspended in water. Owing to the high surface area and an abundance of hydroxyl groups available on the surface, CNF possesses excellent adhesion properties, which is promising for many different applications [6–10]. Figure 1.1 shows an example of 3 wt% CNF content slurry and microscopic image of CNF as compared with CNC.

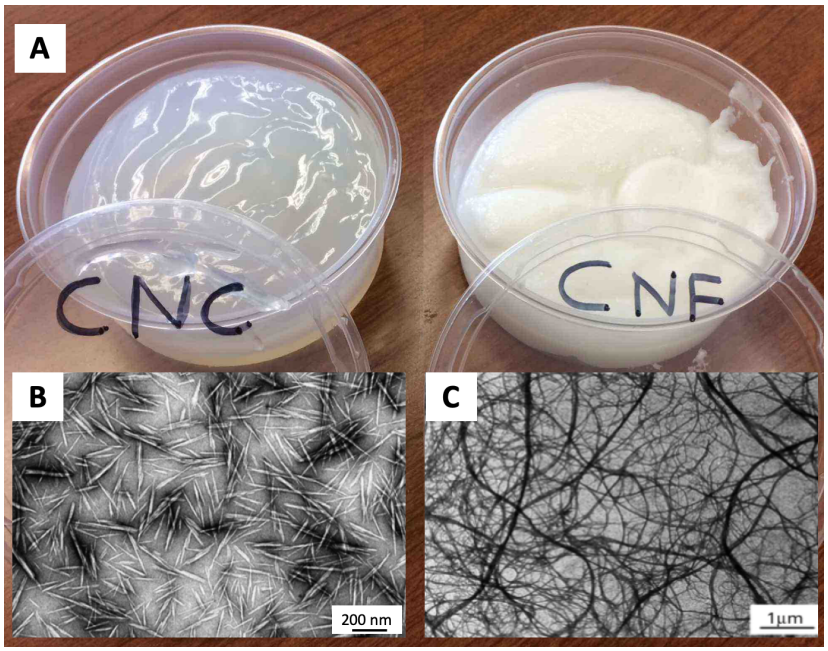

Fig. 1.1. (A) Physical appearance of CNC and CNF suspensions. Transmission electron micrographs of (B) CNC [11] and (C) CNF [12]

Toxicology studies completed thus far have shown cellulose nanomaterials to be safe [13] which eliminates initial concerns regarding consumer safety considerations. In part, owing to the physical form of produced CNF in the form of low consistency slurries and partly the current issues with developing appropriate drying techniques for this highly interesting material, most of the current applications of CNF are limited to using it as an additive for either water-based systems or resins. Figure 1.2 illustrates patents concerning CNF in different fields of application from 2006 to 2013. In almost all cases, CNF was used as an additive in materials at low weight percentages. Therefore, there is a lack of applications that use CNF at higher contents and even as a stand-alone end product. Furthermore, finding applications that use CNF in a large quantity

will help the industries with the potential for producing CNF to grow. For instance, the pulp and paper industry is one of the biggest industries that is currently faced with problems nowadays attributable to a significant decrease in demand for pulp and paper [14]. However, a pulp mill has a major portion of the required machinery for a CNF production line [15] and will be able to produce CNF on a large scale with minor modifications.

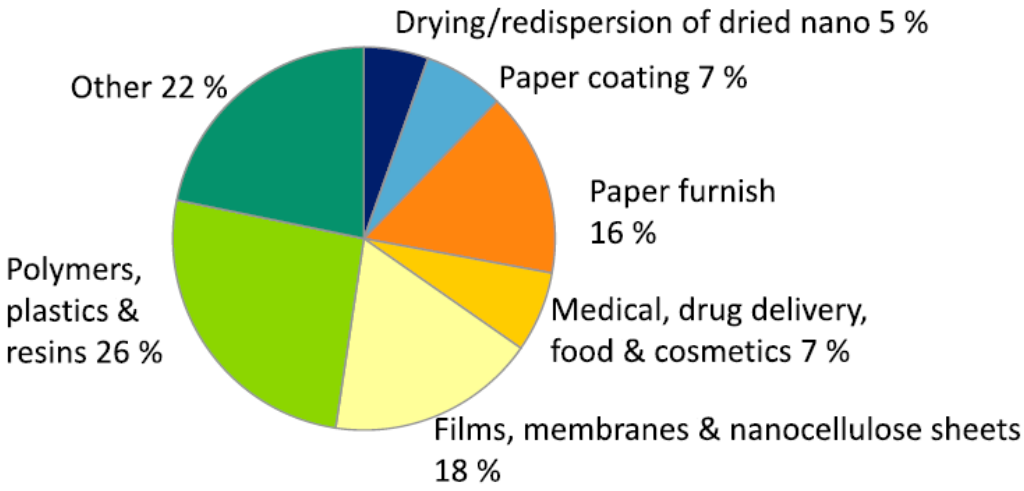

Fig. 1.2. Patents concerning nanocellulose by field of application (2006-2013) [16]

Particleboards (PB) are wood-based composite panels with wide applications including countertops, door cores, floor underlayment, and furniture. Particleboard is also regarded as a sustainable material because it utilizes wood residues from other manufacturing processes that might otherwise be landfilled or combusted. In 2012, North American particleboard manufacturers produced over 3.2 billion square feet of particleboard in 39 different facilities [17]. One major drawback of particleboard is the use of urea-formaldehyde, which is a carcinogenic material [18], in its adhesive formulation and the subsequent formaldehyde emissions both during manufacture and use [19]. Efforts have been made to lower formaldehyde emissions from

particleboard either through the use of an acrylic binder [20] or soy protein resins [21]. As neither of the aforementioned studies succeeded to become commercialized, at this time urea-formaldehyde still continues to be the major resin used in the manufacture of particleboard and the issue of formaldehyde emissions will continue to be persistent.

This dissertation is organized into 5 chapters as outlined below:

Chapter 2 is focused on the manufacturing of particleboard panels using CNF that is isolated from bleached kraft pulp through a refining process as an adhesive binder. The technical feasibility of producing particleboard panels using CNF as the binder is examined and the first set of data and analysis are presented. The production of particleboard through a two-step pressing process is schematically illustrated in Fig. 1.3. Preliminary efforts were also made to understand adhesion mechanisms and the strength development involved in such novel systems. **Chapter 2** has already been published in the form of a peer-reviewed article [7].

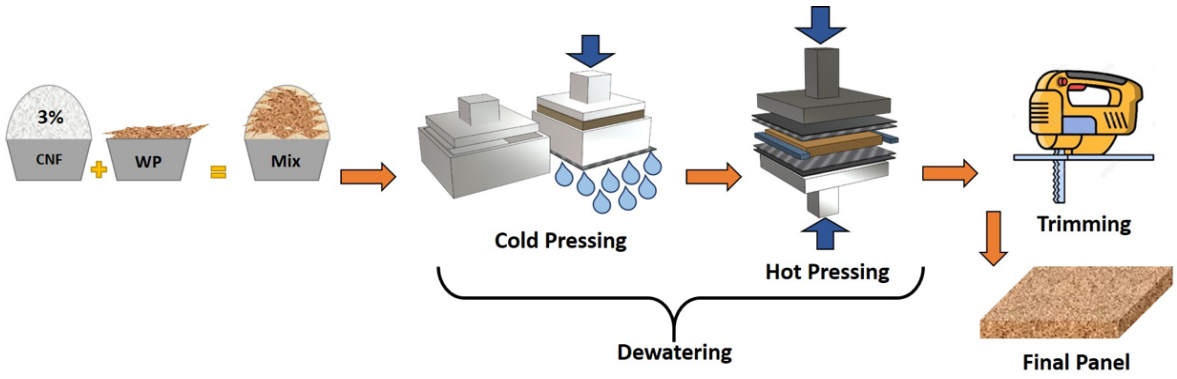

Fig. 1.3. The two-step (cold and hot) pressing process of PB production

The current processing technology to produce composite panels using cellulosic fibers as binder consists of a dewatering process followed by drying in a hot press[2,13-15]. To shorten press cycles and save energy, the majority of the water present in the mixture of wood particles and CNF should be mechanically removed prior to hot pressing in an efficient manner. Therefore, understanding and controlling the water removal behavior of the CNF suspension, both solely and in the form of a mix with other materials is a critical step to optimize the production process.

The original hypothesis of the study discussed in **Chapter 3** is based on the fact that in a CNF suspension, water is mostly in the form of adsorbed water associated with the cellulose surface and is tightly bound to the hydroxyl groups present in the amorphous regions through hydrogen bonding. After mixing wood particles (WPs) with CNF slurry, a large portion of the adsorbed water becomes free water as a result of contact between nanofibrils of cellulose and WPs. Upon consolidation, a considerable amount of free water is removed from the wet furnish by pressing (mechanical dewatering) in a very short period of time and the remaining water in the system can be removed through heating (evaporative dewatering) to produce the final product.

In **Chapter 3**, the dewatering behavior of WP-CNF wet furnish is studied through pressure filtration tests and centrifugation. The effect of wood particle size and particle specific surface area on the dewatering properties of wet furnish is investigated. A method based on Darcy's law for volumetric flow through a porous medium is used to determine the permeability coefficients of wet furnish during filtration test. Characterization of hard-to-remove (HR) water

in wet furnish is also carried out using high resolution isothermal thermogravimetric analysis (TGA) to evaluate thermal dewatering properties of the wet furnish. **Chapter 3** has already been published in the form of a peer-reviewed paper [6].

Regular CNF made at the University of Maine Process Development Center pilot-plant is produced at 90% fines content meaning that 90% of the particles are smaller than 200 micrometers. However, for many applications a highly refined CNF may not be required as the refining processes are mostly energy-intensive and time-consuming, thus adding to the final cost. Therefore, finding an optimal refining level is of crucial importance to producing CNF that can techno-economically fulfil the requirements for the final product.

The reinforcing effect of hardwood- and softwood-derived lignin-containing CNF (LCNF) fibers on the mechanical and physical properties of LCNF-bonded fiberboards were evaluated by Kojima et al. [22]. They found that the flexural characteristics, internal bond strength, and water sorption properties of the fiberboards were significantly improved with the addition of LCNF, in particular for the softwood fiberboard panels. Diop et al. also investigated the effect of using TMP-isolated LCNF as a binder on the physico-mechanical properties of medium-density fiberboard (MDF) panels [23,24]. Results showed that at 20 wt.% LCNF content (dry-basis), the resulting MDF panels met the minimum recommended values for commercial fiberboards in terms of flexural modulus and strength, internal bond strength, and thickness swelling. Overall, LCNF had an acceptable bondability with wood fibers in the fiberboard structure, which can make it a promising replacement for petroleum-based adhesives for fiberboard manufacture.

Old corrugated container (OCC) fibers are high-volume and low-cost recycled materials mostly used as a feedstock for the cost-effective production of papers and containers[25]. OCC mainly consists of cellulose, hemicellulose (low content), lignin, and impurities [26]. OCC has also been utilized as a low-cost source for the production of cellulose and lignocellulose nanomaterials. However, limited studies have dealt with it in this regard [25,27]. There is a lack of a side-by-side comparison of properties of CNF and LCNF produced from different sources using the same method and same pilot-scale facility.

In **Chapter 4 and 5**, side-by-side comparisons between the morphology, physical, and mechanical characteristics of CNF (extracted from bleached kraft pulp) and LCNF (isolated from OCC) with different fines contents are drawn to probe factors affecting the physical and mechanical properties of films made from these materials. To investigate the feasibility of producing PB panels with LCNF, a selection of fine contents from the produced LCNF are used to make the PB panels with the same processing parameters employed to make CNF-bonded PB panels and the physico-mechanical properties of the resulting LCNF-bonded panels are evaluated.

CHAPTER 2

UTILIZATION OF CELLULOSE NANOFIBRILS AS A BINDER FOR PARTICLEBOARD MANUFACTURE

2.1. Chapter Summary

Cellulose nanofibrils (CNF) were investigated as a binder in the formulation of particleboard (PB) panels. The panels were produced in four different groups of target densities with varying amounts of CNF binder. The produced panels were then tested to determine the modulus of rupture (MOR), modulus of elasticity (MOE), internal bond (IB), water absorption (WA), and thickness swelling (TS) properties. Density gradients through the thickness of the panels were evaluated using an X-ray density profiler. The effect of drying on the strength development and adhesion between CNF and wood particles (WP) was investigated, and the effect of surface roughness on the wood-CNF bonding strength was evaluated through lap shear testing and scanning electron microscopy. It was found that at lower panel densities, the produced samples met the minimum standard values recommended by American National Standards Institute (ANSI A208.1) for particleboard panels. Medium-density panels met the standard levels for IB, but they did not reach the recommended values for MOR and MOE. The possible bonding mechanism and panel formation process are discussed in light of microscopic observations and the results of lap shear tests were presented.

2.2. Introduction

Particleboard is a wood composite panel typically manufactured from discrete wood particles combined with a resin or binder under heat and pressure. The resins used in particleboards are mostly made up of formaldehyde-based adhesives, such as urea-formaldehyde (UF) and, to a lesser extent, phenol-formaldehyde (PF) resin [28]. The major concern associated with these resins is the emission of formaldehyde [29], which has been proven to be carcinogenic. Over the past years, several approaches have been taken to reduce formaldehyde emissions from wood-based panels. This includes using liquefied wood (LW), wood meal of black poplar liquefied with a mixture of glycerol and sulfuric acid by heating, for the modification of phenol-formaldehyde [28], organosolv lignin dispersion to partially replace the solids content in a liquid phenol-formaldehyde [30], hydrogen peroxide as a catalyst in the hardening process of urea-formaldehyde[31], low formaldehyde emission acrylic resin [32], and pulp and paper secondary sludge as a urea-formaldehyde co-adhesive [33]. A number of studies focused on the replacement of formaldehyde-based resins with other binders such as epoxidized vegetable oils [34,35] soy-based adhesives[36], tannins and lignin from pulp mill residues[37], and polymeric diphenylmethane diisocyanate (pMDI) [38].

Cellulose nanomaterials that are mainly available in the forms of cellulose nanofibrils (CNF), cellulose nanocrystals (CNC), and bacterial nanocellulose (BC), have attracted considerable interest attributed to the possibility of making strong, light, and biodegradable products from an abundant renewable resource. Some review articles have summarized the applications of these novel materials [39–46]. Cellulose nanomaterials are produced *via* aqueous suspensions with low

consistency, which limits the applications of these materials as additives in systems where dry materials are required. These additive applications also generally consume small amounts of nanocellulose. With the current decline in the demand for pulp and paper worldwide [47,48], finding large-scale applications in which these new materials can be utilized is critical for commercialization purposes.

Using cellulose nanomaterials in their original aqueous state provides a number of advantages; there is no need to dry the material prior to the production of the final product, thereby saving energy. It is possible to preserve the nanoscale dimensions in the final product and take advantage of the high reinforcement capacity of such materials, and it provides the opportunity to use higher amounts of nanocellulose in the product being made. Efforts have been made recently to use CNF as a binder in the formulation of the wood flour boards [49,50], but these studies have been limited in scope and do not provide information on the bonding mechanisms. Veigel *et al.* (2012)[51] utilized CNF as an additive in the formulation of formaldehyde-based adhesives of particleboards and oriented strand boards to improve their mechanical properties. A recent study has been done to use 2,2,6,6-tetramethylpiperidine-l-oxyl (TEMPO) mediated CNF as a reinforcing agent in the manufacture of wood composites from corn thermomechanical fibers[52].

This chapter is focused on the manufacturing of particleboard panels using CNF that is produced through a refining process as a sole binder. Recent work at the University of Maine has shown that the use of CNF as a binder for the production of particleboard is feasible [53,54] . The goal of this study was to evaluate the technical feasibility of producing particleboard panels using CNF as

the binder. We present the first set of data and analysis as well as efforts made to understand adhesion mechanisms and the strength development involved in such novel systems.

2.3. EXPERIMENTAL

2.3.1. Materials

Southern pine wood particles (WP) with an average length of 3.8 mm (aspect ratio of 3.3) and an average moisture content of 7% were supplied by Georgia-Pacific Thomson Particleboard (Thomson, GA, USA). A CNF slurry (containing 3% wt. cellulose nanofibrils) was used as the binder. The CNF was a product of the University of Maine's Process Development Center, which was produced *via* mechanical refining of bleached softwood kraft pulp. The physical form of the 3 wt.% CNF slurry along with a transmission electron microscopy (TEM) image are shown in Fig. 2.1. While there are a large number of fibers that are 50 nm in thickness (Fig. 2.1), a number of fiber fragments or cell wall material in the CNF slurry is still present that have a length scale of a few microns. Polycup™ 5233, formerly known as Kymene®, (30% solids, received from Solenis LLC (Wilmington, DE, USA)) was used in some of the formulations as a formaldehyde-free, water-based, crosslinking agent to enhance the physical and mechanical properties. Throughout this paper this is referred to as the "crosslinking agent." Aspen wood veneer (provided by a local supplier) was used for the lap shear model tests.

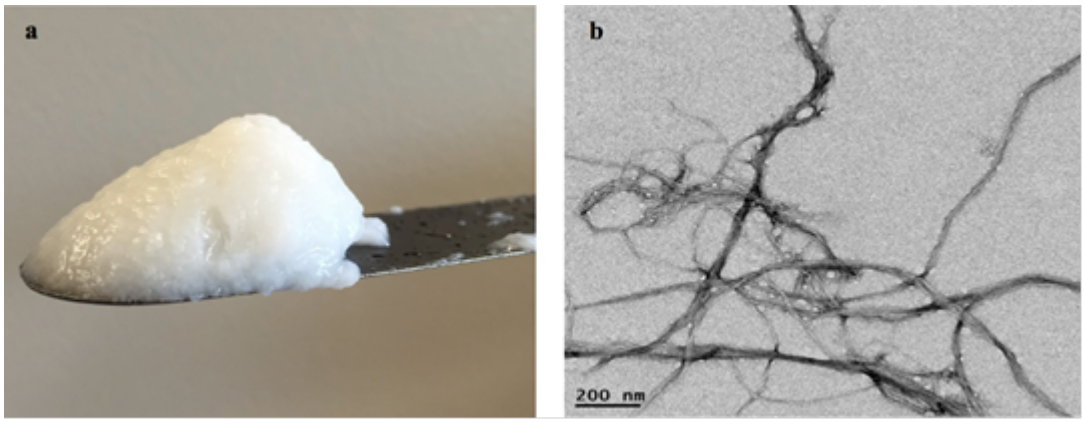

Fig 2.1. Cellulose nanofibrils: (a) physical appearance of a 3 wt.% solids content slurry; and (b) TEM micrograph

2.3.2. Methods

2.3.2.1 Particleboard panel production

The WP with an average moisture content of 7% and CNF slurry at 3 wt.% solids were mixed at mixing ratios of 85% WP-15% CNF and 80% WP-20% CNF (dry weight basis) at room temperature using a stand mixer. The mixture was then poured into a wooden forming box with the internal dimensions of 120 mm × 120 mm × 60 mm that was placed on top of a 40-mesh wire cloth. The mixture filled almost three quarters of the box. A wooden lid was placed on top, and a manual hydraulic press (Dake, Haven, MI, USA) was used to press the mixture and drain the excess water. Most of the free water was drained off during this cold pressing. A small portion of the water was seen to drain from the mixture even before the cold pressing. The solids content (i.e. the oven-dry weight per total weight of the mixture in percent) of the mats before and after cold pressing were approximately 16% and 38%, respectively. This means that the cold pressing

process was able to remove more than 50% of the water. The removed water was observed being quite clean. Then the lid and forming box were removed and the cold pressed mat was pressed and dried using a hydraulic hot press (Carver, Inc., Wabash, IN, USA) at 180 °C for 7 min between two wire mesh cloths. Two metal stops 5-mm in thickness were used for position control. The particleboard panels were produced in four different groups of target density: 0.60 g cm-3 to 0.64 g cm^{-3} (group I), 0.65 g cm^{-3} to 0.69 g cm^{-3} (group II), 0.70 g cm^{-3} to 0.74 g.cm^{-3} (group III), and 0.75 g cm^{-3} to 0.79 g cm^{-3} (group IV). Each density group contained three samples of 15 wt.% and 20 wt.% dry CNF. After trimming, the final dimensions of each panel were 110 mm × 110 mm × 5mm. No significant spring back was observed in the thickness of the PB panels. Each edge-trimmed panel was cut into three 110 mm by 30 mm specimens for the flexural tests. The production procedure is presented in Fig. 2.2.

To evaluate the effect of the addition of crosslinking agent on physical and mechanical properties, 85 wt.% WP and 15 wt.% CNF slurry (dry basis) were mixed at room temperature and 3 pph by weight, *i.e.* 3% on top of the total weight of the WP and CNF slurry mixture, crosslinking agent was added to the mixture. Panels with the crosslinking agent added with the final edge-trimmed dimensions of 110 mm × 110 mm × 5 mm and the target density of 0.65 g cm^{-3} were made along with the control panels in the same manner explained above.

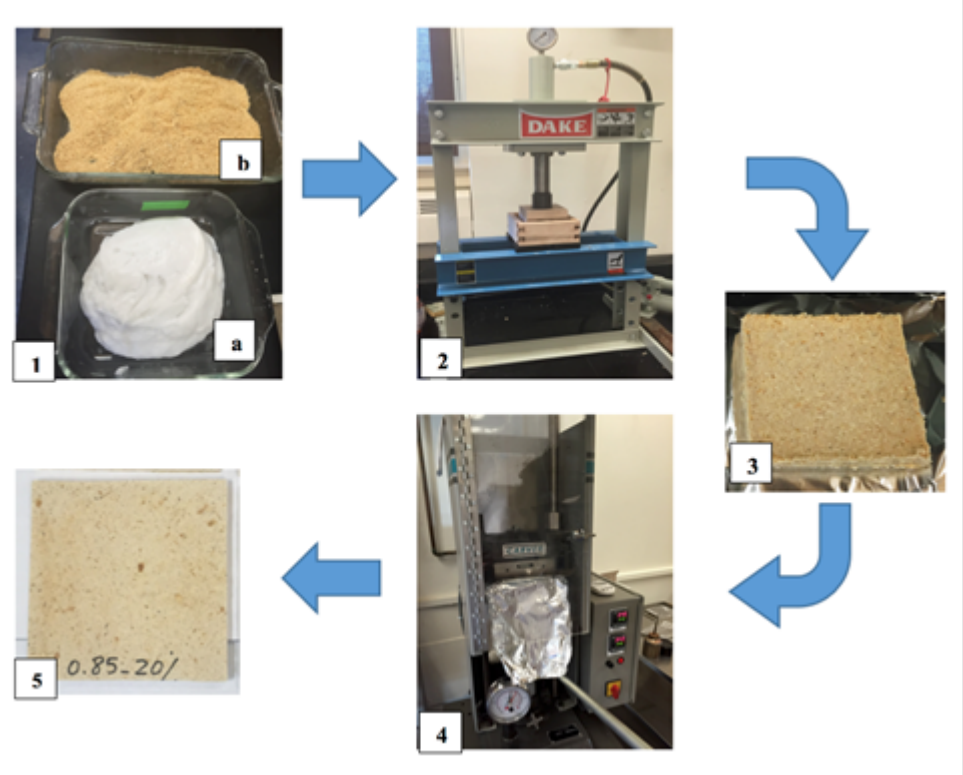

Fig 2.2. PB panel production procedure: (1) raw materials: (a) 3 wt.% CNF slurry and (b) southern pine WP; (2) forming and cold pressing; (3) cold-pressed mat; (4) hot pressing; and (5) final panel

2.3.2.2. Evaluation of mat strength development

In a separate experiment the WP and CNF slurry were mixed at a dry weight basis ratio of 70:30 at room temperature. Then the mixture was poured into a cylindrical mold and was pressed down by a manual hydraulic press (Dake, Haven, MI, USA) to partially drain and form into a wet disk. Five disk-shaped specimens with the nominal diameter of 45 mm and nominal height of 15 mm were made for the strength development test.

The disk-shaped samples were weighed after production. Then they were oven-dried at 120 °C. Every 15 min they were removed, weighed, and returned to the oven until fully dried. The

moisture content (MC %) of the specimens was measured based on the weight of the specimens at each drying level and the oven-dry weight as follows,

$$MC\ (\%) = [(W\text{-}W_o) / W_o] \times 100 \quad (1)$$

where W and W_o are measured weights (g) at each level of drying and the oven-dry weight, respectively. These data were used to construct drying curves to be used to correlate drying time to moisture content. To investigate the strength development of the adhesion between the WP and CNF, a compression test was conducted on the disk-shaped samples after 30, 60, 120, 150, 180, 240, and 300 min of oven-drying at 120 °C. Five oven-dried specimens with a nominal diameter of 45 mm and nominal height of 15 mm were made for each level of drying. The compression test was performed at approximately 23 °C with the crosshead speed of 5 mm/min using an Instron 5500R universal testing machine (Instron, Norwood, MA, USA) with a 10 kN capacity load cell.

2.3.2.3. Lap-shear bonding strength investigation

Rectangular strands of 35 mm × 20 mm were prepared from aspen wood veneer in the longitudinal direction with an average moisture content of 7.5% and an average thickness of 1.25 mm. Lap shear specimens were produced by overlapping two strands bonded together using the CNF slurry. The length of lap area was 20 mm. To investigate the effect of surface roughness on the wood-CNF bonding strength, 150-grit and 400-grit sandpapers were used to sand twenty strands (ten strands of each) at the lap area, with ten control strands not sanded or refreshed surfaces for bonding. Five lap-shear specimens of each category were prepared by using CNF 3 wt.% as binder (at a spread rate of 0.015 g dry mass per glue-line) in-between strands and placing samples between two glass slides held in a paperclip. The assembly was then oven-dried at 120 °C for an hour prior to the lap-shear tests. Adhesive lap shear strength tests were performed to determine the wood-CNF bonding strength. The lap shear test was conducted in accordance with ASTM D4896-01 (2016) with modification using an Instron 4202 (Instron, Norwood, MA, USA) with a 10 kN capacity load cell and the crosshead speed of 0.1 mm/min. This low crosshead speed was required to avoid premature failure of the specimens.

2.3.2.4. Evaluation of flexural properties

For the determination of the modulus of elasticity (MOE) and modulus of rupture (MOR), a three-point bending test was performed on each 110 mm × 30 mm specimen according to ASTM D1037 (2012) with modifications using an Instron 5966 universal testing machine (Instron, Norwood, MA, USA) with a 10 kN load cell capacity. The span length and the crosshead speed were 80 mm

and 3 mm/min, respectively. Specimens were conditioned to approximately 23 °C and 50% RH for at least 48 h prior to testing.

2.3.2.5. Water absorption and thickness swelling evaluation

To investigate the water absorption and thickness swelling of the PB, rectangular specimens were prepared from the broken flexural samples (one specimen from each broken sample). The specimens were 50-mm long, 30-mm wide, and 5-mm thick. The water absorption and thickness swelling of the PB specimens were measured in accordance with ASTM D1037 (method A: 2-plus-22-h submersion in water) (2012).

2.3.2.6. Density profile

The evaluation of density distribution through the thickness of PB panels was conducted using a QMS X-ray density profiler (model: QDP-01X, Quintek Measurement Systems, Inc., Knoxville, TN, USA).

2.3.2.7. Evaluation of internal bond

To evaluate the internal bond (IB) strength of the panels, tension tests perpendicular to the surface were performed according to the ASTM D1037 standard (2012) with modifications using an Instron 5500R universal testing machine with a 10 kN capacity load cell. The specimens with the nominal dimensions of 30 mm × 30 mm × 5 mm (thickness) were prepared from the broken flexural samples (one specimen from each broken sample) and glued to aluminum test fixtures using hot melt adhesive. The testing was conducted at a cross-head speed of 0.4 mm/min.

2.3.2.8. SEM microscopy

For scanning electron microscopy (SEM) imaging, all samples were placed on specimen mounts with double-sided carbon tape, and then grounded on all edges with conductive silver paint. After drying, they were sputter-coated using a Cressington 108 auto sputter coater (Ted Pella, Inc., Redding, CA, USA) with 23 nm of gold-palladium. For a better understanding of the surface morphology of the WP mixed with CNF, scanning electron microscope (SEM) images of the southern pine particles and the particles mixed with 3 wt.% CNF suspension after drying were taken at 20 kV using an Amray 1820 SEM (Amray, Inc., New Bedford, MA, USA). The SEM imaging was also used to investigate the wood-CNF bonding at fractured areas of the lap shear specimens.

2.3.2.9. Statistical analysis of experimental data

All experimental data were statistically analyzed with IBM SPSS Statistics Version 23 (IBM Corp., Armonk, NY, USA,). A two-way Analysis of Variance (ANOVA) was used to investigate the main and interaction effects of the independent variables (density and CNF level). A Duncan's multiple range test (DMRT) was used to evaluate the group means. A t-test was performed to evaluate the effect of the crosslinking agent as an additive. Comparisons were made based on a 95% confidence interval.

2.4. RESULTS AND DISCUSSION

2.4.1. Mechanical and Physical Properties

As expected, it was observed that the density has a considerable effect on the MOR and MOE of the panels. Changing the CNF content of the panels from 15% to 20% did not significantly (*p*-

value = 0.388) change the MOE but increased the MOR values significantly (p-value = 0.003). The effect of the density of the produced PB on MOR and MOE for the panels that contained 15% and 20% CNF is illustrated in Fig. 2.3. This shows that the MOR and MOE increased with an increase in the density of the panels.

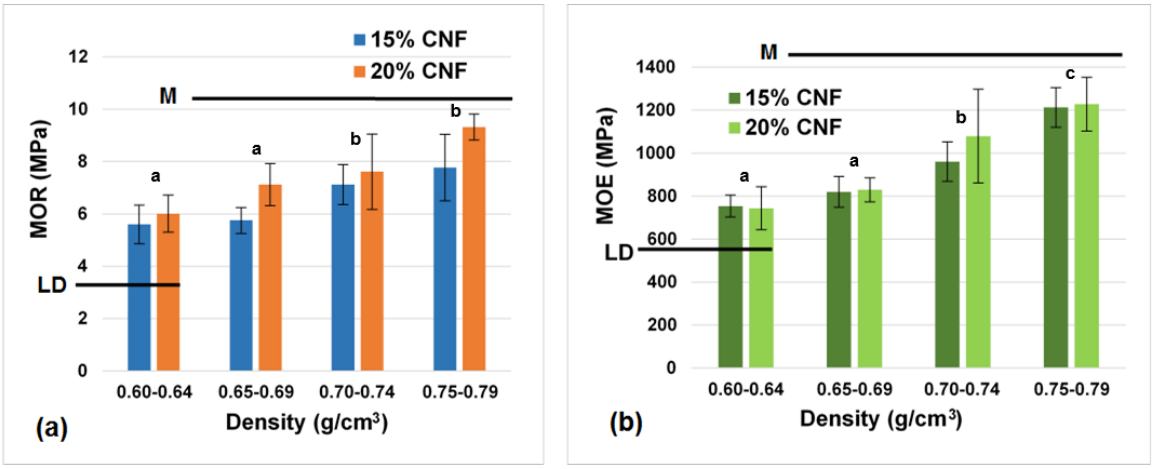

Fig 2.3. Mechanical properties of 15% and 20% CNF-containing panels: (a) MOR (b) MOE. Columns with different letters are significantly different at a significance level of 0.05.

The DMRT test showed that the MOR values of the two lowest density levels were not significantly different from each other (p-value = 0.188). The same was true for the MOR of the two highest density levels (p-value = 0.064). The MOE of the two lowest density levels were not significantly different (p-value = 0.113), whereas all other density levels showed a statistically (p-value < 0.0001) different effect on MOE. As mentioned above, the CNF content did not meaningfully improve MOE, but did so for MOR. This could have been related to the fact that MOE of the panel mainly depended on the elastic moduli of both the WP and CNF. As the moduli of elasticity of CNF particles and southern pine wood are almost similar [55, 56], increasing the proportion of CNF in the formulation of the panel means decreasing the proportion of the WP,

and consequently not noticeably altering the overall value of the MOE. In contrast, the MOR relates to the bonding strength of the adhesive. Therefore, increasing the proportion of CNF as a binder would result in an increase in MOR values.

The lines marked with M and LD in Fig. 2.3 represent the minimum required MOR and MOE for the medium-density and low-density particleboard panels, respectively, based on ANSI A208.1 (2016). As shown in Fig. 2.3, the CNF-bonded panels fulfilled the requirements of the MOR and MOE standard levels for the low-density (less than 0.64 g cm^{-3}) particleboard panels. However, these values were lower than the minimum standard levels of both properties for the medium-density (generally between 0.64 g cm^{-3} to 0.8 g cm^{-3}) panels. To meet the M level requirements, several changes could be made to the PB configuration, such as using larger particles in the core layers and smaller ones in the surface layers. A three-layer layup with higher densities for the panel surfaces as opposed to a one-layer layup is common in the industrial particleboard manufacturing process.

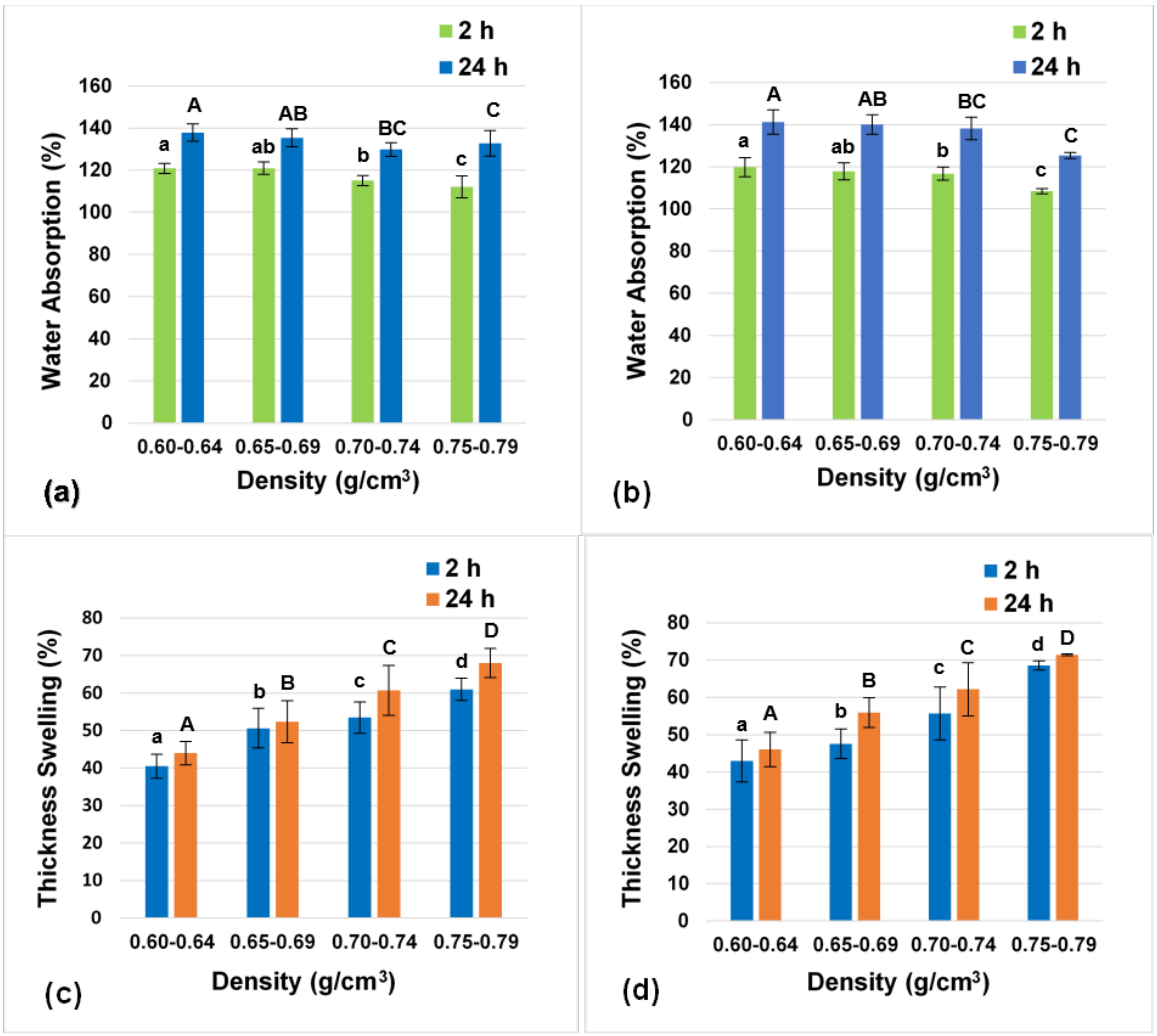

Fig 2.4. Water absorption of (a) 15% and (b) 20% CNF containing panels; thickness swelling of (c) 15% and (d) 20% CNF-containing panels. Columns with different letters are significantly different at a significance level of 0.05.

Water absorption and thickness swelling properties of the produced panels were observed to be affected by the changes in density. However, there was no statistically significant difference between panels that contained 15% and 20% CNF in terms of water absorption and thickness swelling. Figure 2.4 presents the results of water absorption and thickness swelling tests for the panels that contained 15% and 20% CNF after 2 h and 24 h of submersion. It can be seen that for all of the samples, most of the water was absorbed in the first 2 h of submersion. The DMRT test

showed that the thickness swelling values after 2 h and 24 h of submersion were significantly (p-value = 0.000) different for all four density levels. However, the water absorption values after 2 h of submersion were not significantly different for the two lowest density levels (p-value = 0.573). The same was true for the second and third level of density (p-value = 0.054). Overall, with increased densities of the panels, the thickness swelling increased while an inverse effect on water absorption was observed. This was attributed to the packing density of the panel structures. As the density of panels increased (at a constant volume), the structure became more packed. Therefore, the number of pores per volume into which water can penetrate (bulk penetration) decreased, which resulted in water absorption reduction. This is why the water absorption decreased with an increase in the density of panels. However, thickness swelling, increased as the density increased because the number of particles and binders swollen in a constant volume of panel increased with an increase in the density.

Despite considerable thickness swelling and water absorption of panels, all specimens maintained their integrity after the tests were completed. This was an encouraging observation for future research to focus on how low-density insulating panels could have high dimensional stability. It should be mentioned that thickness swelling and water absorption are not limiting factors for interior-grade particleboard panels in the U.S. (ANSI A208.1-2016 (2016)), but tests results are helpful in understanding bonding efficiency.

2.4.2. Effects of Adding a Crosslinking Agent

The addition of the crosslinking agent to the PB formulation altered the mechanical and physical properties of the panels. Results of flexural tests on both crosslinking agent- and non-

crosslinking agent-added panels with the density of 0.65 g.cm^{-3} are presented in Figs. 5a and b. It is observed that adding 3 pph of the crosslinking agent to the PB formulation almost doubled the MOR of the produced panels. It also caused the MOE of the panels to become nearly 1.5 times higher. In fact, the crosslinking agent used in this work was an aqueous solution of polyamidoamine-epichlorohydrin (PAE) resin, which had an azetidinium group (the cationic four-membered ring structure shown schematically in Fig. 2.6a) that could be cross-linked with the carboxyl groups (Fig. 2.6b) remained from pulp bleaching processes on the cellulosic structure of CNF and impart wet-strengthening on the PB structure[57,58].

The results of water absorption and thickness swelling testing performed on the crosslinking agent- and non-crosslinking agent-added specimens (Figs. 2.5c and d) indicated that the addition of the crosslinking agent to the PB formulation dramatically reduced the water absorption and thickness swelling of the panels, which was desirable for particleboard manufacturing. It was shown that the addition of the crosslinking agent decreased the thickness swelling amount by more than half. This was attributable to the fact that the reaction between the azetidinium functional group in the crosslinking agent structure and carboxylic groups in CNF results in a water-insoluble network [58,57].

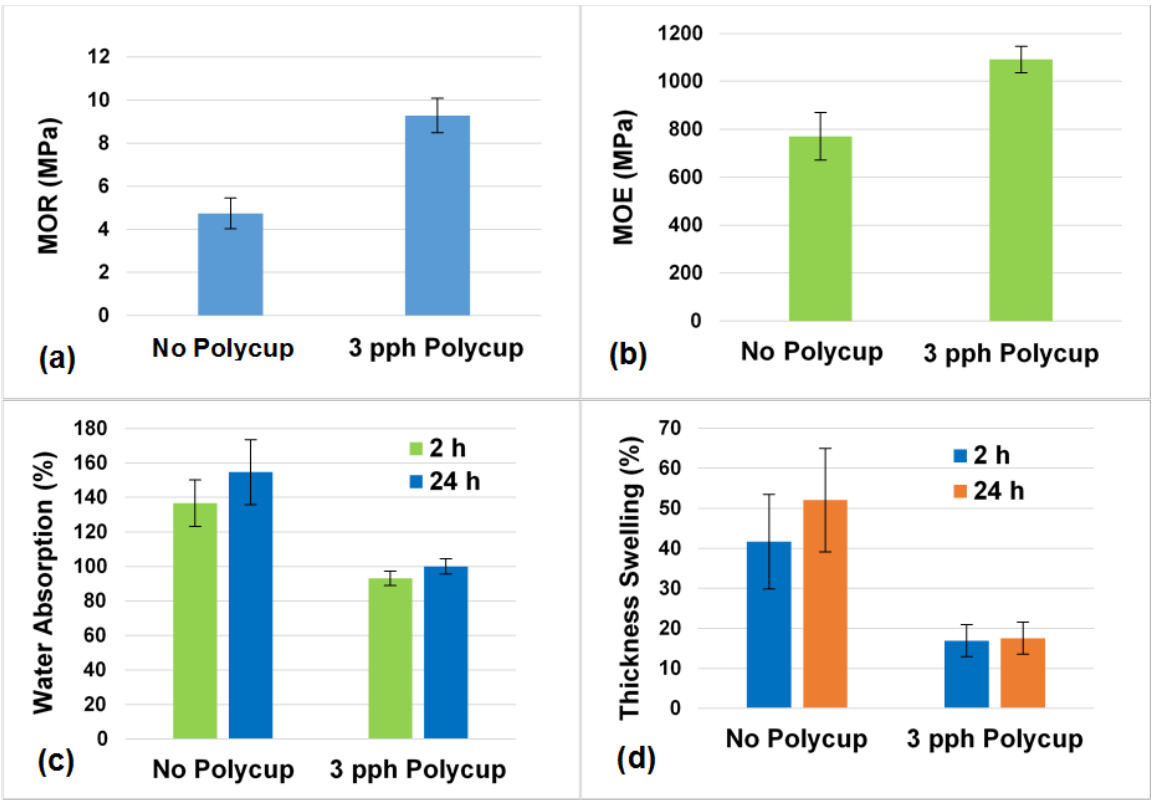

Fig 2.5. Comparison of (a) MOR, (b) MOE, (c) water absorption, and (d) thickness swelling of panels with and without crosslinking agent

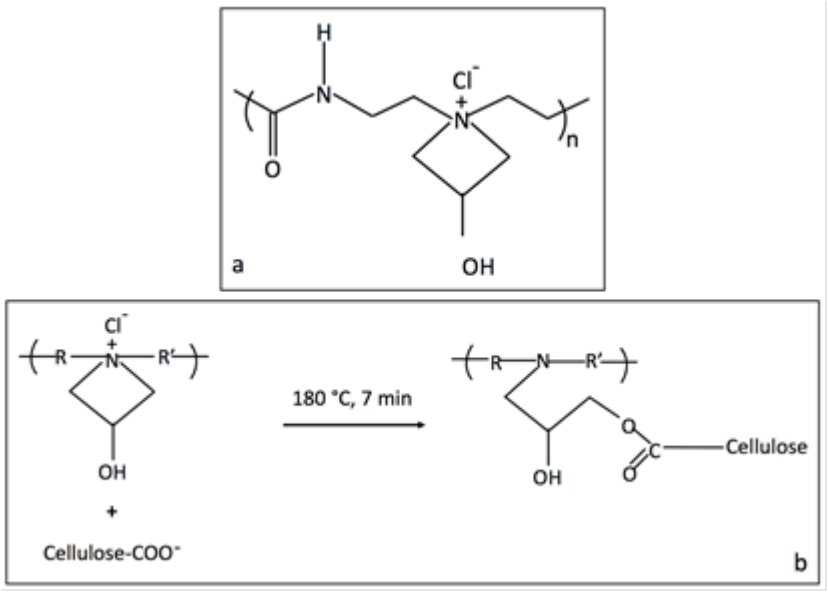

Fig 2.6. (a) Scheme of chemical structure of PAE resins; (b) Reaction between the azetidinium groups of PolycupTM 5233 and carboxyl groups of bleached cellulose

2.4.3. Density Profile

The density profile analysis revealed that all produced PB panels had a U-shaped vertical density profile, which confirmed the higher density in the panel surfaces compared to the core occurred mostly because of a position control pressing type. Density gradients are common in particleboards and can be favorable or unfavorable, depending on their application. While a vertical density gradient can help increase flexural properties without increasing density, the performance of edge gluing and fastening is reduced as a result. Differences in density occur because of the differential heat transfer as well as moisture transport from the mat surfaces that are in contact with press platens to the core, which result in greater densification in the mat surfaces than in the core. If a curable resin is involved, this means that the faces are cured and set at a higher pressure while the core is still curing and sustaining the pressure [59]. In the particular system presented in the current chapter, no curing happened and all bonding took place when the CNF dried. Fig. 2.7 shows the vertical density profiles of two PB panels with different mean density (MD) levels. It was observed that the difference between the surface and core densities was more noticeable at higher mean density levels attributed to the higher level of materials (or larger amount of materials) undergoing the pressure and heat.

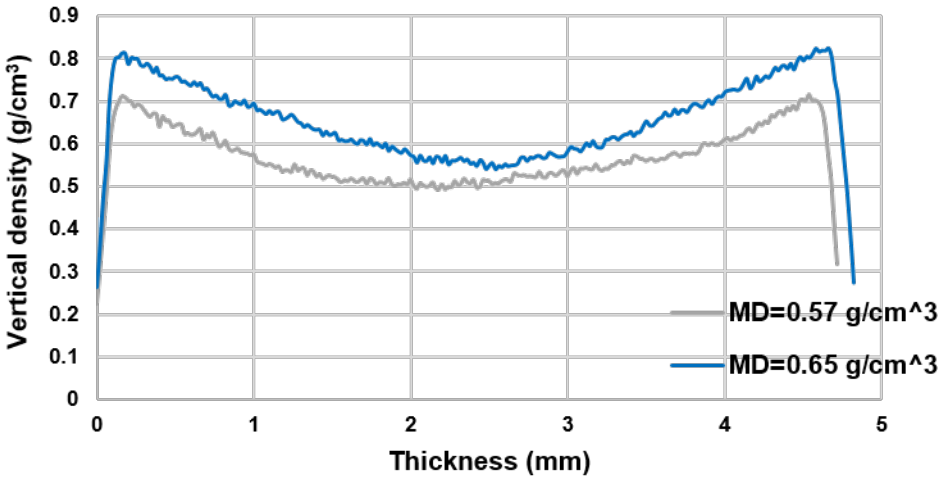

Fig 2.7. Density profile of PB panels at two different mean density levels

2.4.4. Internal Bond

The results of the IB tests for the different groups of density and at CNF levels of 15% and 20% are shown in Fig. 2.8.

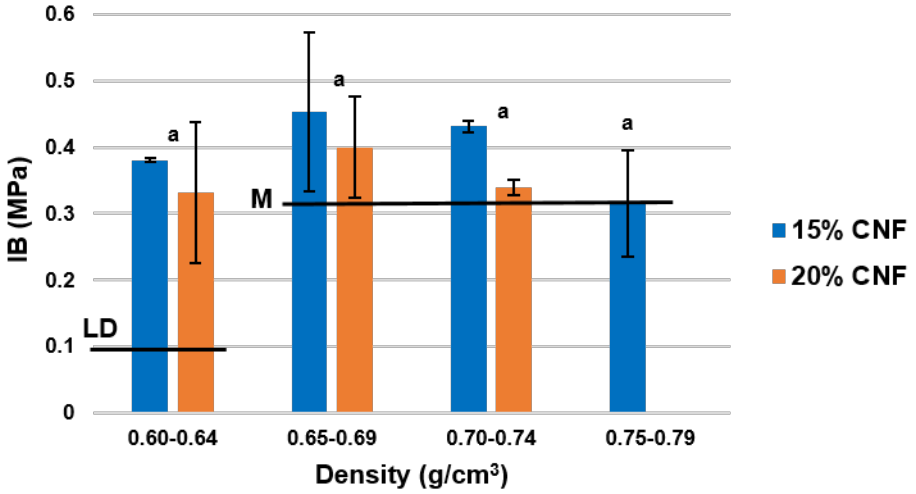

Fig 2.8. Internal bond strength of 15% and 20% CNF containing panels. Columns with the same letters are not significantly different at a significance level of 0.05.

The IB values for the density group of 0.75 g cm^{-3} to 0.79 g cm^{-3} at 20% CNF level were not provided because of unacceptable failure at the interface between the hot melt adhesive and the IB specimen during the test. The DMRT test showed that the IB values of all four groups of density (p-value = 0.103), and two different CNF levels (p-value = 0.128), were not significantly different. This was attributed to the smaller differences in the core densities compared to those in the surface densities of all the panels observed in the density profile analysis. The lines marked with M and LD in Fig. 2.8 represent the minimum IB strength for the medium-density and low-density particleboard panels, respectively, based on ANSI A208.1 (2016). As shown in Fig. 8, the produced panels almost met the requirements of IB strength for both low-density and medium-density particleboard panels.

2.4.5. Strength Development

Drying time was a key factor in the strength development of the adhesion between the CNF and WP. The relationship between drying time and moisture content (MC%) of the disk-shaped samples was first studied. For all samples the moisture content levelled off after approximately 250 min of drying. This information was used to determine the drying time intervals needed to achieve the desired moisture contents for the strength development tests. Figure 2.9c shows the effect of the drying time on the strength development of the disk-shaped samples. As shown in Fig. 2.9d, the relationship between moisture content and compressive modulus of the disks was used as a measure for the strength development of the specimens.

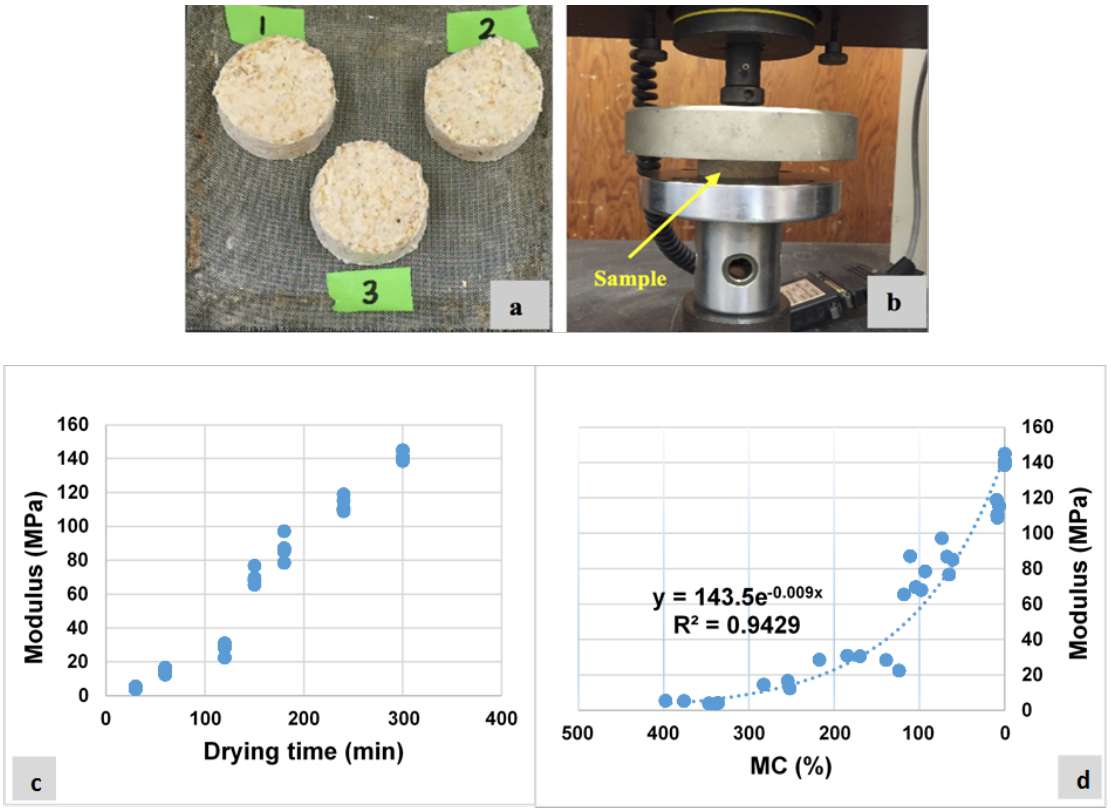

Fig 2.9. (a) Disk-shaped samples used for strength development tests, (b) compression test set-up; Relationship between (c) drying time and compressive modulus, (d) moisture content and compressive modulus of the disk-shaped samples.

It was apparent that increased drying led to increased strength. This happens partly because of the hornification phenomenon, where the dewatering and drying of cellulose nanofibrils results in a strong bond between wood particles and cellulose nanofibrils. Furthermore, drying the samples until the fiber saturation point of wood (approximately 30% moisture content [60] should not substantially change the strength of the samples because of the removal of free water in wood particles and in the mat. However, drying the samples below the fiber saturation point increased the strength of the samples dramatically attributable to the removal of bound water in the cell wall of wood. It was also concluded that at approximately 10% moisture content, 90% of the maximum stiffness was achieved.

2.4.6. Bonding Strength and Mechanism

Results of the lap-shear tests (Fig. 2.10b) indicated that the effect of sanding was significant (*p*-value = 0.037) on the bonding strength. The 400-grit sanded strands had the strongest bond with the CNF, whereas strands that were not sanded had the least bonding strength. These findings were attributed to more microgrooves in the smoother surface that grabbed more CNF and led to better mechanical interlocking of the binder and the substrate. The SEM micrographs of the unsanded control and sanded strands, along with the fractured ones after the lap-shear test, are presented in Fig. 2.11. The SEM micrographs confirmed the higher number and also smaller microgrooves on the surface of the 400-grit sanded strands compared to the other strands. They also verified the presence of nanocellulose fibrils on the surface of the broken strands after lap-shear testing (Figs. 11b, d, and f). Visual observation of the fractured surfaces of the lap shear specimens showed that in all cases, regardless of the surface roughness, an adhesive failure had occurred. The CNF that was used as the adhesive to bond the two strands of wood was fully detached from one side of the specimen, which indicated that the bonding between the CNF and wood surface was not greater than the shear strength of the CNF film. That is why minimal CNF fiber can be seen on the fractured surfaces of the specimens in the SEM micrographs.

The CNFs at low solids content can be largely dispersed and exfoliated in water, and they can result in a three-dimensional network of fibrils upon drying. If wood particles are present in the system, the CNF particles can encompass particles mixed with them and hold them together upon water removal. Considering the exceptionally high mechanical properties of cellulose nanoparticles [61] and excellent hydrogen bonding between cellulose nanoparticles and other types

of cellulosic materials [62], cellulose nanofibrils can bond wood particles to form a strongly bonded composite system. Figure 2.12a depicts a wet mat formed by mixing CNF suspension and wood particles. Such a system was composed of wood particles, CNF, water, and air. Upon dewatering and subsequent drying, a three-dimensional network of CNF was considered to form that held together the wood particles. At the micro/nano scale, it appeared that smaller particles of CNF could penetrate into the porous structure of wood particles that provided strong bonds. Figure 2.12b and c demonstrate how wood particles can be bound together using CNF. Figure 12b shows the surface of a southern pine wood particle used in the production of the particleboard panels. The surface of a similar wood particle after being mixed with a CNF slurry and air-dried overnight is shown in Fig. 2.12c. The CNF fibrils were easily observed as distributed over the particle surface with some particles agglomerated into platelet shapes and some preserving their fibrillar morphology with varying fibril widths. It was thought that at least smaller parts of the CNF particles in the suspension would penetrate into the structures' pores and voids in the wood particles. Once the wood particles with CNF surrounding them were in contact and hot pressed, a three-dimensional network of CNF fibrils formed and encompassed the particles in the panel structure, which gave it strength and stiffness. The strength of the bonds formed between two wood particles would depend on the degree to which the interpenetration of CNF was achieved, and the surface characteristics of the wood particles and CNF.

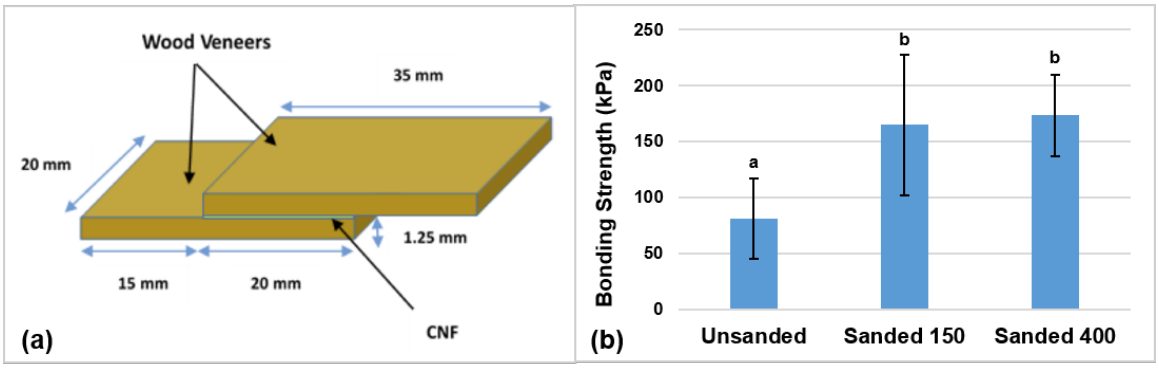

Fig 2.10. (a) Schematic diagram of a lap-shear specimen; (b) Bonding strength of the lap shear specimens with different surface roughness (Columns with different letters were significantly different at a significance level of 0.05).

The adhesion studies presented in this paper solely focused on the effect of mechanical interlocking and disregarded hydrogen bonding as a major contributor to bond strength[63]. The low values of lap shear strength observed in this study imply that hydrogen bonding would be the most important contributor to adhesion in the studied system [64]. The lap shear testing presented in this work may also not be representative of the bonding that happens in an actual wood particle-CNF system. In such a system, CNF can be assumed to encompass wood particles in a three dimensional network where CNF-CNF interactions might actually play a more important role than CNF-wood particle interactions (Fig. 2.12a). These interesting topics are the focus of the authors' current and future research.

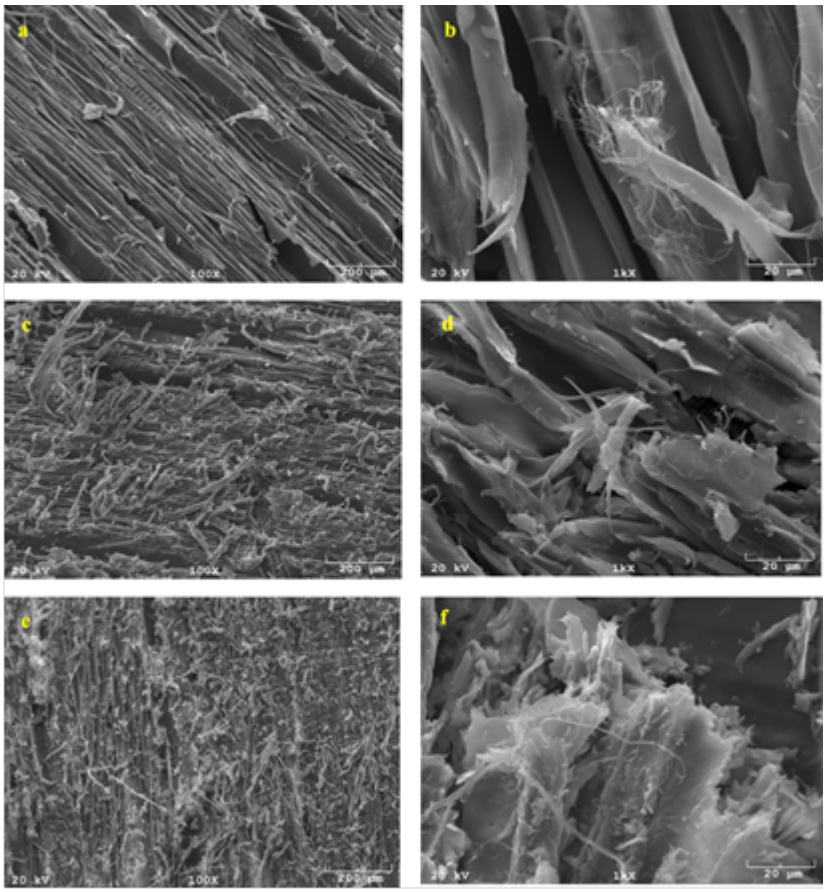

Fig 2.11. SEM micrographs of the surface morphology of (a) unsanded control, (b) broken unsanded, (c) sanded 150 control, (d) broken sanded 150, (e) sanded 400 control, and (f) broken sanded 400 strands.

The findings presented in this article provide a sound basis for a more focused effort on alternative applications of cellulose nanomaterials, particularly CNF as a binder in composite systems. However, the processing method presented in current paper to produce PB panels is different from that used for PB manufacturing on an industrial scale. For CNF to be used as binder in particleboard manufacturing, future research should be directed towards processes that minimize the amount of water in the mat to be pressed in the hot press. This calls for attaining a balance between the amount of water that can be tolerated in the press and that required for effective hydrogen bonding to occur.

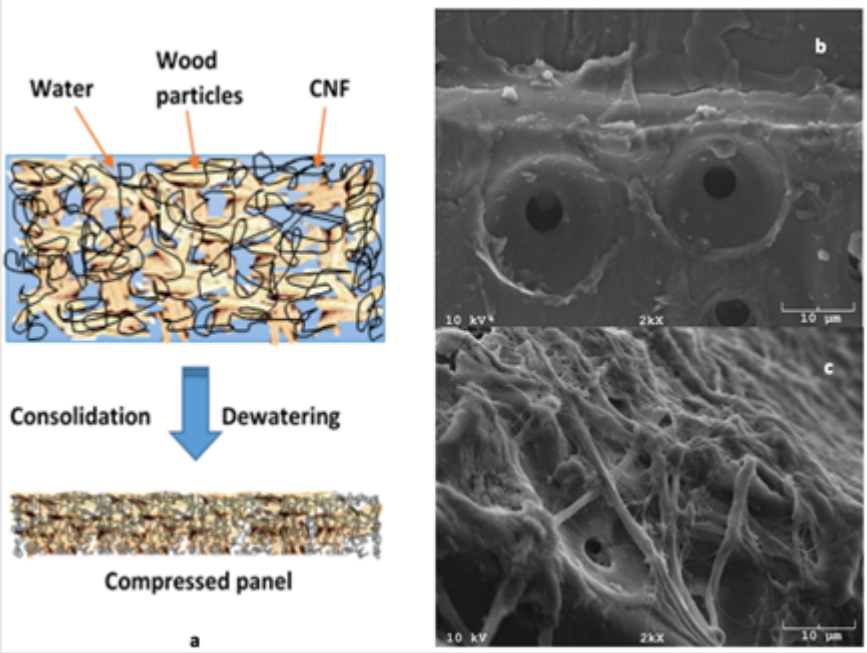

Fig 2.12. (a) Consolidation and dewatering phenomenon followed by drying led to bond formation at micro/nano scale; SEM image of (b) the surface of a southern pine particle and (c) a southern pine particle mixed with a 3% solids content CNF after air-drying overnight.

2.5. CONCLUSIONS

1. The PB panels manufactured using CNF as an adhesive binder were shown to meet the industry requirements in terms of mechanical properties for low density grades. The MOR and MOE of the produced panels increased with increased density levels.

2. The panel's density affected the water absorption and thickness swelling properties inversely. Water absorption decreased as the density of the panels increased. However, increased density led to an increase in the thickness swelling of the panels.

3. Moisture removal plays a major role in the strength development of the adhesion between WP and CNF.

4. The effect of sanding was shown to be significant on the strength of the WP-CNF bonding. The 400-grit sanded lap shear specimens had higher bonding strength values compared to the 150 grit sanded ones. The unsanded lap shear specimens had the weakest bonding strength.

CHAPTER 3

DEWATERING BEHAVIOR OF A WOOD-CELLULOSE NANOFIBRIL PARTICULATE SYSTEM

3.1. Chapter Summary

The novel use of aqueous suspensions of cellulose nanofibrils (CNF) as an adhesive/binder in lignocellulosic-based composite applications requires the removal of a considerable amount of water from the furnish during processing, necessitating a thorough understanding of the dewatering behavior referred to as "contact dewatering". The dewatering behavior of a wood-CNF particulate system (wet furnish) was studied through pressure filtration tests, centrifugation, and characterization of hard-to-remove (HR) water, i.e. moisture content in the wet furnish at the transition between constant rate part and the falling rate part of evaporative change in mass from an isothermal thermogravimetric analysis (TGA). The effect of wood particle size thereby particle specific surface area on the dewatering performance of wet furnish was investigated. Permeability coefficients of wet furnish during pressure filtration experiments were also determined based on Darcy's law for volumetric flow through a porous medium. Results revealed that specific particle surface area has a significant effect on the dewatering of wet furnish where dewatering rate significantly increased at higher specific particle surface areas. While the permeability of the systems decreased over time in almost all cases, the most significant portion of dewatering occurred at very early stages of dewatering (less than 200 seconds) leading to a considerable increase in instantaneous dewatering when CNF particles come in contact with wood particles.

3.2. Introduction

Cellulose nanofibrils (CNF) have received a tremendous level of attention over the past few years as potential binders, reinforcing fillers, paper coatings, oxygen barrier films, and filaments attributable to the unprecedented specific strength of the individual nanofibrils, low density, superb adhesion properties, chemically tunable surface functionality, renewability, and biological abundance of a material obtained from sustainable resources. Finding novel applications which can highly benefit from outstanding intrinsic properties of CNF has been the subject of numerous recent studies [54,65–72].

CNF consists of nano and micro-scale cellulosic fibers suspended in water and is mostly available in the form of a low-consistency (less than 4 wt.%) aqueous suspension. It offers excellent adhesion properties attributed to a very high specific surface area and a vast number of hydroxyl groups available on the cellulosic surfaces, which make this type of material a superior candidate for many different applications[1,10]. The utilization of CNF as well as lignin-containing CNF (LCNF) as binders in the formulation of particleboards and medium density fiberboards has been reported [65,73–76]. Potential applications of CNF as a binder for the production of laminated papers[77], reinforcing natural fiber yarns[78], and self-assembly processes [78,79] have been recently proposed.

The current processing technology to produce composite panels using CNF or LCNF as binder consists of a dewatering process followed by drying in a hot press [2,13-15]. To shorten press cycles and save energy, the majority of the water present in the mixture of wood particles and CNF

(hereafter “furnish” or “mattress”) must be mechanically removed prior to hot pressing in an efficient manner. Therefore, understanding and controlling the water removal behavior of the CNF suspension, both solely and in the form of a mix with other materials is a critical step to optimize the production process.

The terms “dewatering” and “drainage”, herein, refer to liquid (assuming only water) removal from the solid-liquid mixtures during a filtration process. The material structure forming as dewatering progresses is referred to as “filter cake”. To date, the dewatering behavior of cellulosic suspensions and furnishes has been studied by many researchers mostly through filtration or rheological theories or combination of the two[80–89]. Paradis et al. used a modified dewatering apparatus equipped with a cone-and-plate rheometer to determine the drainage resistance coefficient of different grades of paper-making stock under a known shear condition. The influence of shear rate on the drainage resistance was also investigated, which pointed out that the drainage rate changes as a result of the change in the characteristics of the filter cake as drainage progresses[82]. Dimic-Misic et al. studied the effect of shear stress as well as swelling (expressed as the water retention value at a relatively low consistency) of micro and nanofibrillated cellulose (MNFC) on the dewatering behavior of the cellulose furnishes. It was found that the nanofibrillar suspension added to the pulp-pigment particles furnish predominantly governs the rheological and dewatering responses. Highly swelled nanofibrillated cellulose was shown to have a significantly difficult dewatering owing to plugging the bottom layer of the filter cakes with ultrafine fibrils. A noticeable gel-like structure as well as shear-thinning behavior –i.e. the decrease in viscosity under increasing shear rates–

were seen for all the MNFC suspensions and furnishes, thus more efficient dewatering at higher shear rates could be attained [80,81].

The influence of CNF flocculation upon charge neutralization by the addition of salt on the dewatering ability of CNF suspension was investigated using a pressure dewatering method and it was determined that the dewatering ability of the CNF suspension is affected by the type and concentration of the salt [83]. Rantanen et al. [84] studied the effect of adding MNFC to the formulation of high filler content composite paper in the web dewatering process using a gravimetric dewatering evaluation. The results revealed that increasing the MNFC fibrillation decreased the dewatering performance, however, this could be tuned by *in situ* precipitation of precipitated calcium carbonate (PCC) to achieve a desirable combination of strength and processing performance [84]. Further assessments have been done to enhance the dewatering capability of MNFC suspensions and furnishes under an ultra-low shear rate (approx. 0.01 s^{-1}), including the addition of colloidally unstable mineral particles (such as undispersed calcium carbonate), acid dissociation of the surface water bound to the nanofibrils of cellulose by adding ultrafine calcium carbonate nanoparticles, and controlling the rheological properties with respect to length and aspect ratio of fibrils [80,85,86].

Clayton et al. studied the dewatering mechanisms of a range of biomaterials, including lignite, bio-solids, and bagasse, through mechanical thermal expression (MTE) using a compression-permeability cell. It was revealed that at lower temperatures the predominant dewatering mechanism is mechanical dewatering referred to as "consolidation" by the authors. However, thermal dewatering plays a more important role at higher temperatures[87]. A dynamic model

was developed by Rainey et al. to predict the filtration behavior of bagasse pulp incorporating steady state compressibility and permeability parameters obtained from experimental data [88]. Hakovirta et al. employed a method to improve the dewatering efficiency of pulp furnish through the addition of hydrophobic fibers and demonstrated that adding a low percentage of hydrophobic fibers to the pulp furnish could impact freeness and water retention properties, thus a considerable improvement in the dewatering efficiency was attained[89]. A method was used to measure the permeability of fiber mats at different flow rates during the medium density fiberboard manufacturing process using Darcy's law [48]. Lavrykova-Marrain and Ramarao employed two mathematical models based on conventional cake filtration theory and multiphase flow theory by applying Darcy's law to describe dewatering of pulp fiber suspensions under varying pressure [90]. A model was also developed to predict the permeability of cellulose fibers in pulp and paper structures based on Kozeny-Carman theory assuming fibers are either cylindrical or band-shape in a two-dimensional network [91]. Darcy's law was also applied to predict the weight of CNF-containing paper coatings through filtration theory [92].

The original hypothesis of this study is based on the fact that in a CNF suspension, water is mostly in the form of adsorbed water associated with the cellulose surface and is tightly bound to the hydroxyl groups present in the amorphous regions through hydrogen bonding. After mixing wood particles (WPs) with CNF slurry, a large portion of the adsorbed water turns into free water as a result of contact between nanofibrils of cellulose and WPs, a phenomenon termed here as 'contact dewatering' first reported by our research group [54,65]. Upon consolidation, a considerable amount of free water is removed from the wet furnish by pressing

(mechanical dewatering) in a very short period of time and the remaining water in the system can be removed through heating (evaporative dewatering) to produce the final product.

In this chapter, the dewatering behavior of WP-CNF wet furnish was studied through pressure filtration tests and centrifugation. The effect of wood particle size and therefore particle specific surface area on the dewatering properties of wet furnish was investigated. A method based on Darcy's law for volumetric flow through a porous medium was used to determine the permeability coefficients of wet furnish during filtration test. Characterization of hard-to-remove (HR) water in wet furnish was also carried out using high resolution isothermal thermogravimetric analysis (TGA) to evaluate thermal dewatering properties of the samples. The results of this study will be helpful in the design of processing equipment for the production of wet-formed CNF bonded composite panels.

3.3. Materials and Methods

3.3.1. Materials.

Southern yellow pine wood particles (WP) with an average aspect ratio of 3.3 and average moisture content of 7% were supplied by Georgia-Pacific Thomson Particleboard (Thomson, GA, USA). The CNF was received in the form of a slurry of 3 wt.% cellulose nanofibrils from the University of Maine's Process Development Center, which was the product of mechanical refining of bleached softwood kraft pulp. The properties of this CNF material are published elsewhere[18]. Polypropylene (PP) granules with the average diameter of 2.5 mm were provided by Channel Prime Alliance Inc. (Des Moines, IA, USA).

3.3.2. Particle size distribution.

To investigate the effect of WP size on the dewatering behavior of the wet furnish, particles were separated based on the size using a Retsch AS 200 laboratory sieve shaker (Retsch®, Haan, Germany). Particles were screened into six different size ranges, including larger than 2 mm (Group I), larger than 1.4 mm and smaller than 2 mm (Group II), larger than 1 mm and smaller than 1.4 mm (Group III), larger than 0.5 mm and smaller than 1 mm (Group IV), larger than 0.25 mm and smaller than 0.5 mm (Group V), and finally dust (Group VI).

The sieved particles were then weighed and the weight fractions of each particle size range was calculated based on the total weight of the given sample of WPs. Results are presented in Fig. 1. As shown in Fig. 3.1, WPs with the sizes ranging from 0.5 mm to 1.4 mm had the highest weight fraction, almost 60%, of the entire sample.

To determine the average specific surface area of the wood particles in each range/group, three different samples of wood particles, each sample about 5 grams in weight, were selected from each size range. The average thickness of particles in each sample was calculated through measuring the thicknesses of one hundred particles randomly selected from the given sample. The average length and surface area of each given sample were measured by an optical (digital) photograph of the sample and then processing the digital image using the ImageJ image processing software version 1.49v (National Institutes of Health, USA). Assuming that particles are in the form of small cuboids and having the average values of length, thickness, and surface

area, the average specific surface area of particles in a given sample can be approximated using Eq. 3.1:

$$S\acute{S}A = \frac{2 \times \left[\left(\acute{S}\right) + \left(\acute{a} + \acute{b}\right) \times \acute{t}\right]}{w} \tag{3.1}$$

where $S\acute{S}A$ is the average specific surface area (cm^2/g), ($\acute{S}$) is the average top view surface (cm^2), $\acute{a}$ is the average length (cm), $\acute{b}$ is the average width (cm), $\acute{t}$ is the average thickness, and w is the sample weight (g). The average width of the particles can be easily calculated by having the average top view surface and the average length through Eq. 3.2:

$$\acute{b} = \frac{\acute{S}}{\acute{a}} \tag{3.2}$$

The average values of specific surface area for each particle size group are illustrated in Fig. 3.1. It is clearly shown that the smaller the wood particle size, the higher the specific surface area.

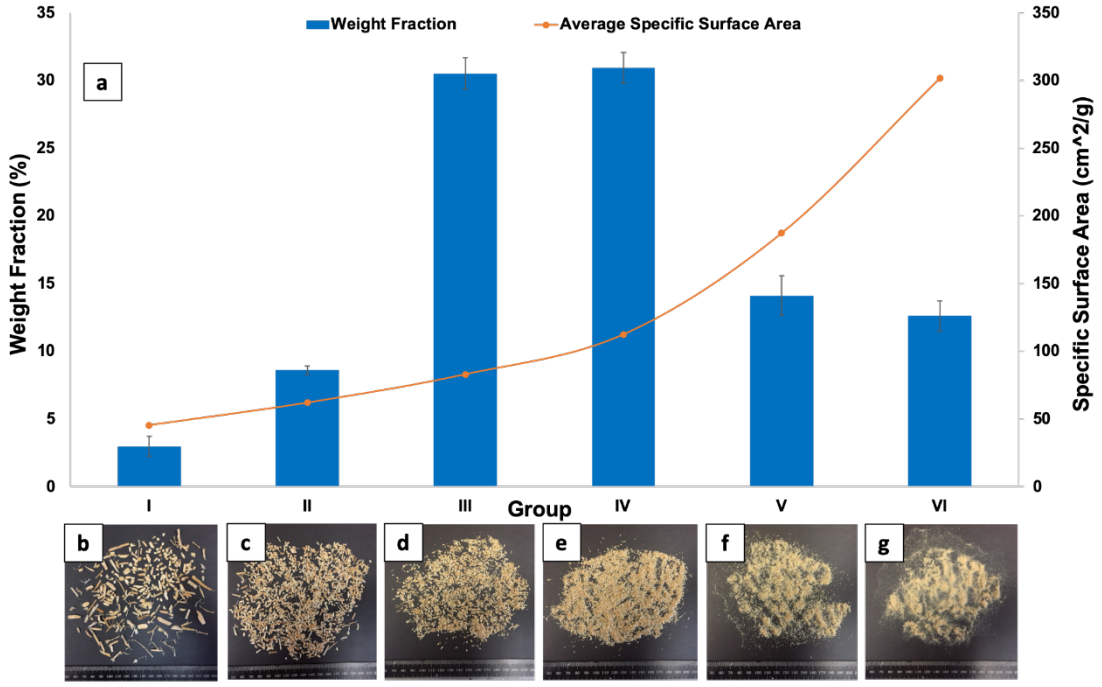

Fig. 3.1. (a) WP size distribution and average specific surface area values in a given sample. WPs (b) larger than 2 mm (Group I) (c) larger than 1.4 mm and smaller than 2 mm (Group II) (d) larger than 1 mm and smaller than 1.4 mm (Group III) (e) larger than 0.5 mm and smaller than 1 mm (Group IV) (f) larger than 0.25 mm and smaller than 0.5 mm (Group V) (g) dust (Group VI).

3.3.3. Pressure filtration.

A pressure filtration test was used as a method to study the dewatering behavior of the wet furnish. To investigate the effect of particle size on the dewatering of the wet furnish, samples of WPs with deferent sizes from Groups I through VI (excluding Group IV that had close *SŚA* to Group III) were selected and mixed with a CNF slurry at 3 wt.% solids content. The mixing ratio of WPs to CNF was 7:3 based on dry weights of the constituents. Samples of pure CNF slurries with consistencies of 3 and 10 wt.% (prepared by squeezing adequate amount of water out of CNF 3 wt.% slurry to reach 10% consistency) were also used to compare the dewatering behavior of pure CNF with that of WP-CNF mixes. The reason for choosing CNF 10 wt.% was

that it had the same solids content as the mix samples. Pressure filtration tests were then carried out on the prepared samples at a pressure of 172 kPa (approx. 25 psi) for 30 minutes using an OFITE® low pressure bench mount filter press (OFI Testing Equipment, Inc., Houston, TX, USA). Samples of 100 g from each formulation were loaded into the cylindrical chamber of the device on top of a metal screen and a filter paper. A small digital scale along with a glass Erlenmeyer flask on top were placed under the chamber outlet to collect and weigh the removing water (Fig 2d). The changes in the weight of collected water through time were recorded by a video camera from which dewatering values were extracted.

3.3.4. Determination of permeability.

Darcy's law for liquid flow through a porous medium was used to determine the permeability of pure CNF and WP-CNF mixtures. A schematic of pressure filtration is illustrated in Fig. 2a-c. According to Darcy's law, the specific volumetric flow rate ($\dot{V}$) is related to the pressure drop through the filter cake ($\Delta \boldsymbol{P}$), permeability of the filter medium ($\boldsymbol{k}$), viscosity of the fluid (μ) and the cake thickness (h):

$$\dot{V} = \frac{d\left(\frac{V}{A}\right)}{dt} = \frac{\Delta P\ k}{\mu\ h} \tag{3}$$

where $\left(\frac{V}{A}\right)$ represents volumetric liquid flow per unit area and $\boldsymbol{t}$ is the drainage time. The thickness of filter cake ($\boldsymbol{h}$) can be also obtained from Eq. 4 taking into account a balance between

the volume of fibers trapped in the filter cake and the volume of fibers that were present in the water which has passed through the membrane at any given time[35]:

$$h = \frac{V\ \phi_0}{A\ \phi_m} \tag{4}$$

where ϕ_0 and ϕ_m are volume fraction of fibers in the slurry and in the filter cake, respectively. In the case of wet furnish, fibers refer to the sum of cellulose nanofibrils and wood particles. The volume fraction of fibers can be easily obtained based on solids content of the slurry and the densities of fibers and water:

$$\phi = \frac{s\ \rho_w}{s\ \rho_w + (1-s)\ \rho_f} \tag{5}$$

where s, ρ_w, and ρ_f are solids content of the slurry, density of water (for simplification assumed 1 g/cm^3), and density of fibers, respectively. Rewriting Eq. 3 based on Eq. 4 will yield:

$$\left(\frac{V}{A}\right) d\left(\frac{V}{A}\right) = \left(\frac{\Delta P\ k\ \phi_m}{\mu\ \phi_0}\right) dt \tag{6}$$

Equation 3.7 can be derived from Eq. 3.6 by integration. Equation 3.7 actually describes the dewatering behavior based on the permeability and fiber volume fraction of the filter cake. This

equation clearly demonstrates that the volumetric flow of water per unit area of the filter cake has a square root relationship with the pressure drop through the filter cake, permeability of the cake, volume fraction of fibers, and dewatering time.

$$\frac{V}{A} = \sqrt{\frac{2\,\Delta P\,k\,\phi_m\,t}{\mu\,\phi_0}} \tag{3.7}$$

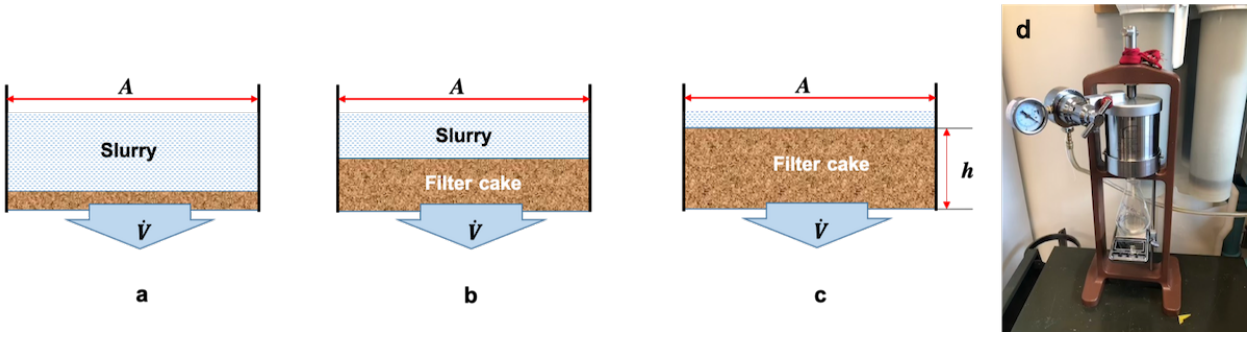

Fig. 3.2. Schematic of the filtration model: (a) shortly after the beginning (b) in the middle (c) at the end of filtration experiment. (d) Filter press and test setup.

It should be noted that during the dewatering of wet furnish, the permeability of the filter cake changes due to the densification and compression of the filter cake over the time. To determine the permeability of wet furnish, Eq. 3.7 can be rearranged in the form of Eq. 3.8.

$$\left(\frac{\mu\,\phi_0}{2\Delta P\,\phi_m}\right)\left(\frac{V}{A}\right)^2 = \kappa t \tag{3.8}$$

Volumetric liquid flow $\left(\frac{V}{A}\right)$ can be calculated based on the filtrate mass (g) over filtration time (s), density of water (g/mm^3), and cross-sectional area of the filter cake (mm^2), which is roughly equivalent to the cross-sectional area of the cylindrical chamber, using the following equation:

$$\frac{V}{A} = \frac{m_w}{\rho_w A} \tag{3.9}$$

where m_w and A are mass of removed water and cross-sectional area of the filter cake, respectively. The left-hand side of Eq. 3.8 for each corresponding volumetric flow can be calculated and plotted versus time. The permeability of filter cake at each time interval can then be determined by fitting a straight line to the resultant curve in the corresponding time interval and finding the slope of the lines.

3.3.5. Centrifugation.

Water retention value (WRV) of wet furnish gives a useful measure of the performance of fibers and particles relative to the dewatering behavior of the furnish. Samples of WP-CNF mixtures along with pure CNF 3 wt.% and 10 wt.% were prepared using the same preparation method as the pressure filtration experiment. Samples of WP Group I were excluded from the experiment owing to insufficiency of large WPs. The WRVs of the samples were determined through centrifugation at 2200 rpm for 15 minutes using a CLAY ADAMS DYNAC® II table top centrifuge (Becton, Dickinson and Company, Franklin Lakes, NJ, USA). In order to separate the water removed during the centrifugation from the wet furnish and collect the leftover furnish, a Pierce™ Protein Concentrator PES tube was used. A round piece of filter paper was cut out of

the filter paper used for the pressure filtration test and placed underneath the samples prior to centrifugation to have control over the liquid flow and not to clog the tube membrane. After centrifugation, the leftover furnish was removed and weighed to determine the weight of centrifuged furnish. Samples then were dried in an oven at 105 °C until they reached the constant weights. The water retention values were calculated using Eq. 3.10.

$$\mathrm{WRV\%} = \frac{W_w - W_d}{W_d} \times 100 \tag{3.10}$$

where W_w and W_d are the wet weight of the sample after centrifugation and the oven-dry weight of the sample, respectively.

3.3.6. Hard-to-remove water.

Evaporative dewatering is another important mechanism of water removal occurring during the hot pressing process. To investigate the influence of particle size on the evaporative dewatering of the wet furnish, high resolution isothermal thermogravimetric analysis (TGA) was used based on the method first proposed by Park et al.[93] for measuring what was termed "hard-to-remove (HR) water", in softwood bleached kraft pulp fibers. HR water content is defined as the water content in fibers at the beginning of the transition between the constant rate zone and the dropping rate zone (between Part (2) and Part (3) in Fig. 3.3) of the evaporative change in mass (1st derivative curve). It can be calculated by dividing the mass of water in the fiber associated with the starting point (Point (a) in Fig. 3.3) of the transition stage by the mass of the dried fiber (Point (b) in Fig. 3.3), i.e. y divided by x in Fig. 3.3. To find the beginning of the transition stage, the starting point on the changes of the evaporative change in

mass, i.e. 2nd derivative curve is first located. Then the corresponding weight of water (value of "y") at Point (a) from the TG curve is found. The HR water value can then be calculated by simply dividing the obtained "y" value by the dry weight of the sample (value of x).

Samples of WPs (with an average moisture content of 7%) from Groups III, IV, V, and VI were selected and mixed with a CNF slurry at 3 wt.% solids content. The mixing ratio of WPs to CNF was 7:3 on a dry-weight basis. The resultant mixtures had an average solids content of about 10 wt.%. Samples of pure CNF and pure WP slurries with the same solids content (3 wt.%) were also prepared and tested using a TGA (model Q500, TA Instruments, New Castle, DE, USA) with a heating regime of ramping up (100 °C/min) to 120 °C and then continuing isothermally at 120 °C for 30 minutes to assure that samples are fully dried. WPs with the size of larger than 1.4 mm -i.e. Group I and II- were excluded from the experiment due to the difficulty in filling the small TGA pans with relatively large WPs. To compare the HR water content of pure CNF with larger cellulosic fibers, samples of pure (3 wt.% consistency) softwood bleached kraft pulp were also tested. To investigate the effect of using a nonpolar and hydrophobic materials instead of WP in the formulation of the mix, samples of 70% PP granules mixed with 30% CNF 3 wt.% (dry-basis) were made and tested as well. The initial mass of each sample was about 100 mg.

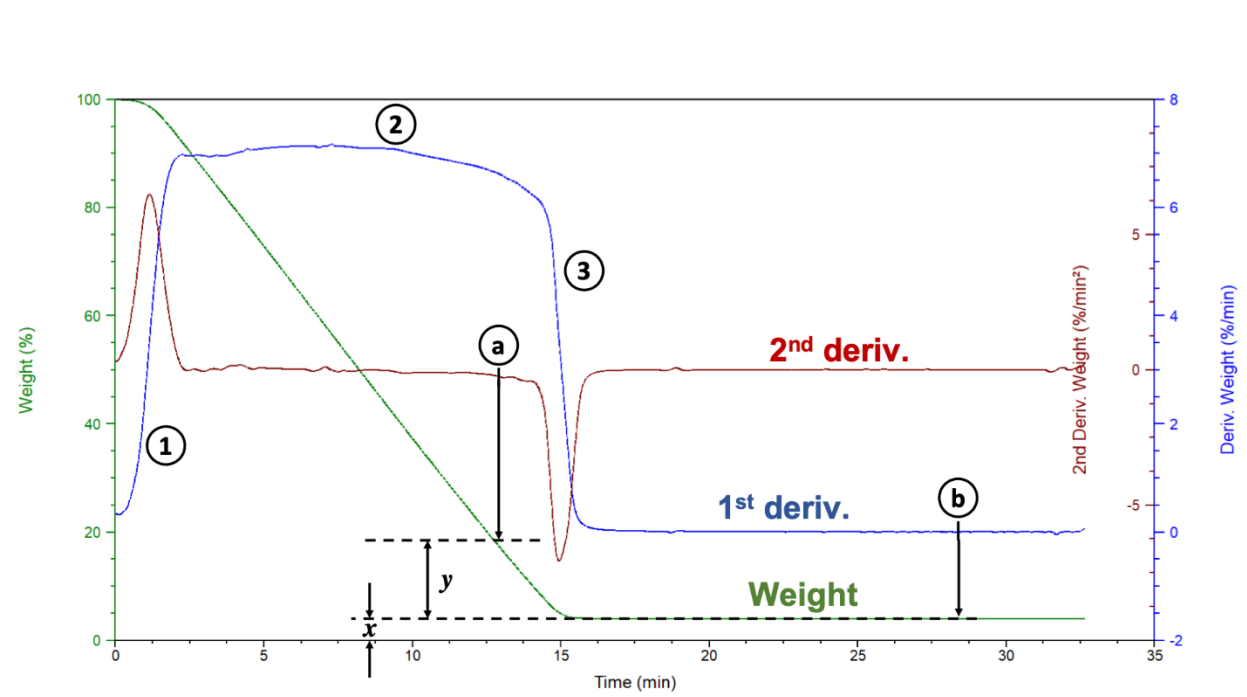

Fig. 3.3. Representation of drying response during an isothermal heating protocol used to define hard-to-remove water. Point (a) corresponds to the starting point of the transition between the constant rate zone and dropping rate zone of the DTG curve and Point (b) indicates the constant zone of the TG curve corresponds to mass of the fully dried fibers.

3.3.7. Statistical analysis.

The experimental data were statistically analyzed using IBM SPSS Statistics Version 25 (IBM Corp., Armonk, NY, USA). A one-way ANOVA test was carried out to statistically compare the HR water properties as well as WRV results. Duncan's multiple range test (DMRT) was also used to evaluate the group means. Comparisons were drawn based on a 95% confidence level.

3.4. Results and Discussion

3.4.1. Pressure filtration.

Pressure filtration tests revealed that the dewatering rate generally decreases over time, regardless of the material formulation. Samples of pure CNF 10 wt.% (with the same water content as the WP-CNF mixtures) exhibited considerably lower amounts and rates of water removal within the same period of time compared to the mixtures with the same solids content (Fig. 3.4a, b). This also happened for the case of CNF 3 wt.% within the first 200 seconds of the filtration during which in other formulations most of the water removal occurred and dewatering rate started to level off. The dewatering rate of CNF 3 wt.%, however, continued to decrease until almost 20 minutes after the experiment started. This may support the original hypothesis that most of the water in a WP-CNF mix is in the form of free water owing to contact dewatering and could be easily removed from the system, however in pure CNF suspensions, adsorbed water predominantly exists, which is harder to drain. Higher levels of water removal at the end of the test in CNF 3 wt.% compared to other formulations may be related to the lower consistency of CNF 3 wt.% samples which was lower than all other formulations.

Among WP-CNF samples, those with smaller particle sizes- i.e. Groups V and VI- in general exhibited the highest levels of water removal during filtration experiments (Fig. 3.4a). This can be attributable to the smaller size, thus higher specific surface area, which resulted in higher levels of contact dewatering. The lowest level of dewatering (Fig. 3.4a) and smallest change in the rate of dewatering (Fig. 3.4b) occurred throughout the filtration of WP with the largest particle size and smallest specific surface area (Group I). This can be also explained by lower

levels of contact dewatering in particles with smaller specific surface area. WP-CNF samples of Group V and VI showed to have a small amount of drainage even before applying any pressure. As shown in Fig. 3.4b, the initial increases in the dewatering rates of these two formulations within the first 10 seconds of the filtration is attributable to the pressure adjustments at the beginning of the experiments.

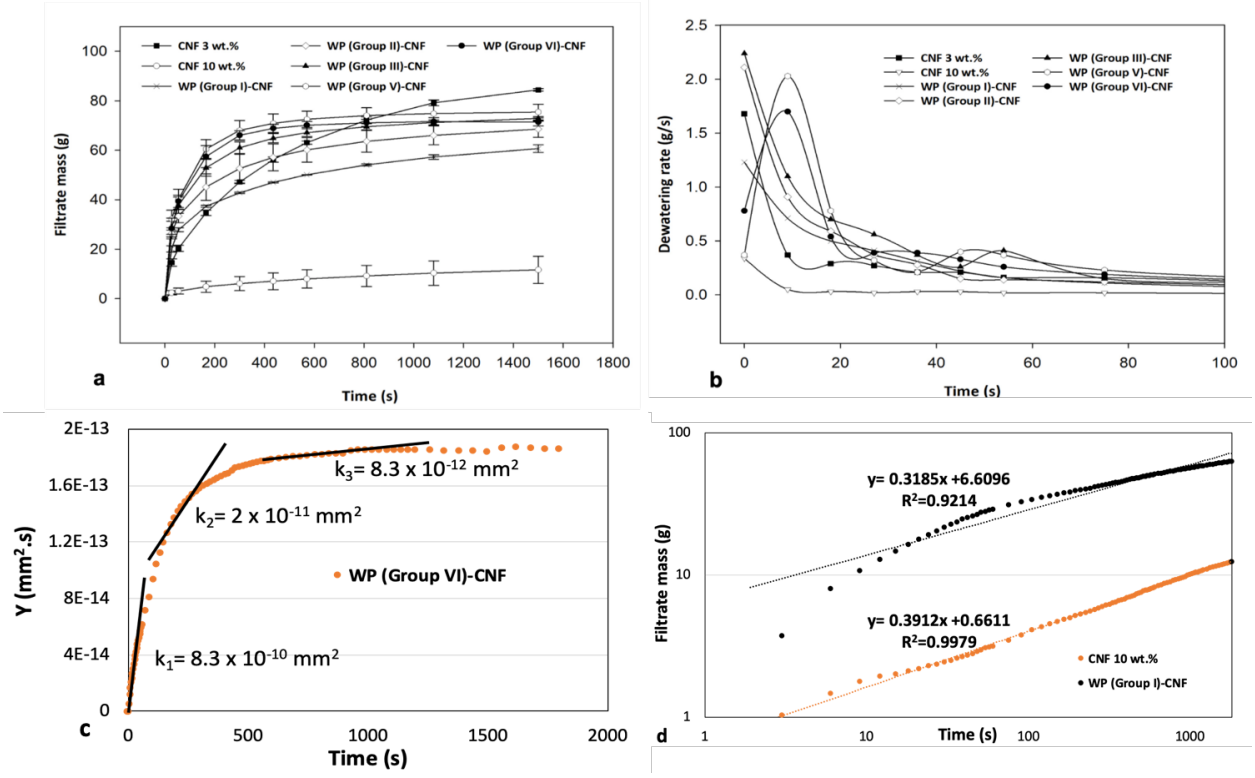

Fig. 3.4. Average (a) water removal (b) dewatering rate over filtration time for various material formulations. Representations of (c) parameter "Y" over filtration time to determine the permeability values and (d) filtrate mass versus filtration time to determine the instantaneous dewatering values.

3.4.2. Permeability.

Permeability values of the samples were determined using Equation 3.8. The values of $\left(\frac{V}{A}\right)$ at each time were calculated through Equation 3.9 by inserting the corresponding filtrate mass, density of water (1000 kg/m^3), and the cross-sectional area of the cylindrical chamber (4.6x10^{-3} m^2). The obtained volumetric flow values along with the pressure (172 kPa), viscosity of water (10^{-3} Pa.s) were then plugged into the Equation 8. Initial volume fraction of fiber (ϕ_0) and volume fraction of fiber at the end of the experiment (ϕ_m) were also calculated through Eq.3.5 and by measuring the solids of furnish before and after each filtration test.

Permeability values were obtained by plotting the left-hand side of the Eq. 3.8 (herein "Y") over time and fitting a line to the resultant curve at certain time intervals. As for nearly all the formulations, the resultant curves corresponding to Eq. 3.8 showed three different regions with significantly different slopes- i.e. at the beginning, before reaching the plateau, and the plateau-, the permeability values for each formulation were determined over these three regions. Therefore, the obtained k_1, k_2, and k_3 values respectively corresponded to the permeability of wet furnish at the beginning of the filtration, before reaching the point at which the dewatering rate started to level off, and at the level where no changes were seen in the dewatering rate. The obtained permeability values for each formulation are presented in Table 3.1. It can be seen that almost for all cases, the permeability decreases as the filtration goes on. The reduction in the permeability coefficient is more significant in WP (Group V and VI) mixtures with lower

particle sizes. This can be attributed to the higher compaction and densification of smaller particles upon dewatering, which resulted in lower porosity in these materials.

Table 3.1. Average values of permeability over three regions and instantaneous dewatering.

Formulation	Permeability (m^2)			Instantaneous dewatering (g)
	k_1	k_2	k_3	
CNF 3 wt.%	10^{-16}	$7x10^{-17}$	$1.7x10^{-17}$	3.3
CNF 10 wt.%	$1.1x10^{-17}$	$1.1x10^{-17}$	10^{-17}	0.66
WP (Group I)-CNF	$6.5x10^{-16}$	$8.5x10^{-17}$	$4.5x10^{-17}$	6.61
WP (Group II)-CNF	$9.3x10^{-16}$	$8.3x10^{-17}$	$3.3x10^{-17}$	9.56
WP (Group III)-CNF	$6.9x10^{-16}$	$4x10^{-16}$	$2.7x10^{-16}$	10.59
WP (Group V)-CNF	$7.7x10^{-16}$	$5.7x10^{-17}$	$8x10^{-18}$	8.52
WP (Group VI)-CNF	$8.3x10^{-16}$	$2x10^{-17}$	$2x10^{-18}$	9.55

Our observations in the lab and pressure filtration results indicated that the contact dewatering starts almost instantaneously after CNF particles come in contact with wood particles. To have a better understanding of how much water was instantaneously removed at the beginning of filtration, the average instantaneous dewatering value for each formulation was obtained by plotting the logarithm of the average filtrate mass versus the logarithm of time and then fitting a straight line to the resultant curve. The intercept of the regression line yielded the logarithmic value of the instant dewatering. As presented in Table 3.1, CNF 10 wt.% has a significantly lower instantaneous dewatering value compared to that of the WP-CNF mixtures. The amount of the water immediately removed at the beginning of the filtration is even considerably lower in CNF 3 wt.%, as compared with that of the mixes. It clearly shows that, in general, adding WPs to CNF helps with the dewatering. For comparison the instantaneous dewatering of the 3wt.% CNF

increased by 100% when the largest wood particles were added to the system. This was increased by 220% when Group III wood particles were mixed with CNF.

3.4.3. Water retention value.

Water retention values of wet furnishes are shown in Fig. 3.5. Results simply showed that the level of final water removed is almost the same among CNF 10 wt.% and WP-CNF mixes with the same solids content. Higher level of water retention in CNF 3 wt.% shows that the percent ratio of water contained in the sample after centrifugation, within the same time and speed, is much higher compared to other formulations. As WRV test only measures the final amount of removed water, these tests cannot capture the change in the rate of dewatering unless tests are done for very short periods of time.

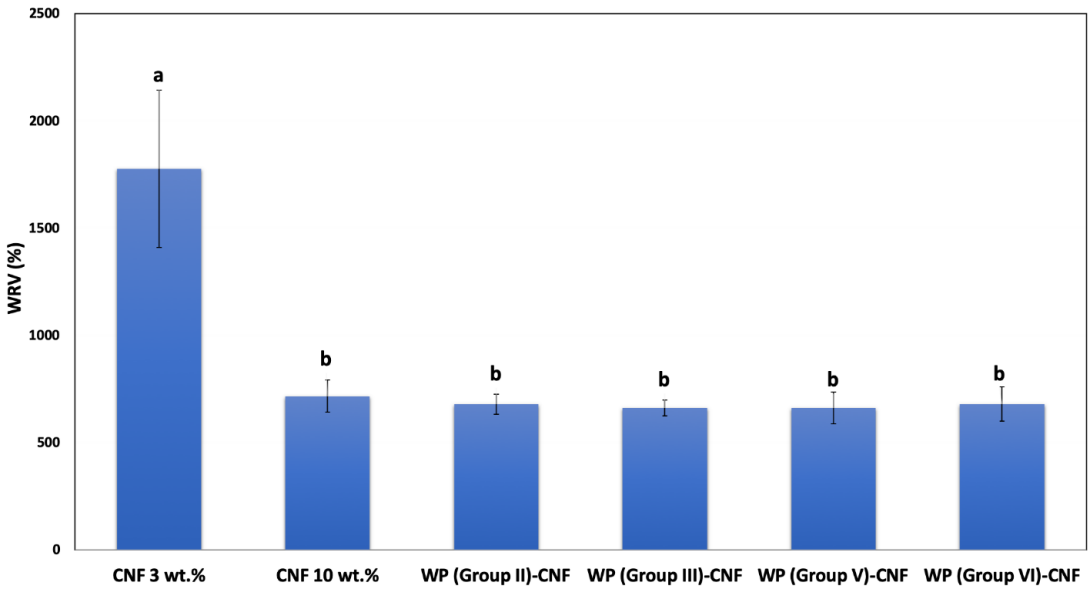

Fig. 3.5. Average water retention values. Common letters over bars indicate no significant difference at 95% confidence level.

3.4.4. Hard-to-remove water.

Results of HR water measurements are shown in Fig. 3.6. The HR water values of neat CNF samples were significantly higher than those of neat pulp and neat WP slurries with the same consistency. This can be interpreted as a higher amount of adsorbed water in the structure of CNF 3 wt.% slurry compared to pulp 3 wt.% and WP 3 wt.% suspensions as a result of much higher surface area and higher level of bound water in the fibrillar structure of the CNF. Moreover, WPs contain lignin, which is presumed to be less hydrophilic than neat CNF and pulp samples. Among the mixes, samples of PP-CNF showed the lowest levels of HR water attributable to the hydrophobicity and non-polarity of PP particles, no water is absorbed by PP particles compared to WP with higher level of water absorption thus easier water evaporation. There were no significant changes observed among the HR water values of WPs (with different sizes) and CNF mixtures. This can be explained by taking into account the role of permeability on the one hand and the effect of particle size upon contact dewatering on the other hand. It was expected that smaller wood particles, because of having higher specific surface areas, should lead into higher amounts of contact dewatering. However, larger particles will cause easier evaporation owing to higher permeability. These two factors might have counter effects leading to no considerable difference in HR values.

In the work by Park et al., HR water content was measured in pulp fibers by determining the onset of transition between constant rate and falling rate zones through 2nd derivatives. The values found for softwood bleached kraft pulps were in the same range as our results, i.e. between 2 and 4 g/g. However, the solids content used in the study was not clearly mentioned.

In another work, Sen et al.[94] used another method to calculate the HR water for pulp fibers by integrating the area above the 1st derivative curve in the constant and falling rate zones, and compared this method with the method used by[93] Park et al. The authors refined cellulose fibers to liberate microfibrils with different sizes ranging from several microns down to hundreds of nanometers. The values obtained for the microfibrillated cellulose at an initial consistency of 9.1 wt.% are between 4 and 4.5 g/g, which were again in the same range as our results. Overall, although the results of HR water were useful for understanding the evaporative dewatering behavior of the wet furnish, the method did not seem to be capable of illustrating the effect of particle size on the contact dewatering clearly.

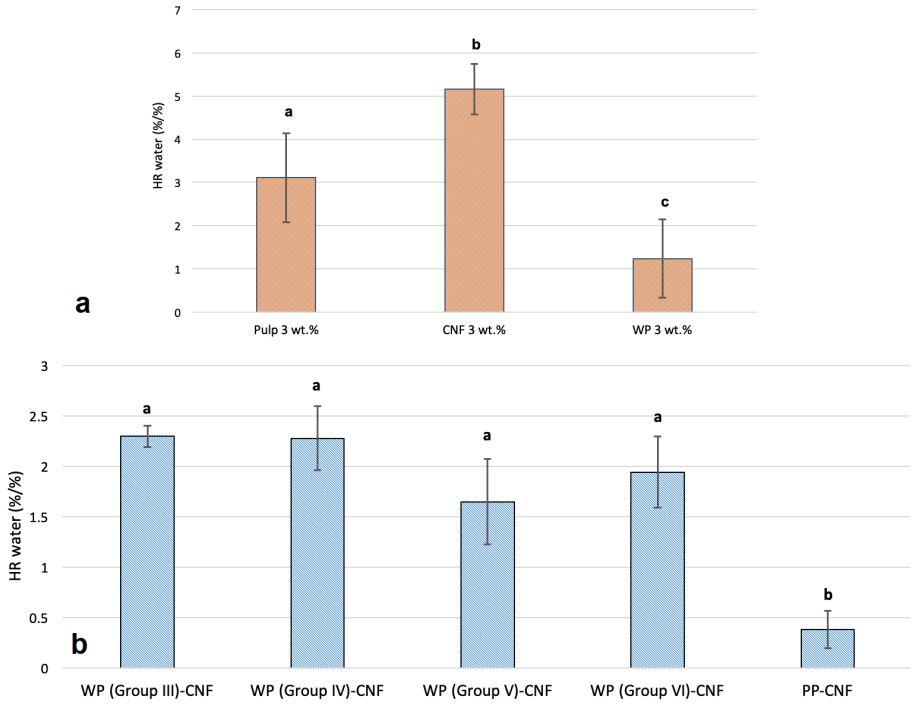

Fig. 3.6. HR water values of (a) neat samples (b) mixed samples. Common letters over bars indicate no significant difference at 95% confidence level.

3.5. Conclusions

Production of composite panels using CNF as an adhesive/binder is accompanied by a considerable level of water removal prior to hot pressing, which impacts pressing efficiency and energy consumption. This study focused on the dewatering behavior of WP-CNF particulate systems to understand and hence control the water removal from wet furnish. It was hypothesized that the size of WPs and consequently the specific surface area affects the level of contact dewatering, resulting from contact between nanofibrils of cellulose and WPs upon mixing. Pressure filtration tests were carried out to investigate the effect of particle size on the mechanical dewatering of wet furnish. It was found that among WP-CNF mixtures in general, those with smaller particle size had higher levels of water removal during filtration experiments. The lowest level of dewatering and smallest change in the drainage rate occurred during the filtration of WP with the largest particle size and smallest specific surface area (Group I). Samples of pure CNF 3 wt.% and 10 wt.% generally exhibited lower rates of water removal, as compared with those of WP-CNF mixes. This may support the original hypothesis that most of the water in a WP-CNF mix is in the form of free water as a result of contact dewatering and can be easily removed from the system, however in pure CNF suspensions, adsorbed water predominantly exists, which is harder to drain. The determination of the permeability coefficients of wet furnishes showed that regardless of the material formulation, the permeability of the wet furnish decreases over filtration time. The reduction in the permeability coefficients is more significant in WP mixtures with lower particle sizes (Group V and VI). This can be attributable to the higher compaction and densification of smaller particles upon dewatering that resulted in lower porosity.

Water retention values of wet furnish were measured through centrifugation technique. Results revealed that the amount of final water removed is almost the same among CNF 10 wt.% and WP-CNF mixes with the same solids content indicating that water retention values cannot capture the change in the rate of dewatering and therefore are unable to quantify contact dewatering. Samples of pure CNF 3 wt.% showed to have significantly higher level of water retention compared to other formulations, which simply means that the level of water contained in these samples after centrifugation under the same conditions is much higher compared to other formulations.

Characterization of HR water was also carried out to study the influence of particle size on the evaporative dewatering of wet furnish using high resolution isothermal thermogravimetric analysis (TGA). It was revealed that samples of neat CNF had higher values of HR water compared to neat pulp and neat WP suspensions with the same consistency. Samples of CNF mixed with PP showed the lowest levels of HR water attributed to the hydrophobicity and non-polarity of PP particles. Among the samples of CNF mixed with different sizes of WPs, no significant changes in HR water values were observed.

Overall, the study of the dewatering properties of WP-CNF particulate system via pressure filtration tests was the most effective way to quantify the effect of contact dewatering. Further studies are required for highlighting the direct influence of particle surface area on contact dewatering. Furthermore, the effects of other particle characteristics such as absorptivity, bulk density, compaction, and porosity need to be clearly examined.

CHAPTER 4

CELLULOSE AND LIGNOCELLULOSE NANOFIBRIL SUSPENSIONS AND FILMS: A COMPREHENSIVE COMPARISON

4.1. Chapter Summary

A comparative study on the morphology and physico-mechanical properties of cellulose nanofibrils (CNF) produced from bleached kraft pulp and lignocellulose nanofibrils (LCNF) produced from recycled old corrugated container (OCC) fibers in the form of slurries and films was conducted. The effects of raw material and fines content on the physico-mechanical properties were investigated. Suspensions of 3 wt.% consistency and films of both CNF and LCNF at different fines contents including 50, 60, 70, 80, 90, and 100% were prepared using the same production system and underwent a range of experiments and analyses. The morphology of the fibers was assessed through optical and atomic force microscopy techniques. Turbidity measurements and the laser diffraction technique were also carried out on the suspensions to investigate the suspension turbidity and particle size and particle size distribution with respect to the film transparency. The morphology of the produced films were also investigated by scanning electron microscopy. To evaluate the surface properties, contact angle and surface free energy measurements were carried out on the films. Mechanical properties of the films were evaluated through uniaxial tensile tests. Multiple stepwise linear regression analyses were also conducted to assess how the mechanical properties of the films can be predicted from morphological and physical characteristics of the suspensions and films. Results showed that in most cases the effect of raw material and fines content as well as the interaction effect of the two on the mechanical and physical properties were significant at a significance level of 0.05.

Multiple regression analyses also revealed that for both CNF and LCNF, the density of the films had the major effect on the modulus of the resulting films. The strengths of the CNF films were significantly influenced by the density and interfacial contact angle values, whereas the film density, particle size d[0.1] index, and surface roughness had significant effects on the strength values of the LCNF films.

4.2. Introduction

A number of sustained efforts are being made towards the production, development and commercialization of sustainable, biodegradable and health-friendly materials and products. In this regard, cellulose nanomaterials are of a growing interest because of possessing exceptionally outstanding characteristics such as large specific surface area, low density, outstanding mechanical properties, renewability and biodegradability that make them fascinating building blocks for functional materials [1,2]. Cellulose nanomaterials are mainly classified into three groups including cellulose nanofibrils (CNF), cellulose nanocrystals (CNC), and bacterial cellulose (BC). CNF and CNC are produced through top-down methods involving mechanical, chemical, or combination of the two to isolate nano-scale elements from wood and agricultural/forest residues, while BC is produced in a bottom-up process by bacteria and microorganisms [3,4].

CNF is one of the most commonly produced and commercialized types of cellulose nanomaterials today. It is mostly produced in the form of a low-consistency (less than 4 wt.%) aqueous suspensions of nano-scale cellulose fibers. Owing to the high surface area and an

abundance of hydroxyl groups available on the surface, CNF possesses excellent adhesion properties, which is promising for many different applications [6–10].

Lignocellulose nanofibrils, also known as lignin containing CNF (LCNF) isolated from wood with minimum chemical pretreatment have also received tremendous attention in bioproducts engineering. In comparison to the isolation of CNF from bleached pulp, the lower cost of raw materials attributed to the saving of the pulp bleaching step, easy processing and lower energy consumption of LCNF production make it a low-cost and promising material to be utilized on industrial scale[95]. Similar to CNF derived from bleached pulp, LCNF has a branched structure of fibrils with a thickness varying from 10 to 50 nm and length of several microns [23]. Numerous studies have been carried out on the production (isolation), utilization, and characterization of LCNF and their respective products. For example, Wang et al. conducted one of the pioneering research studies on the production of LCNF with two different lignin levels (5 and 10%) through a process of acid hydrolysis and a subsequent high-pressure homogenization of the lignin-containing kraft wood pulps and characterization of crystallinity, morphology, interfacial contact angle, and thermal stability of the resulting materials[96]. The results of X-ray diffraction (XRD) spectroscopy confirmed a decrease in the intensity of peaks with an increase in the lignin content of cellulose fibers indicating a reduction in the relative degree of crystallinity. The transmission electron microscopy (TEM) of the LCNF showed a semi-rod like structure of the fibers with an average diameter of 0.2 μm and length of several microns. Higher water contact angle values were also seen for the films of LCNF with higher lignin content[96]. Bian et al. [97]used a fully recyclable dicarboxylic acid hydrolysis to isolate lignin-containing cellulose nanofibrils

(LCNF) and nanocrystals (LCNC) from unbleached hardwood chemical pulps with different lignin contents. They found that the LCNF yield was higher than that of LCNC through this method and the aspect ratio (the ratio of the length to the diameter) of the isolated fibers was highly influenced by the lignin content of the starting materials. Delgado-Aguilar et al.[98] studied the effect of lignin content on the reinforcing properties of stone groundwood pulp (SGW)-derived LCNF as a low-cost alternative to Tempo-oxidized CNF for papermaking applications. It was revealed that pulps with lower residual lignin fraction (2-3%) had higher nanofibrillation yield than those with higher lignin content. Therefore, the highest strength development happened to the paper samples reinforced with the lowest lignin-containing LCNF. It was also shown that the isolated LCNF had quite the same reinforcing effect as TEMPO-oxidized CNF on the resulting paper samples.

The influence of residual lignin upon mechanical, physical, barrier, and surface properties of LCNF films was studied by Rojo et al[99]. LCNF fibers with varying lignin fractions were produced from Norway spruce SO_2-ethanol-water (SEW) pulp via microfluidization process and then made into films (nanopapers) for the evaluation of morphological, tensile, surface, and barrier properties. It was found that similar to the role of lignin in native wood, it acted as a cementing agent between the cellulose nanofibrils in the structure of the respective nanopaper. Therefore, the nanopapers made of LCNF with higher lignin contents had less and smaller micropores, hence smoother surfaces. The presence of lignin in LCNF also improved the dewatering of LCNF fibers throughout the filtration process of the film formation. Higher hydrophobicity and better oxygen barrier properties were also observed for the LCNF films

with higher lignin contents which can be very promising for packaging and composites applications. Horseman et al.[100] studied the morphology and thermal stability of LCNF fibers produced from thermo-mechanical pulp (TMP) along with the mechanical and physico-chemical properties of LCNF composite films. It was revealed that compared to neat CNF, LCNF had lower thermal stability. As the films of neat LCNF could not reach the mechanical properties of neat CNF films, different additives including polyvinyl alcohol (PVA), CNC, bentonite, CNF, and talc were used to reinforce the composite film structure. The addition of all additives except talc showed to improve the Young's modulus and ductility of the resulting LCNF films.

Faruk et al. [101]conducted research on the enhancement of bio-based poly urethane rigid foams with the aid of lignin and nanocellulose. It was found that addition of lignin and nanocellulose helped improve the compressive modulus and strength as well as impact properties. The density of the foams slightly increased and a significant reduction (almost 80%) in the open cell content was observed by adding lignin and nanocellulose into the foam formulation. Ding et al.[102,103] worked on improving the compatibility, hydrophilicity, and mechanical properties of polysulfone ultrafiltration membranes by adding lignocellulose nanofibrils into the membrane formulation. Results indicated that morphology, thermo-stability, hydrophilicity, and mechanical characteristics of the membranes were significantly improved upon the incorporation of the lignocellulose nanofibril, which can be considered as a promising replacement for costly and wasteful chemical modifiers and processing to develop high-performance ultrafiltration membranes. The reinforcing effect of hardwood- and softwood-

derived LCNF fibers on the mechanical and physical properties of LCNF-bonded fiberboards were evaluated by Kojima et al.[22]. They found that the flexural characteristics, internal bond strength, and water sorption properties of the fiberboards were significantly improved with the addition of LCNF, in particular for the softwood fiberboard panels. Diop et al. also investigated the effect of using TMP-isolated LCNF as a binder on the physico-mechanical properties of medium-density fiberboard (MDF) panels[23,24]. Results showed that at 20 wt.% LCNF content (dry-basis), the resulting MDF panels met the minimum recommended values for commercial fiberboards in terms of flexural modulus and strength, internal bond strength, and thickness swelling. Overall, LCNF had an acceptable bondability with wood fibers in the fiberboard structure, which can make it a promising replacement for petroleum-based adhesives for fiberboard manufacture.

Old corrugated container (OCC) fibers are high-volume and low-cost recycled materials mostly used as a feedstock for the cost-effective production of papers and containers[25]. OCC mainly consists of cellulose, hemicellulose (low content), lignin, and impurities [26]. OCC has also been utilized as a low-cost source for the production of cellulose and lignocellulose nanomaterials. However, limited studies have dealt with it in this regard [25,27]. Tang et al. studied the effectiveness of enzymatic hydrolysis of OCC pulp fibers after phosphoric acid hydrolysis on the CNC yield. It was found that enzymatic hydrolysis helped increase the CNC yield about 10% and enhanced the dispersion, thermal stability, and crystallinity of the isolated particles [25]. Yousefhashemi et al.[27] also worked on the extraction of LCNF fibers from OCC by ultra-fine grinding and investigated the synergy between LCNF and cationic starch-nanosilica for

paperboard production. Results revealed that the incorporation of nanosilica-starch system in the paperboard formulation significantly reduced the pulp freeness, which helped with the dewatering of the LCNF-containing furnish and increased the tensile and tear indices of the resulting paperboard.

The refiner-based production of CNF at the University of Maine uses the fraction of particles smaller than 200 micrometers as a measure for quality purposes. Regular CNF is produced at 90% fines content; this means that 90% of the particle are smaller than 200 micrometers. However, for many applications a highly refined CNF may not be required. Therefore, energy-intensive and time-consuming may not improve product quality only adding to the final cost. Therefore, finding an optimal refining level is a crucial importance to producing CNF that can techno-economically fulfil the requirements for the final product. Furthermore, both CNF and LCNF reported in the literature are produced from many different sources using various production methods, which makes comparisons difficult.

There is a lack of property comparisons of properties of CNF and LCNF produced from different sources using the same method and same pilot-scale facility. The aim of this study was to draw comparisons between the morphology, physical, and mechanical characteristics of CNF (extracted from bleached kraft pulp) and LCNF (isolated from OCC) with different fines contents and to probe factors affecting the physical and mechanical properties of films made from these materials.

4.3. Materials & Methods

Cellulose nanofibrils (CNF) were kindly supplied in the form 3 wt.% suspensions at six different fines contents (fines%) including 50, 60, 70, 80, 90, and 100% by the University of Maine's Process Development Center (PDC). CNF suspensions were the products of mechanical refining of bleached softwood kraft pulp. Lignocellulose nanofibrils (LCNF) were produced at the PDC by multi-step mechanical refining of recycled old corrugated container (OCC) to yield 3 wt.% suspensions of different fines% starting from 50% and going up to 100% using the same processing equipment CNF were produced by. Fines content was determined by analyzing the images taken from fiber suspensions using a MorFi TechPap Compact fiber analyzer.

4.3.1. Optical microscopy

Light microscopy was used to assess the micron-level morphology of CNF and LCNF fibers. A very dilute (approx. 0.01 wt.%) suspension of each material was prepared and sonicated for 30 sec to partially disintegrate agglomerated fibrils and a 0.05 ml droplet was placed on a microscope glass slide and left to air-dry. The dried fibers were then observed under an AmScope™ optical microscope at a magnification of 10X (Model ME520TA, Irvine, CA, USA). The average diameters of fifty fibrils for each fines level were measured using ImageJ software version 1.49v (National Institutes of Health, USA).

4.3.2. Atomic force microscopy

The topography and roughness of the fibers were studied through atomic force microscopy (AFM) using a tabletop ezAFM atomic force microscope (NanoMagnetics Instruments, Oxford, UK). Suspensions of very dilute (approx. 0.01 wt.%) CNF and LCNF fibers from each material

were prepared and sonicated for thirty seconds for a better fiber dispersion. A 0.05 ml droplet was placed on a glass slide cover attached to the AFM sample holder and left to air-dry. For film samples, a 5 mm by 5 mm piece of each film was placed on a sample holder and securely attached with a double-sided tape in between. A 2D scan of 10 μm by 10 μm area in the dynamic mode was done on each sample. Average surface roughness of fibers was then measured from the resultant AFM micrographs.

4.3.3. Turbidity

The turbidity of the CNF and LCNF suspensions was measured using a portable turbidity meter (AQUAfast AQ3010, Thermo Scientific Orion, USA). Suspensions of 0.1 wt.% were prepared and sonicated for 1 min. The turbidity meter system basically includes a light source and a detector to monitor and measure the light scattered at an angle of 90° with respect to the incident light beam, which is directly related to the size, shape, and refractive index of the suspended particle. Nephelometric Turbidity Unit (NTU) is a standard measure of an aqueous suspension optical clarity, which is nearly zero when the suspension is composed of fully-fibrillated nanoparticles. A poor fibrillation of particles results in a higher NTU value attributable to an increase in the suspension turbidity [104].

4.3.4. Laser diffraction analysis

The laser diffraction technique was used to determine the relative particle size of CNF and LCNF using a Malvern Hydro 2000s laser diffraction equipment (Malvern Panalytical Ltd, Malvern, UK). Suspensions of very dilute (approx. 0.01 wt.%) CNF and LCNF were prepared and added one at a time into the sample opening in the equipment and circulated throughout

the system. The laser diffraction system basically involved a mechanism to detect the scattered light after the incident laser beam hit the suspended particles. The device had a certain algorithm to yield the apparent particle size information based on the scattered light angle and intensity, assuming that the size of the particle is equivalent to the diameter of a sphere having the same apparent volume (hydrodynamic volume) as the particle.

4.3.5. Film formation

Films of pure CNF and LCNF at different fines% were produced using a vacuum filtration system, consisting of a vacuum pump, a 1 L flask, and a Büchner funnel. All suspensions were initially diluted to a solids content of 1% and then poured into the Büchner funnel with a 2.5 μm pore size Whatman™ (Grade 5) filter paper placed at the bottom of the funnel. A vacuum pressure of 27 inHg (approx. 95 kPa) was applied to the suspensions for about 10 min until most of free water was removed. The formed film along with the filter paper underneath were placed between two dry Whatman™ Grade 5 (2.5 μm pore size) filter papers. To have uniform surface and thickness in final films, the formed films along with the filter papers were placed between two stainless steel disks and the entire assembly was dried in an oven with (2.5 kg) load on top of the sample at 75 °C for 24 h. It was generally observed that keeping the very first filter paper attached to the formed film after the vacuum pressure process and during the oven drying helped prevent the final film from wrinkling and waviness.

4.3.6. Density & porosity measurement

To measure the density of produced films, six rectangular (70 mm x 20 mm) specimens of each formulation were cut out from the produced films (two specimens from each film) and then

conditioned in a conditioning chamber at a relative humidity of 53±2% and temperature of 23±2 °C for 24 h to reach a constant mass and moisture content. The conditioned samples were then weighed to determine the average density of the films. The porosity of each sample was also calculated through Equation 1, assuming that the density of cellulose fibers is 1.5 g/cm^3:

$$Porosity\% = (\frac{\rho_c - \rho_f}{\rho_c}) \times 100 \quad (1)$$

where ρ_f *and* ρ_c are the densities of the film and cellulose fibers, respectively.

4.3.7. Tensile tests

To evaluate the mechanical properties of the films, tensile tests were carried out using an Instron 5942 Universal testing machine (Instron, Norwood, MA, USA) with a 500 N capacity load cell. Three dog-bone specimens (overall length: 70 mm; overall width: 20 mm, gauge length: 20mm, gauge width: 10 mm, inner shoulder length: 25 mm, outer shoulder length: 15 mm) were cut out of each film (total of six test coupons per formulation) and conditioned in a conditioning chamber at a relative humidity of 53±2% and temperature of 23±2 °C for 24 h. The specimens were then tested at a loading rate of 2 mm/min with an initial gauge length of 20 mm. Tensile moduli and strengths of the film samples were obtained from the stress-strain curves.

4.3.8. Scanning electron microscopy

For a better understanding of surface morphology and tensile failure modes of the films, the surfaces of the films and fractured cross-sections of the tensile specimens were observed under

a Hitachi TM3000 tabletop scanning electron microscope (Hitachi, Ltd., Chiyoda, Tokyo, Japan). The tabletop SEM did not require sputter coating of samples prior to imaging.

4.3.9. Surface free energy

To investigate the surface properties of the films, a two-sessile drop (water and diiodomethane) contact angle measurement technique was employed using a Mobile Surface Analyzer (MSA, KRÜSS GmbH, Hamburg, Germany). The surface free energy (SFE) was determined through the Owens, Wendt, Rabel, and Kaelble (OWRK) model (Kaelble, 1970; Rabel, 1971).

4.3.10. Transparency

The transparency of the films was optically investigated by overlaying each film on a piece of printed paper to compare the clarity of the picture seen through different films. To relatively quantify the transparency of the films, an image processing technique was employed using ImageJ software version 1.49v to measure the average of digital numbers (DNs) values, assigned to each pixel (ranging from 0 to 255) in a similarly selected section of the pictures taken from all different films. The relative transparency (clarity%) was calculated using Equation 2:

$$Clarity\% = \frac{D_{ctrl}}{D_{film}} \times 100 \quad (2)$$

where D_{ctrl} and D_{film} are, respectively, the average digital numbers of a selected section of the picture in the absence and presence of the film.

4.3.11. Statistical analysis

A two-way analysis of variance (ANOVA) was conducted to investigate the main and interaction effects of variables (starting raw material and fines content) in a full factorial design. A Duncan's Multiple Range Test (DMRT) was used as a post hoc test to evaluate the differences among a group means if a significant effect was observed. Multiple stepwise linear regression analyses were carried out to find a statistical model to predict the mechanical properties of the films from other characteristics of the fibers and films. All statistical analyses were carried out at a 0.05 significance level (0.95 confidence interval) using IBM SPSS Statistics Version 25 (IBM Corp., Armonk, NY, USA).

4.4. Results & Discussion

4.4.1. Morphology of fibers

Optical micrographs of the CNF and LCNF fibers at different fines% are shown in Figure 1a-l. The micrographs were captured from the largest fragments seen in the microscopic view as the nano-scale fibrils are barely visible with an optical microscope. It can be seen that regardless of the material type, there is a decrease in the fiber size as the fines% increases attributed to further increases in the level of refining. In consequence, higher levels of fibrillation can be perceptible for higher fines% due to an increase in the number of fibrillated structures visible in the form of branching fibrils partially detached from a larger fiber. As shown for both CNF and LCNF, a smaller number of the fibrils branched off a larger pulp fiber seen at the two lowest fines contents, i.e. 50 and 60%, can be a sign that fibrillation has occurred, to a lesser extent, even in the aforementioned fines%. The average values of fiber diameter (thickness) for different fines%

of CNF and LCNF derived from the image processing of the optical micrographs are presented in Table 4.1. The relatively high CV% values seen in Table 4.1 are because of the fact that the thickness measurements were carried out on a wide range of fibril sizes within each fines content. As seen, the average diameter of fibers in both CNF and LCNF samples generally tended downward upon further refining. There was about 86% reduction in the average fiber thickness by refining from 50% to 100% fines levels for both CNF and LCNF. This can translate into a considerable increase in the specific surface area of the fibers, which can be the major reason for most of the changes in the material behavior.

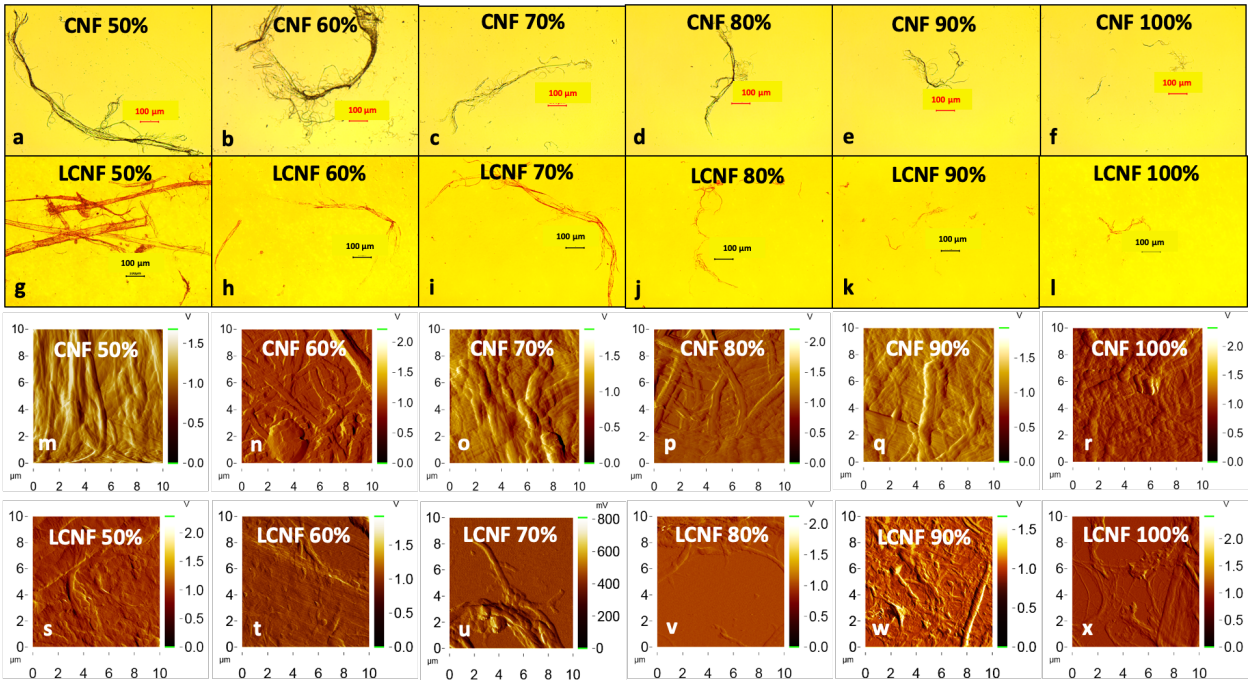

Fig. 4.1. Optical micrographs of (a-f) CNF (g-l) LCNF, and AFM micrographs of (m-r) CNF (s-x) LCNF fibers.

Results of the AFM in the amplitude mode for the 2D scan of the CNF and LCNF fibers are shown in Figure 1m-x. AFM was used to investigate the topography and surface roughness of

the samples. The average surface roughness of both CNF and LCNF obtained from AFM micrographs at different fines% is presented in Table 4.1. It can be observed that regardless of the material type, the surface roughness slightly changed with a change in fines%, however, the statistical analyses showed that the differences were not significant at a significance level of 0.05. Generally speaking, the average roughness values ranged from 60 to almost 200 nm.

4.4.2. Particle size analysis

Laser diffraction tests were conducted to determine the apparent particle size of the suspended CNF and LCNF fibers. Results were acquired in the form of a fraction of fibers that are smaller than a particular size. For instance, if for a given sample d[0.5] is 20 microns, then 50% of the fibers in that sample are smaller than 20 microns. As presented in Table 1, the laser diffraction outcomes also confirmed an overall reduction in the fiber size for both CNF and LCNF samples as a result of refining.

Table 4.4.1. Fiber thickness and apparent particle size obtained from optical micrographs and laser diffraction, respectively, as well as average surface roughness measured by AFM

Formulation	Optical microscopy	Laser diffraction			AFM
	Average fiber thickness (μm)	d [0.1]* (μm)	d [0.5] (μm)	d [0.9] (μm)	Average surface roughness (μm)
CNF 50	14 (92.2)+	22.13	111.45	733.50	0.08 (20.9)
CNF 60	12 (66.9)	22.38	116.31	829.68	0.12 (43.7)
CNF 70	6 (82.1)	16.41	79.59	390.97	0.15 (23.1)
CNF 80	5 (44.3)	17.66	91.75	743.07	0.06 (32.2)
CNF 90	4 (43.1)	11.16	57.34	218.91	0.10 (22.8)

CNF 100	1 (58.5)	6.56	35.03	99.59	0.19 (35.7)
LCNF 50	15 (91.3)	17.07	86.56	582.98	0.14 (44.4)
LCNF 60	10 (72.8)	16.89	88.26	539.46	0.11 (62.4)
LCNF 70	9 (98.2)	16.81	91.56	474.82	0.09 (68.0)
LCNF 80	7 (90.7)	14.28	74.24	344.36	0.10 (83.1)
LCNF 90	1 (43.6)	10.75	54.95	187.33	0.12 (48.6)
LCNF 100	2 (73.1)	6.80	37.98	99.70	0.09 (37.6)

[+] Values in parentheses are coefficients of variation (CV%)

* d[x] indicates the (x) fraction of the fibers in a given sample, which belong to a range of particle sizes smaller than a particular size in microns

Figures 4.2a and b show the particle size distribution at each fines content for both CNF and LCNF samples. As illustrated in these figures in most case, the distribution of particle size had a slight shift toward the left side the particle size (x) axis indicating a reduction in particle size with an increase in fines content, regardless of the material type. In some cases such as CNF 100%, LCNF 90 and 100%, the reduction in particle size was more noticeable than other fines levels (Figures 4.2a and b). Comparing CNF 100% with LCNF 100%, the largest volume of fibers in CNF 100% had an average particle size of around 65 microns, whereas the majority of fibers in LCNF 100% had an average particle size of around 85 microns. The largest portion of both CNF and LCNF fibers in other fines contents had average particle sizes ranging from 85 to 100 microns.

4.4.3. Turbidity of the suspensions

Results of the turbidity measurements are shown in Figure 4.2c. Statistical analysis of the results indicated that the effect of raw material (bleached kraft or OCC) and fines content as well as the interaction effect of the two were significant at a 95% confidence interval, which means that in general, the material type and fines content had significant effects on the turbidity of the suspensions. It can be also concluded that the effect of fines content on the turbidity was significantly different when the material type changed.

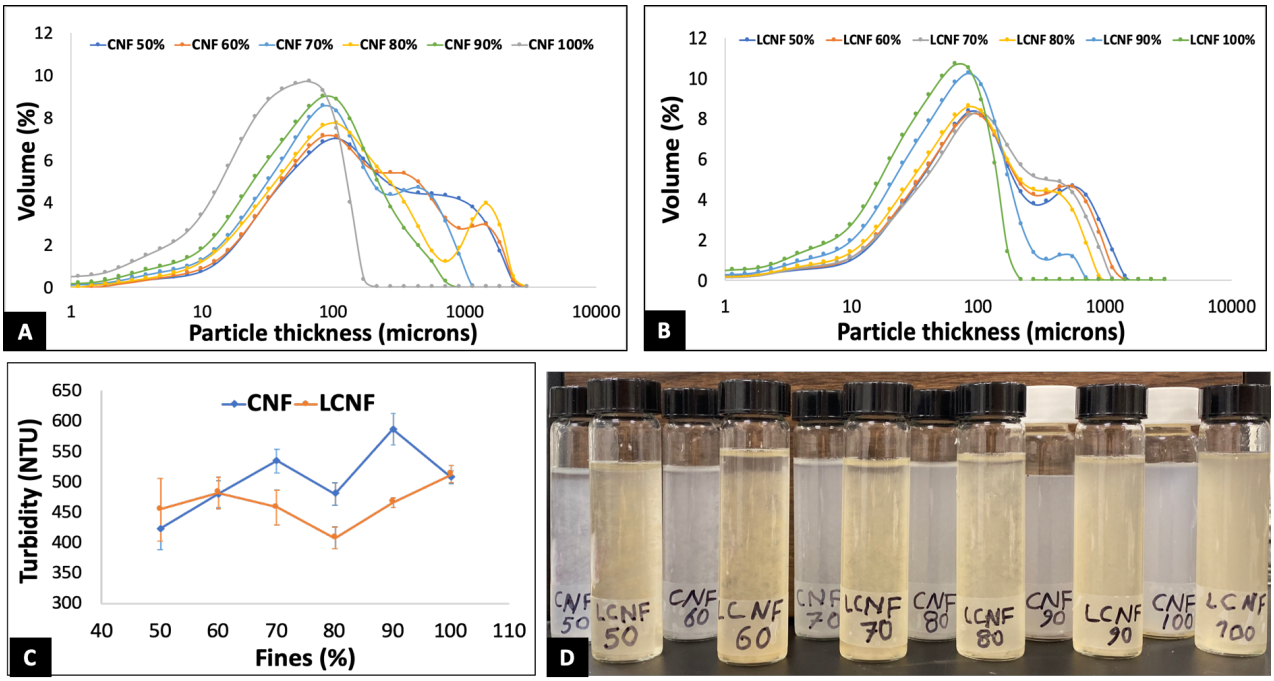

Fig. 4.2. Apparent particle size distribution (A) CNF (B) LCNF, (C) turbidity of fibers, and (D) CNF and LCNF 0.1 wt.% suspensions 10 seconds after agitation.

It is expected that the turbidity of CNF suspensions decrease as a result of greater fibrillation and reduced particle size and turbidity measurements have been used as quality parameter to define the quality of CNF [104]. However, as shown in Figure 4.2c, in most cases the average turbidity of suspensions increased with an increase in fines content in this study. This was more

perceptible in CNF suspensions. This behavior can be attributed to the flocculation of fibers in lower fines content, which made some clear (fiber-free) spots in the suspensions consisting predominantly of clear water, thus decreasing the turbidity values measured by the turbidity meter (Figure 4.2d). Higher levels of flocculation observed in LCNF suspensions compared to the CNF slurries with the same fines content resulted in lower average turbidity (lower NTU values) for the LCNF samples. Furthermore, the number of scattering objects (particles) increases with an increase in the degree of refinement, which can be another reason for the increase in the turbidity values of suspensions with higher fines contents. The expected trend of decreasing turbidity as a result of higher degrees of fibrillation should still hold at fibrillation levels beyond 100% fines.

4.4.4. Morphology of film surfaces

SEM images of the surfaces of film produced from the CNF and LCNF suspensions evaluated above are presented in Figure 4.3a-l. Going from 50 to 100 fines%, a size reduction mostly in the fiber diameter was evident, regardless of material type. It can be also seen that as the fines content increased, the size of micropores on the surface of the films became smaller, which can be evidence that finer fibers formed films with smoother surfaces and less porosity.

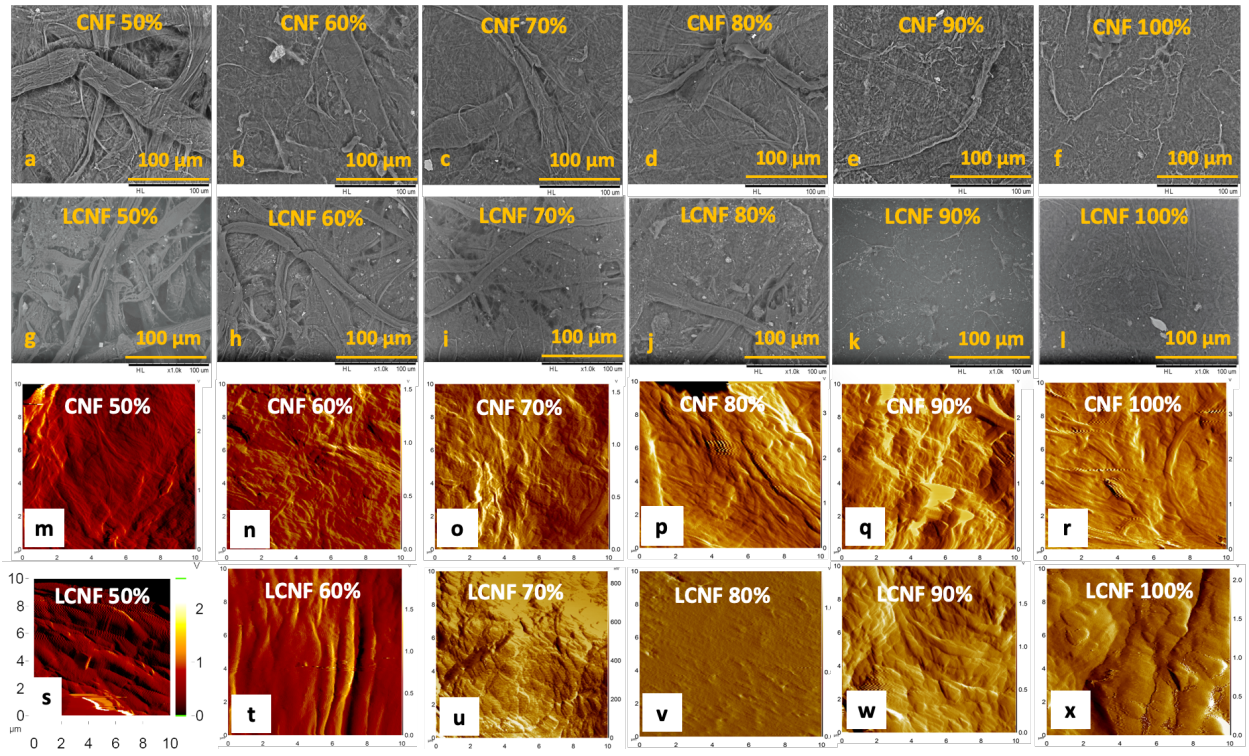

Fig. 4.3. SEM micrographs of (a-f) CNF (g-l) LCNF, and AFM micrographs of (m-r) CNF (s-x) LCNF film surfaces.

To further analyze the surface morphology of films surface, AFM was used on a 10 µm x 10 µm scanning area (Figure 4.3m-x). It is worth noting that the area of SEM film images was slightly larger than 200 µm x 200 µm. Comparing the AFM images of the two types of materials (CNF vs LCNF), one could easily notice the entanglement of the CNF fibrils analogues to SEM images of the same material. This, however, was not the case in LCNF films as the images of different LCNF fines exhibited some variability in the topography of film surfaces. It is also important to note that LCNF films were relatively more challenging to scan by AFM as opposed to CNF films. This was presumably because of the increased roughness of LCNF film surfaces especially at low fine levels (i.e. 50% and 60%) where the fibers could be easily noticed protruding from the film surface.

4.4.5. Surface properties of films

For a deeper understanding of the surface characteristics of the films, contact angles and surface free energies were successively determined. Figure 4.4a shows the results of water contact angle measurements for different formulations. As seen, contact angle values of the LCNF films are generally higher than those of the CNF ones. This means that the LCNF is generally more hydrophobic than the CNF, which is attributable to higher hydrophobicity of lignin compared to cellulose [105]. Furthermore, the crosslinking of polysaccharides by lignin in the plant cell wall forms an obstacle to water absorption and wetting [106]. Other researches also reported that increases in lignin content resulted in higher interfacial contact angles, thus higher hydrophobicity of the resulting films [99].

It can be also observed that the surface behavior of the CNF and LCNF films is quite different in response to the refining. Comparing 50% to 100% fines, CNF became less hydrophilic, while LCNF showed lower levels of hydrophobicity upon increased refining. Such a decrease in hydrophilicity of CNF upon further refinement has been previously reported and can be partly attributed to lower hydroxyl (O-H) groups availability on the surface of the CNF films that can interact better with each other and form strong internal hydrogen bonding upon further refining, thus lower hydrophilicity on the surface [9]. In the case of LCNF, the opposite trend might be attributed to better accessibility of cellulose surface hydroxyl groups as a result of greater fibrillation.

The surface free energies and their polar and dispersive components as well as contact angle values for all the CNF and LCNF values are presented in Table 4.2. In some instances the

diiodomethane contact angle and the resultant surface free energy values were not available (N/A) owing to the very quick absorption of the diiodomethane droplets by the substrate after introducing to the surface in such a way that the surface analyzer was not able to do the measurement. For CNF surfaces, a clear decreasing trend in the polar component of surface free energy is observed which is in line with the lower hydrophobicity at higher refining levels.

4.4.6. Transparency of films

The transparency of the films was visually evaluated through the comparison of the clarity of the background picture seen through each film (Figure 4b-g). As illustrated in Figure 8a-f, the transparency of CNF films increased as the fines% went up. The clarity differences among the first three fines levels, i.e. 50, 60, and 70, seemed to be more significant than those among the three highest fines% (80, 90, and 100). This can be attributed to the average thickness of the fibers at different fines content. Particles with lower thickness scatter the incident light to a smaller extent, as compared to thicker particles, hence higher transparency. Transparency values of the CNF films also showed to have a linear negative correlation ($y = -0.3093x + 18.465$; $R^2 = 0.925$) with the thickness of CNF fibers. As seen earlier in the morphology and analysis of particle size, the average particle size decreased as the fines content increased, which resulted in an increase in the transparency of the CNF films. Going from 80% to 100% fines, the reduction in the particle size was lower, thus smaller changes in the transparency. It was not feasible to evaluate the transparency of the LCNF films (even the films of 100% fines) through the foregoing method because of relatively high opacity.

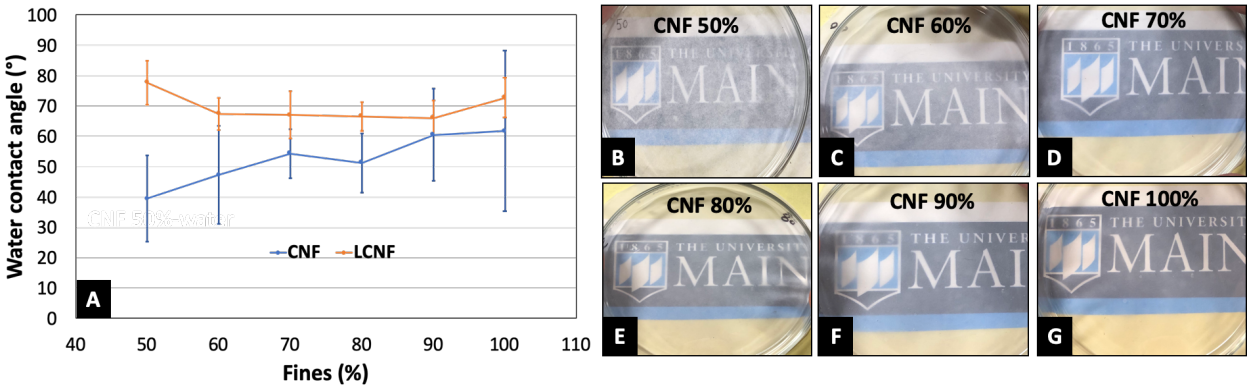

Fig. 4.4. (A) Water contact angle, (B-G) transparency examination of CNF films.

Results of the transparency quantification for the CNF films based on the image processing method are presented in Table 4.2. The Results of transparency quantification also indicated that the transparency of the films increased by increasing fines%. The changes, however, are comparatively smaller among the three highest levels of fines% (80, 90, and 100).

Table 4.4.2. Average thickness, transparency and surface properties of the films.

Material & fines%	Average film thickness (mm)	Trans-parency (%)	Diiadomethane contact angle (°)	Surface free energy (mN/m)	Polar (mN/m)	Dispersive (mN/m)
CNF 50	0.11 (4.46)	13.70 (4.27)+	50.17 (9.2)	61.31 (18.01)	27.13 (31.15)	34.18 (7.55)
CNF 60	0.10 (8.66)	15.37 (3.98)	49.35 (19.01)	56.81 (27.28)	22.18 (46.44)	34.64 (15.04)
CNF 70	0.10 (7.41)	16.14 (6.05)	50.28 (15.37)	52.15 (18.54)	18.04 (29.66)	34.12 (12.66)
CNF 80	0.10 (6.97)	16.93 (3.45)	53.01 (8.81)	53.33 (16.73)	20.75 (30.2)	32.58 (8.13)
CNF 90	0.09 (5.52)	17.62 (6.28)	54.89 (21.11)	47.01 (34.72)	15.5 (62.58)	31.51 (21.01)
CNF 100	0.09 (5.78)	18.04 (3.8)	51.57 (12.43)	47.34 (40.54)	13.94 (111.76)	33.4 (10.81)
LCNF 50	0.37 (11.77)	N/A*	N/A	N/A	N/A	N/A
LCNF 60	0.18 (7.72)	N/A	42.3 (2.52)	47.45 (6.81)	9.01 (29.74)	38.44 (1.43)
LCNF 70	0.13 (3.6)	N/A	N/A	48.63 (7.81)	8.75 (43.42)	39.87 (-)
LCNF 80	0.10 (4.61)	N/A	N/A	N/A	N/A	N/A
LCNF 90	0.10 (5.48)	N/A	45.84 (20.75)	46.86 (18.33)	10.3 (33.59)	36.56 (14.03)
LCNF 100	0.09 (6.99)	N/A	N/A	42.29 (7.26)	7.64 (40.18)	34.65 (-)

+ Values in parentheses are coefficients of variation (CV%)

*Values are not available (N/A)

4.4.7. Mechanical properties of films

Tensile properties of the films were evaluated through uniaxial tension tests and results are shown in Figures 4.5c and d. As shown in Figure 4.5c, tensile elastic modulus values of the CNF films were generally higher than those of the LCNF films at the same fine%. This can be in general attributed to higher Young's modulus of cellulose compared to lignin[107], which caused the resultant films of CNF to have higher moduli and better hydrogen bonding capacity of CNF compared to LCNF. The films of LCNF with 10 wt.% lignin content made of TMP fibers by Horseman et al [100] also showed to have lower tensile modulus and strength values compared to their CNF films. Tensile strength values were also higher in the CNF films. This can be explained by the presence of lignin in the structure of LCNF that hinders, to a certain extent, the formation of direct hydrogen bonding between cellulose molecules as well as impurities commonly found in recycled OCC fibers.

The observed differences between the mechanical properties of the CNF and LCNF films were partly related to the differences in the density values (Figure 4.5a). These differences are more noticeable at lower fines%, i.e. 50 and 60, with comparatively larger density differences. Multiple regression analyses were carried out to examine which characteristics of the fibers and films have significant effects on the tensile properties of the produced films at a significance level of 0.05. Results revealed that for both CNF and LCNF, density of the films had a significant effect on the modulus of the resulting films. The strength of the CNF films were significantly influenced by the density and water contact angle values of the films. However, film density, particle size d[0.1] index, and surface roughness had significant effects on the

strength values of the LCNF films. It should be noted the differences in both contact angle and surface roughness values originate from the difference in particle size, in other words contact angle and surface roughness are dependent on the particle size. Stress-strain representations of CNF and LCNF at different fines contents are also illustrated in Figure 4.6a-f. As seen, in almost all cases the toughness of CNF films were higher than that of LCNF at the same fines%, which is attributed to the higher ductility of lignin compared to cellulose[108]. The differences in the toughness values of CNF and LCNF were more evident at the lower fines contents, which can be related to the fiber shortening happening during pulp refining, accordingly, the ductility decreases[109].

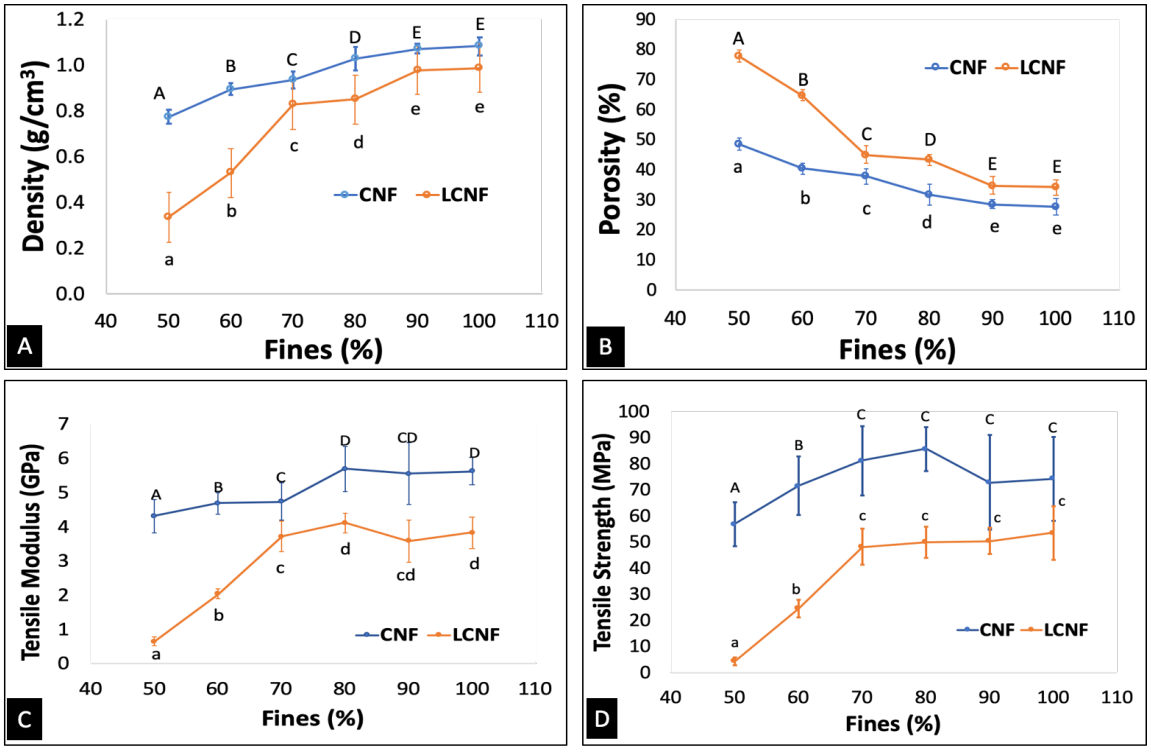

Fig. 4.5. (A) Density (B) porosity, (C) tensile modulus, and (D) tensile strength of the films as function of fines%. Common letters on the graph for each series indicate no significant difference at 95% confidence interval.

To eliminate the effect of the density from the tensile properties (elastic modulus and strength) of the films, the elastic modulus and strength values should be normalized based on the corresponding density values of the films. The normalized values can then be compared with each other to investigate the effect of material type and fines content on the tensile properties of the films. In this regard, the correlation between the density and tensile properties was found by plotting the density of the films against their tensile properties and finding the equation that can closely describe the correlation between the variables. The predicted density values were then obtained by plugging the actual values of the mechanical properties into the acquired equation. The normalized modulus and strength values were then calculated by dividing the actual modulus and strength values of the films by the corresponding predicted density values.

Figures 4.7a and b show the normalized tensile modulus and strength of the CNF and LCNF films at different fines contents. Statistical analyses revealed that the effects of raw material and fines content on both normalized modulus and strength were significant at a confidence interval of 95%. The interaction effect of raw material and fines content on the tensile properties were also significant at the same significance level, which implies that when the material type changes the effect of fines content on the tensile properties of the films would significantly change.

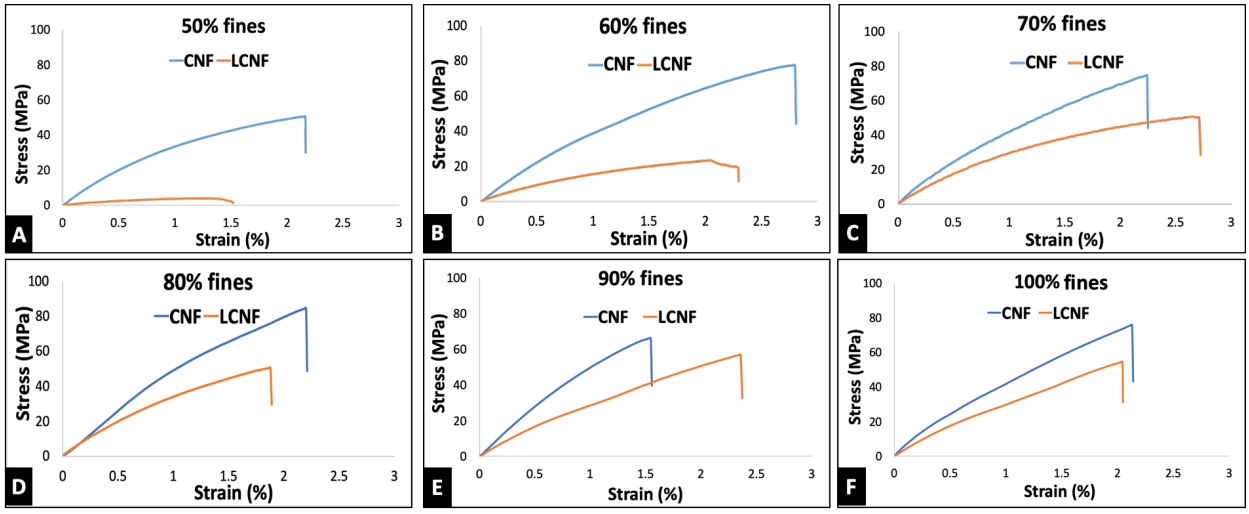

Fig. 4.6. Tensile stress-strain representations of the CNF and LCNF films

As shown in Figure 4.7a, the moduli of the films significantly increased as the fines content increased from 50% to 70%, regardless of the material type. However going from 70% to 100% fines, no significant change was observed in the modulus values of both CNF and LCNF films. Significant increases in the strength values of both CNF and LCNF films only occurred as the fines content increased from 50% to 60%. No significant changes were seen when going to higher fineness from 60% to 100%, regardless of material type (Figure 4.7b).

SEM micrographs of the fracture surfaces of the CNF and LCNF film tensile samples are shown in Figures 7c-n. As shown in the figure, a laminar structure of fibers through the thickness of the films was observed to form in almost all cases. This laminar structure seemed to have a relatively more ordered orientation in the films with higher fineness levels, which can be related to smaller size and larger specific surface area of finer particles, hence better packing. It can be also seen that in lower fines% (mostly 50 and 60), the failure mode was either fiber pull-out or

breakage (Figures 4.7c, d, i, and j), whereas in the films of finer fibers failure happened predominantly because of fiber breakage (Figures 4.5e-h and k-n).

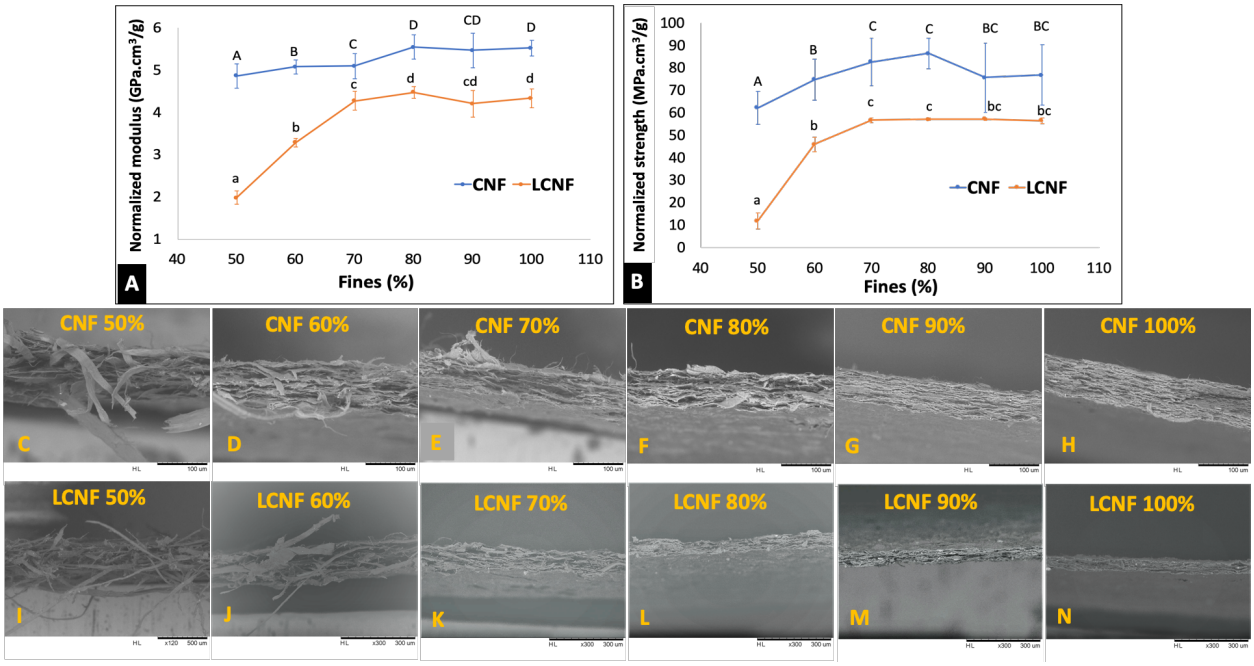

Fig. 4.7. Normalized (A) tensile modulus (B) tensile strength of the films. SEM micrographs of the fracture surface of the (C-H) CNF (I-N) LCNF films. Common letters on the graph for each series indicate no significant difference at 95% confidence interval.

Multiple regression analyses were also conducted after the normalization of tensile properties to assess the effect of other fiber and film characteristics on the normalized modulus and strength values of the films. Results showed that after normalizing the effect of density, d[0.1] and d[0.9] particle size indices had significant effects on the modulus of the CNF films, whereas the modulus values of the LCNF films were significantly influenced by only d[0.9] index. The water contact angle and d[0.1] index had significant influences on the strength the CNF films. However, the strength values of the LCNF were significantly affected by the d[0.9] particle size

index and surface roughness of the films. A summary of the multiple regression analyses results before and after normalization are presented in Table 4.3.

Table 4.4.3. Results of multiple regression analysis between the mechanical properties of the films and other predictors.

Tensile properties	Before normalization		After normalization	
	Model	R^2	Model	R^2
CNF modulus	M‡ = 0.165 + 5.1 x D‡	0.583	M = 6.352 - 0.094 x d[0.1] + 0.001 x d[0.9]	0.639
CNF strength	S = -19.382 + 78.375 x D + 0.398 x CA	0.674	S = 79.053 – 1.413 x d[0.1] + 0.443 x CA	0.651
LCNF modulus	M = -0.617 + 4.737 x D	0.803	M = 4.819 – 0.003 x d[0.9]	0.521
LCNF strength	S = -57.020 + 97.689 x D + 2.385 x d[0.1] – 123.103 x SR	0.974	S = 80.869 – 0.055 x d[0.9] – 225.870 x SR	0.668

‡ M: modulus; D: density; S: strength; CA: water contact angle; SR: surface roughness

4.5. Conclusions

A wide variety of experiments were conducted to study the morphology, mechanical properties, surface characteristics, turbidity, and transparency of CNF and LCNF suspensions and films at different fines% including 50, 60, 70, 80, 90, and 100%. Results of the morphological analyses on the CNF and LCNF fibers illustrated that fibrillation occurred, to a lesser degree, even at the 50 and 60 fines%. In general, the average diameter (thickness) of both CNF and LCNF fibers decreased upon further refining. A reduction of about 86% in the average fiber diameters was captured by refining from 50% to 100% fines levels for both CNF and LCNF, which is equivalent to a noticeable increase in the specific surface area of the fibers and can be

extremely promising for a number of applications. The average surface roughness of both CNF and LCNF fibers, however, did not significantly change with an increase in fines%. The average roughness values generally ranged from 60 to almost 200 nm.

SEM of the fractures surfaces of the CNF and LCNF film tensile samples demonstrated the presence of a laminar structure of fibers formed through the thickness of the films in almost all cases. The laminar structure showed to be well-oriented in the films with higher fineness levels. Contact angle measurements of the films indicated that LCNF films were generally more hydrophobic than the CNF ones. It was also observed that the surface behavior of the CNF and LCNF films differently changes upon refining from 50 to 100 fines%. The CNF samples showed to become less hydrophilic, while the LCNF ones showed lower levels of hydrophobicity by increasing the fines levels.

Results of the mechanical tests revealed that the CNF films, in general, had higher tensile elastic modulus and strength values compared to the LCNF films at the same fine%. The differences, however, were related largely to the differences in the density of the CNF and LCNF films in particular at lower fines%. Regardless of the material type, dramatic rises (about 32% for CNF and 532% for LCNF) in the tensile modulus values of the films were observed as the fines contents increased from 50 to 80%. Going from 50 to 70 fines%, the averaged strength values of the films also showed a significant increase (almost 1.5-fold in CNF and 12-fold in LCNF). Multiple regression analyses also showed that the density of the films had the major effect on the elastic modulus of the both CNF and LCNF films. The strength of the CNF films were significantly affected by the density and contact angle, while the film density, particle size d[0.1]

index, and surface roughness had significant influences on the strength values of the LCNF films. In conclusion, it was found that in most cases either CNF with relatively lower fines% (70 and 80%) or LCNFs derived from an inexpensive source, i.e. OCC, can meet the technical requirements to be economical replacements for the regular 90% fines CNF in many applications.

CHAPTER 5

ASSESSMENT OF CELLULOSE AND LIGNOCELLULOSE NANOFIBRILS FOR PARTICLEBOARD BONDING APPLICATIONS

5.1. Chapter Summary

This chapter is mainly focused on the adhesion properties of cellulose and lignocellulose nanofibrils as renewable replacements for resin adhesives in particleboards. A comparison of cellulose nanofibrils (CNF) and lignocellulose nanofibrils (LCNF) in terms of energy requirements and the corresponding energy costs needed for the pilot-scale production of CNF and LCNF with varying fines contents has been drawn. Lap-shear strength of CNF and LCNF, at different fines fractions was investigated as an indicator of bondability. Mechanical and sorption properties of particleboard (PB) panels made with LCNF with a selection of fines contents (i.e. 50, 70, 80, 90%) were also evaluated. Results indicated that at a given fines level, production of CNF had generally higher energy consumption and costs, as compared with LCNF. Results of the lap-shear test indicated that the lap-shear strength values of CNF samples were generally higher than those of LCNF at fines contents above 60%. The PB panels made with LCNF 50% fines had the lowest stiffness values. From 50 to 70% fines contents, a 40% increase was observed in the average stiffness of the LCNF-bonded panels. The average flexural strength values of the panels also increased by 57%, going from 50 to 70% fines contents. An overall reduction was detected in the water absorption and thickness swelling values of the LCNF panels when the fines% increased from 50 to 70%. The thickness swelling of the panels also did not significantly change between LCNF at 80 and 90% fines content samples. From both

technical and economic standpoints, LCNF 70% fines content was found to be the optimal binder formulation for particleboard manufacture.

5.2. Introduction

With the increasing number of efforts nowadays to produce, develop, and commercialize sustainable, environment- and health-friendly products, cellulose nanomaterials have received growing attention attributed to possessing excellent characteristics such as mechanical robustness, low density, exceptional adhesion properties, biodegradability, and sustainability that make these materials phenomenal candidates for functional materials and end products [1,42]. Cellulose nanomaterials are mainly produced either through top-down processes involving mechanical, chemical, and so forth, to isolate nano-scale cellulose (like cellulose nanofibrils and cellulose nanocrystals) from wood, agricultural and forest residues or in a bottom-up process by bacteria and microorganisms to form bacterial cellulose [3,4].

One of the most widely produced and utilized types of cellulose nanomaterials are cellulose nanofibrils (CNF) well-known for their superb adhesion properties attributed to their high surface area and profusion of surface hydroxyl groups, which is very promising for bonding applications. CNF is mostly produced in the form of a low-consistency (about 3 wt.%) aqueous suspension of cellulosic nanofibers and based on the final application can be utilized in dry or wet states [6–8,10,49,110,111].

Lignocellulose nanofibrils (LCNF) are also isolated from wood and forest residues with minimum chemical pretreatment. LCNF have also been of growing interest in bioproducts engineering applications because of their relatively low-cost precursors compared to CNF

attributed to the removal of the pulp bleaching step, easy processing and lower energy consumption [23,95] . A number of researchers have focused on the production, utilization, and evaluation of LCNF and their composites to date. Utilization of stone groundwood pulp (SGW)-derived LCNF as a low-cost alternative to Tempo-oxidized CNF for papermaking applications and the effect of lignin content on their reinforcing properties were studied by Delgado-Aguilar et al. [98]. It was found that lower lignin contents resulted in higher strength development in the LCNF-reinforced papers. Isolated LCNF materials also showed almost the same reinforcing effect as TEMPO-oxidized CNF on the paper samples.

Rojo et al [99] studied the influence of residual lignin on physico-mechanical, barrier, and surface properties of LCNF films. It was revealed that lignin acted as a cementing agent between the cellulose nanofibrils in the structure of the resulting film, thus, LCNF with higher lignin contents formed films with smoother surfaces. The LCNF with higher lignin contents also had more efficient dewatering during the filtration process of film formation and the resulting films had higher hydrophobicity and better oxygen barrier properties encouraging for packaging and composites applications. Incorporation of lignin and nanocellulose in the formulation of bio-based poly urethane rigid foams improved the compressive modulus and strength as well as impact resistance. The addition of lignin and nanocellulose also slightly increased the density of the rigid foams and significantly reduced the number of open cells [101]. Ding et al. [102,103] studied the effect of adding LCNF to the formulation of polysulfone ultrafiltration membranes on their hydrophilicity, compatibility, and mechanical properties. Results showed that the incorporation of the LCNF helped improve the morphology, thermo-stability, hydrophilicity, and mechanical properties of the resultant membranes significantly, which can be considered as a promising

alternative to cost-intensive chemical modifiers and processing to enhance high-performance ultrafiltration membranes.

Utilization of CNF and LCNF as binders or reinforcing agents in the binder formulation of wood composite panels has been the main focus of much research [7,10,23,49,50,112–114]. Kojima et al. [22] investigated the reinforcing effect of LCNF isolated from hardwood and softwood fibers on the mechanical and physical properties of LCNF-bonded fiberboards and found that addition of LCNF helped with improvement of the flexural properties, internal bond strength, and water absorption of the fiberboards, particularly in the case of softwood fiberboard panels. Thermomechanical pulp (TMP)-derived LCNF used as an adhesive binder in the formulation of medium-density fiberboard (MDF) panels [23]. Results showed that the produced MDF panels at 20 wt.% LCNF content (dry-basis) were able to meet the minimum flexural properties, internal bond strength, and thickness swelling requirements of the commercial fiberboards. In general, the strong bonding between LCNF and wood fibers makes LCNF a promising replacement for resin adhesives in fiberboards.

Old corrugated container (OCC) recycled fibers have also been used as high-volume and low-cost feedstock rich in cellulose and lignin for the cost-effective production of cellulose and lignocellulose nanomaterials [25,26]. However, a limited number of studies have focused on the isolation, utilization, and characterization of LCNF derived from OCC [25,27]. In this chapter comparisons of CNF and LCNF (with varying fines contents) in terms of energy consumption and the corresponding energy cost required for the pilot-scale production along with lap-shear strength as an indicator of bondability have been made. Then the physico-mechanical characteristics of particleboard panels made of LCNF (as a sole binder) with a selection of fines

contents were evaluated to explore the optimal LCNF fines content, which is both technically and economically suitable for particleboard manufacture.

5.3. Experimental Section

5.3.1. Materials

Cellulose nanofibrils (CNF) were kindly provided at six different fines contents (fines%) including 50, 60, 70, 80, 90, and 100% by the University of Maine's Process Development Center (PDC). Fines content is defined as the fraction of fibers (in percentage) that have lengths smaller than 200 micrometers. CNF were in the form of 3 wt.% suspensions isolated from bleached softwood kraft pulp through mechanical refining. Old corrugated container (OCC) papers with an average thickness of 0.3 mm and 200 grams per square meter were also provided by the PDC. Southern pine wood particles (WP) with an average moisture content of 7% and an average length of 3.8 mm (aspect ratio of 3.3) were supplied by Georgia-Pacific Thomson Particleboard (Thomson, GA, USA).

5.3.2. LCNF Production

The pilot-scale production of LCNF was carried out using the University of Maine's nanomaterial pilot facility in the PDC. The OCC paper (linerboard) was used as a precursor for the production of LCNF. The manufacturing process of the LCNF was basically the same as the pilot-scale production of regular CNF suspension via disk refining. The production process mainly consisted of mixing OCC pulp and tap water in a hydropulper (Figure. 5.1a) to reach a 3 wt.% consistency, pumping the resulting suspension into a buffer tank (Fig. 5.1b), and recirculating the suspension through a disk refiner (Figure 5.1c) until the desired fines content is

achieved. Two refiners with different grinding plates in series were used to refine the fibers at different levels. One of the refiners was used to reach 50 to 80% fines contents and the other one was used to achieve higher fines (> 80%). Going to the higher fines fractions took significantly more time to achieve the desired fines%. A power meter was used to record the energy consumption during the refining process at certain time intervals and the results were then plotted against the fine%. To measure the fines content at each step, fractions of the LCNF suspension were collected every 30 minutes and evaluated using a TechPap MorFi analyzer. LCNF suspensions of 50, 60, 70, 80, 90, and 100% fines% at an average consistency of 3.5 wt.% were produced and collected for the next steps.

5.3.3. Lap-shear

Bondability of the CNF and LCNF was evaluated through lap-shear tests according to ASTM D4896-01 (2016) with modification using an Instron 5942 Universal testing machine (Instron, Norwood, MA, USA) with a 500 N capacity load cell. Rectangular pieces of 50 mm by 20 mm were prepared from the liner papers to be used as substrates. Lap-shear specimens were then prepared by cutting and overlapping two paper substrates bonded together using about 0.4 g of the binders (at 3 wt.% solids content) in-between. The dimensions of the lapping area were 10 mm (length) by and 20 mm (width). Specimens were then pressed at 2 MPa and 180 °C for one minute using a hydraulic hot press (Carver, Inc., Wabash, IN, USA). The produced lap-shear samples were then conditioned in a chamber at a relative humidity of 53±2% and temperature of 23±2 °C for 24 h prior to testing. Six replicates of each formulation were produced and tested at a loading rate of 1 mm/min and an initial gauge length of 30 mm.

5.3.4. Scanning electron microscopy (SEM)

For a better understanding of the failure modes at the binder-substrate lapping area, the fractured surfaces of the lap-shear specimens were observed under a Hitachi TM3000 tabletop scanning electron microscope (Hitachi, Ltd., Chiyoda, Tokyo, Japan). No sputter coating of samples was required prior to imaging for the tabletop SEM.

5.3.5. PB Panel production

The WP were mixed with the LCNF 3 wt.%-solids slurry (at 50, 70, 80, and 90% fines contents) at a mixing ratio of 85% WP to 15% LCNF (dry-basis) at room temperature using a stand mixer. A metallic forming box with the internal dimensions of 125 mm × 125 mm × 65 mm placed on top of a 40-mesh wire cloth was used. The mixture was then poured into the forming box with a metallic lid placed on top to transfer the load and apply a uniform pressure to the mixture. The assembly was then cold-pressed to the thickness of approximately 20 mm using a manual hydraulic press (Dake Corporation, Grand Haven, MI, USA) to drain the excess water. More than 70% of the free water was drained off during the cold pressing. The lid and forming box were then removed and the cold pressed mat was hot-pressed to the final thickness of 10 mm at 180 °C for 15 min (almost bone-dry) between two wire mesh cloths and caul sheets using a hydraulic hot press (Carver, Inc., Wabash, IN, USA). Two metal stops 10-mm in thickness were used for position control during the hot pressing. The particleboard panels were produced with a target density of 0.85 g/cm^3. The final dimensions of the produced panels after trimming were 120 mm x 120 mm x 10 mm. PB panels were produced in four different formulations (four different LCNF fines%), including LCNF 50, 70, 80, and 90.

5.3.6. Flexural tests

Three-point bending tests were conducted for the determination of the modulus of elasticity (MOE) and modulus of rupture (MOR) of the PB panels. Three samples with the dimensions of 120 mm x 30 mm x 10 mm were prepared from each panel (6 replications per each formulation) in accordance with ASTM D1037 (2012) with modifications using an Instron 5942 Universal testing machine (Instron, Norwood, MA, USA) with a 500 N capacity load cell. The span length and the crosshead speed were 80 mm and 3 mm/min, respectively. Specimens were conditioned in a chamber at a relative humidity of 53±2% and temperature of 23±2 ^{o}C for at least 48 hours prior to testing. The density of each specimen right after conditioning and prior to testing was measured. The average density for each formulation is as follows: LCNF 50 (0.92 g/cm^3), LCNF 70 (0.90 g/cm^3), LCNF 80 (0.82 g/cm^3), and LCNF 90 (0.82 g/cm^3). The differences observed in the average panel densities can be attributable to the loss of total wet furnish in some formulations during panel production.

5.3.7. Sorption properties evaluation

Water absorption and thickness swelling test were carried out in accordance with ASTM D1037 (2012) (method A: 2-plus-22-h submersion in water) to investigate the sorption properties of the produced panels. Rectangular specimens with the dimensions of 50 mm by 30 mm were cut out of the broken flexural samples (one specimen out of each broken sample) and then submerged in a tub of water for 24 hours overall at room temperature. The water absorption and thickness swelling of the specimens were measured after 2 and 24 hours of submersion.

5.3.8. Statistical analysis

The results of the mechanical and physical properties of the PB panels were statistically evaluated using a one-way analysis of variance (ANOVA). A Duncan's Multiple Range Test (DMRT) was used as a post hoc test to evaluate the differences between group means when a significant effect was observed. For the statistical analyses of the lap-shear results, a two-way ANOVA was used to investigate the main and interaction effects of the independent variables (material type and fines content) in a full factorial design. Simple effects follow-up tests were used when the interaction effect was significant to explore the difference between the groups within one level of each independent variable. Multiple stepwise linear regression analyses were conducted to find a statistical model to describe the shear strength property behavior of the lap-shear specimens as well as the flexural and sorption properties of the panels from other characteristics of the fibers and films. All statistical analyses were assessed at a significance level of 0.05 (0.95 confidence interval) using IBM SPSS Statistics Version 2 (IBM Corp., Armonk, NY, USA).

5.4. Results and Discussion

5.4.1. Nanofiber production and characterization

The energy (electricity) consumed to produce LCNF at different fines% from OCC along with the energy cost based on the average industrial electricity rate in the State of Maine (7.98 ¢/kWh [115]) are presented in Figures 5.1e and f. The information about the energy consumption and cost for the production of CNF from northern unbleached softwood kraft (NBSK) at the same fines contents that was kindly provided by PDC is also shown in Figures 5.1e and f. to make a side by

side comparison with LCNF production. It is noteworthy that the energy measurements were based on the total (gross) energy applied to the system, which consisted of the net energy applied to the pulp and the energy needed to run the refiner with pulp going through without any load applied to the pulp. As shown in Figures 5.1e and f, the energy consumption and the corresponding energy cost of CNF production is noticeably higher than those of LCNF at the same fines fraction. From 50 to 80 fines% the average difference between the energy consumption of CNF and LCNF at each fines level is roughly 870 kWh per metric ton (MT), which can be translated into almost 70 U.S. dollars (USD) per metric ton. It increased to 1450 kWh/MT (116 USD/MT) and 4270 kWh/MT (341 USD/MT) for 90 and 100% fines contents, respectively. Taking the average price of the starting materials (NBSK: 1300 USD/MT [116] vs. OCC: 120 USD/MT [117]) into account, the difference between the production costs of CNF and LCNF at a certain fines% would be significantly higher.

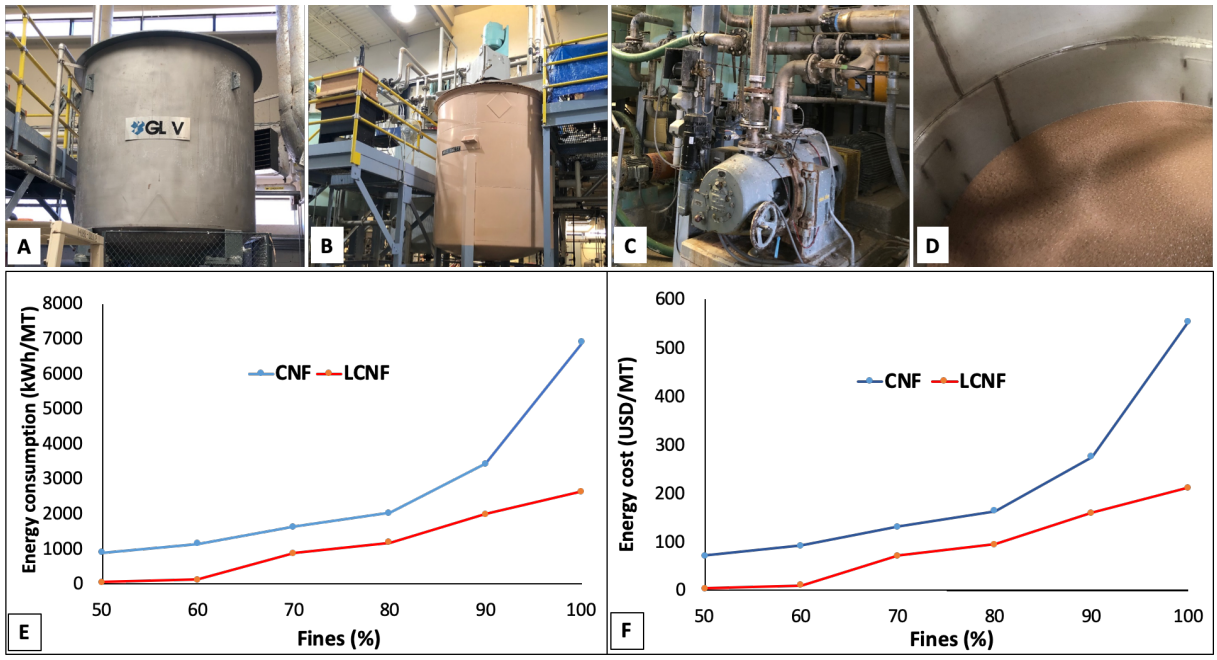

Fig. 5.1. (a) Hydropulper, (b) buffer tank, (c) refiner, (d) physical appearance of LCNF suspension, (e) electricity consumption and (f) energy cost (at an average electricity rate of 7.98 ¢/kWh) versus fines contents.

Results of the particle size analyses on the CNF and LCNF suspensions, interfacial contact angle and mechanical characterization on the films are summarized in Table 5.1 for a better comparison with the results of further characterizations discussed in this chapter. Detailed information and explanations are presented in the previous chapter.

Table 0.1 Particle diameter (thickness) indices, water contact angle, and normalized tensile modulus and strength values based on the films densities

Formulation	d [0.1]* (μm)	d [0.5] (μm)	d [0.9] (μm)	Water contact angle (°)	Tensile modulus ($GPa.cm^3/g$)	Tensile strength ($MPa.cm^3/g$)
CNF 50	22.13	111.45	733.50	39.5 (37.76)+	4.86 (6.03)	62.18 (11.84)
CNF 60	22.38	116.31	829.68	47.3 (34.16)	5.08 (3.28)	74.75 (12.33)

CNF 70	16.41	79.59	390.97	54.4 (14.78)	5.10 (5.85)	82.63 (12.91)
CNF 80	17.66	91.75	743.07	51.3 (18.89)	5.54 (5.22)	86.38 (7.76)
CNF 90	11.16	57.34	218.91	60.5 (25.00)	5.46 (7.58)	75.65 (20.34)
CNF 100	6.56	35.03	99.59	61.7 (42.94)	5.52 (3.27)	76.86 (17.45)
LCNF 50	17.07	86.56	582.98	77.75 (9.38)	1.98 (7.83)	11.79 (31.41)
LCNF 60	16.89	88.26	539.46	67.4 (8.03)	3.29 (3.14)	45.91 (6.98)
LCNF 70	16.81	91.56	474.82	67.02 (11.07)	4.28 (5.32)	56.61 (1.60)
LCNF 80	14.28	74.24	344.36	66.55 (7.09)	4.47 (2.96)	57.05 (1.02)
LCNF 90	10.75	54.95	187.33	66.09 (8.59)	4.20 (7.44)	57.17 (0.7)
LCNF 100	6.80	37.98	99.70	72.69 (9.00)	4.33 (5.25)	56.46 (1.97)

[+] Values in parentheses are coefficients of variation (CV%)

* d[x] indicates the (x) fraction of the fibers in a given sample, which belong to a range of particle thickness smaller than a particular thickness in microns

5.4.2. Lap shear

Lap-shear tests were carried out to evaluate the shear strength of the lapping area between the binder and the paper substrate as a measure of bonding strength. The possible failure modes in a lap-shear test can be typically categorized as (i) the interfacial debonding between the adhesive binder and the substrate (i.e. adhesive failure), (ii) the fracture within the adhesive binder (i.e. cohesive failure in the binder), and (iii) the cohesive failure within the substrate (Fig. 5.2b-d). Results of the lap-shear test are shown in Fig. 5.2e. It can be observed that the shear strength values of both CNF- and LCNF-bonded samples at 50 and 60 % fines contents were not significantly different (at a 0.05 significance level), whereas for the fines contents higher than 60%, the shear strength values of the CNF-bonded samples were generally higher than those of the LCNF ones. This can be explained by examining at the SEM micrographs of

the fractured surfaces after lap-shear tests. As shown in Fig. 5.3 (a-d and m-p), in the case 50 and 60% fines contents and regardless of the binder type, the failure occurred mainly because of the interfacial debonding between the binder (CNF or LCNF) and the OCC substrate (adhesive failure mode) in a manner that the binder was fully detached from one side of the lapping area, which indicates that the bonding between the binder and the OCC liner was weaker than the shear strength of the binder or the substrate. However, for the fines contents higher than 60%, cohesive failure occurred within the binder, regardless of the binder type (Fig. 5.3 e-l and q-x).

Multiple regression analyses were conducted to examine which characteristics of the fibers and films had significant effects on the shear strength of the CNF- and LCNF-bonded lap-shear specimens at a significance level of 0.05. Results indicated that the shear strength of the CNF-bonded samples was mainly influenced by the particle size d[0.1] index, while the normalized tensile strength of the LCNF films had the predominant effect on the shear strength of the LCNF samples (Table 5.2). It is also shown that for the CNF samples, d[0.1] index alone explains 67% of the changes in the shear strength, whereas for the LCNF specimens, the normalized tensile strength is responsible for only about 50% of the variations. Therefore, the relatively low shear strength values of the CNF and LCNF samples at the lower fines contents (≤ 60%) can be attributed to the relatively high particle thicknesses and low tensile strength values, respectively. At the higher fines% (> 60), the increasing shear strength values of the CNF samples can be explained by the significant reduction observed in the d[0.1] values, whereas for the LCNF samples the shear strength did not significantly change as there was no significant change in the normalized tensile strength values of the corresponding films (Table 5.1).

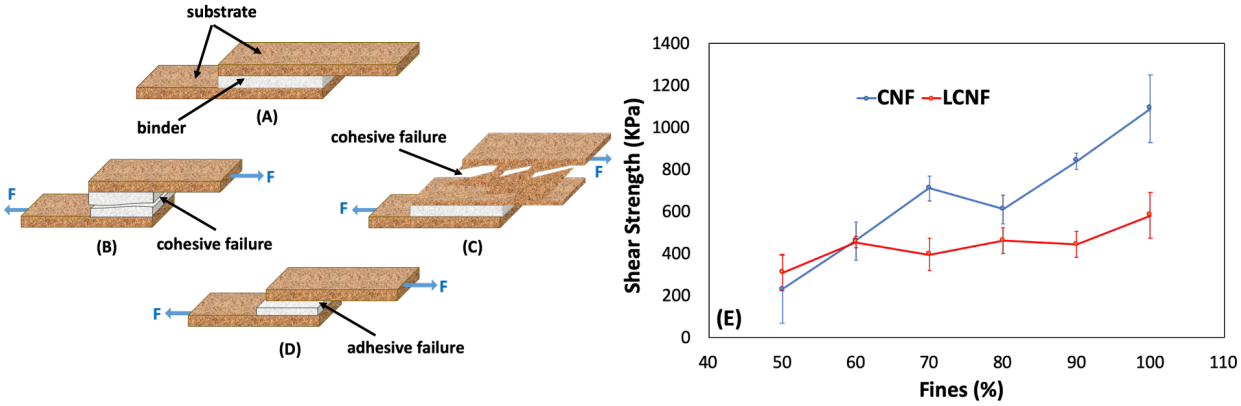

Fig. 5.2. Schematic of (A) lap-shear testing sample, (B) cohesive failure within binder, (C) cohesive failure within substrate, and (D) adhesive failure. (E) lap-shear strength of CNF and LCNF at different fines%

5.4.3. Mechanical and physical properties of the PB panels

Three-point bending tests were carried out to evaluate the flexural properties of the produced PB panels. As shown in Fig. 5.4a, the LCNF 50%-bonded panels had the lowest stiffness of all. A 20% increase in the fines contents (i.e. from 50 to 70%) resulted in an almost 40% increase in the average stiffness of the panels. However, the stiffness values of the LCNF 70, 80, and 90% panels were not significantly different at a significance level of 0.05. Figure 5.4b illustrates the MOR values of the LCNF-bonded panels. It can be seen that the average strength values increased from 6.25 to 9.81 MPa (approx. 57% change) when the fines contents increased from 50 to 70%. The average MOR values of the LCNF 70% panels was higher than those of LCNF 80% and 90%. Results of the multiple regression analyses at a 95% confidence interval revealed that the normalized tensile strength of the LCNF films is the dominant factor that influenced both MOE and MOR of the panels (Table 5.2). Therefore, the observed changes in the MOE values can be explained by the trend seen in the tensile strength of the corresponding films

(Table 5.1). The trend observed in the flexural strength of the panels can also be attributed to the percolation threshold. At the lower fines contents, the number of fibers with a relatively high aspect ratio (ratio of length to diameter) is lower, thus the strength of the resultant panel is only governed by the adhesion between wood particles and binder (Case I in Fig. 5.5). However, at higher fines fractions, a percolating network of LCNF fibrils connected to each other is highly possible to occur, which could form a film structure encompassing wood particle in the particleboard structure (Case II in Fig. 5.5). Therefore in addition to LCNF-WP adhesion, the strength of the forming films of nanofibrils (percolating network) plays an important role in the overall strength of the PB panel[15] .

Results of the water absorption and thickness swelling tests after 2 and 24 hours of submersion are presented in Fig. 5.4c and d. As shown for all cases, most of the water was absorbed during the first 2 hours of submersion. A roughly 10% increase in the average water absorption values and 7% raise in the average thickness swelling were observed in the last 22 hours of submersion. The overall reduction seen in the water absorption and thickness swelling values of the panels when the fines% increased from 50 to 70% can confirm the formation of stronger bonding in the wood-LCNF particulate system that absorbed less water and consequently had less thickness swelling. From 70 to 90% fines fraction, there was no significant change in the water absorption of the LCNF-bonded panels. The thickness swelling of the panels also did not significantly change between LCNF 80% and 90% samples. It is noteworthy that all PB specimens maintained their integrity after the sorption tests, despite their considerable thickness swelling and water absorption.

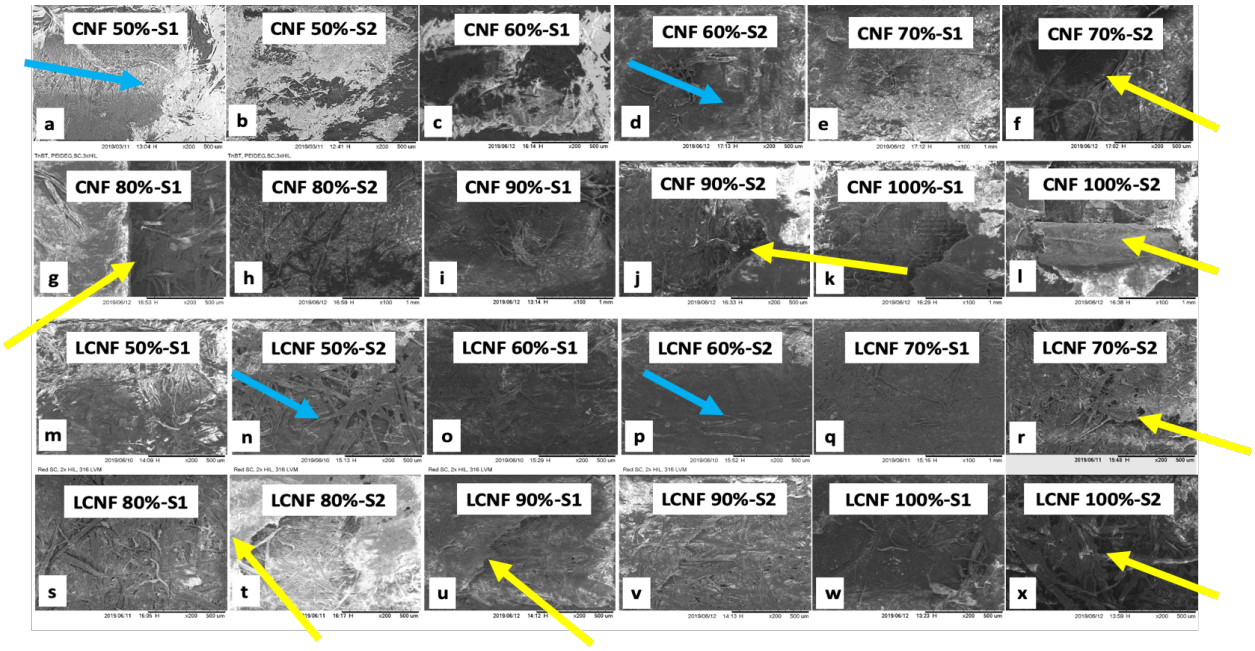

Fig. 5.3. SEM micrographs of fractured surfaces of (a-l) CNF and (m-x) LCNF-bonded lap-shear samples

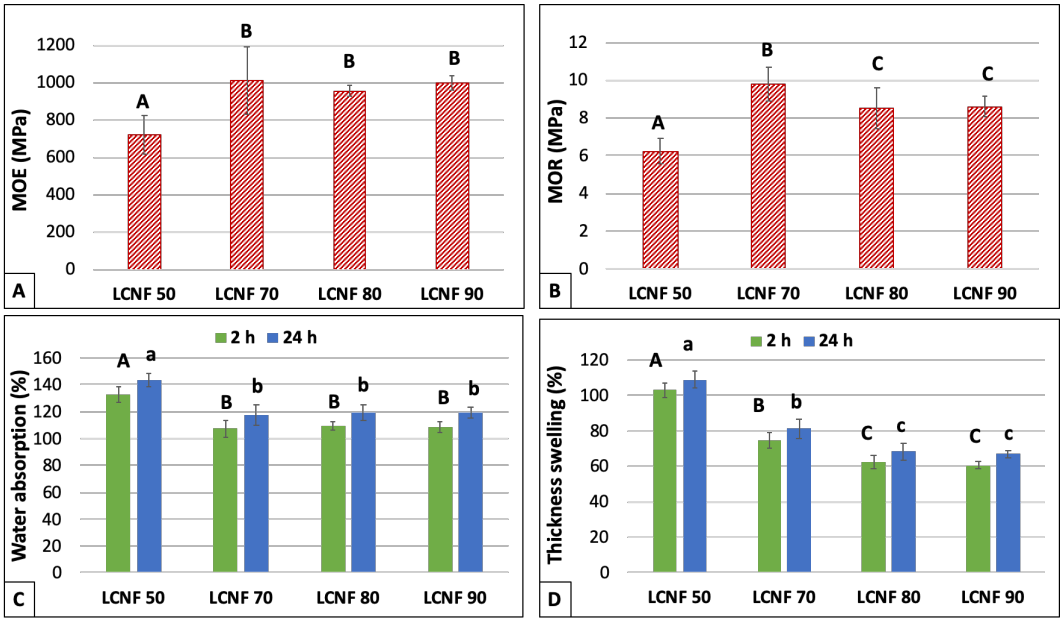

Fig. 5.4. (a) Modulus of elasticity, (b) modulus of rupture, (c) water absorption, and (d) thickness swelling of LCNF-bonded PB panels

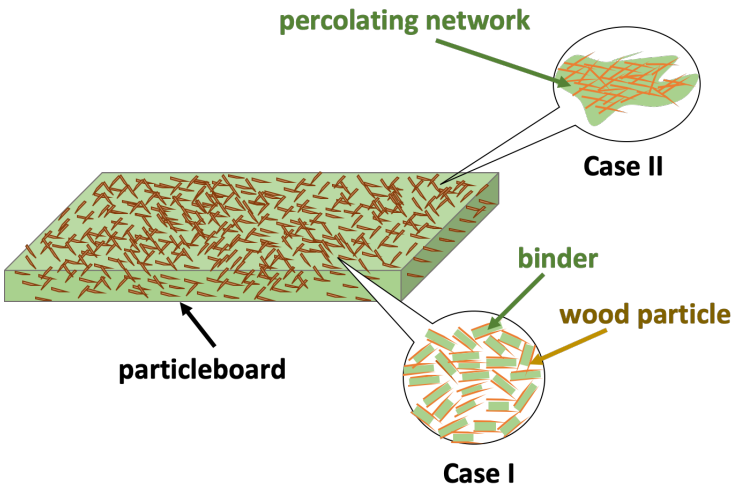

Fig. 5.5. Schematic of possible wood particle and binder arrangements in the particleboard structure

Table 5.2. Results of multiple regression analysis between the mechanical and physical properties of the testing samples and other predictors

Properties	Model	R^2
CNF shear strength (kPa)	SS‡ = 1307.748 – 42.644 x d[0.1]	0.670
LCNF shear strength (kPa)	SS = 265.569 + 3.823 x S	0.532
MOE (MPa)	MOE = 650.865 + 5.992 x S	0.812
MOR (MPa)	MOR = 5.630 + 0.058 x S	0.812

‡SS: lap shear strength; M: normalized film tensile modulus; S: normalized film tensile strength; D: panel density;

In conclusion, the results of energy consumption and cost analyses along with the physico-mechanical characterization showed that LCNF 70% fines content can be considered as the optimum binder formulation for the production of particleboard panels.

5.5. Conclusions

Binding properties of cellulose and lignocellulose nanofibrils along with the analysis of production costs in terms of energy consumption and the corresponding energy costs were

studied. It was found that at the same level of fines%, the energy consumption and cost of CNF production is remarkably higher than those of LCNF. From 50 to 80 fines% the average difference between the energy consumption of CNF and LCNF at each fines level is nearly 870 kWh (70 USD) per metric ton. The differences increased to 1450 kWh/MT (116 USD/MT) and 4270 kWh/MT (341 USD/MT) for 90 and 100% fines contents, respectively. Results of the lap-shear tests indicated that the shear strength values of both CNF and LCNF samples at 50 and 60% fines contents were not significantly different (at a 0.05 significance level), while CNF samples generally had higher lap-shear strength at fines contents above 60%.

The flexural and sorption properties of particleboard panels made with LCNF with a selection of fines contents have also been investigated. Results revealed that the PB panels made with LCNF 50% had the lowest stiffness values. From 50% to 70% fines contents, a 40% increase was observed in the average stiffness of the LCNF-bonded panels. The stiffness of the LCNF 70, 80, and 90% panels, however, were not significantly different at a significance level of 0.05. The average flexural strength values of the panels also showed a 57% increase when the fines contents increased from 50 to 70%. It was also observed that the LCNF 70% panels had higher MOR values, as compared to LCNF 80 and 90%. Results of sorption properties evaluation confirmed an overall reduction in the water absorption and thickness swelling values of the LCNF panels when the fines% increased from 50 to 70%, whereas no significant change was observed in the water absorption of the panels, when going from 70 to 90% fines fraction. The thickness swelling of the panels also did not significantly change between LCNF 80% and 90% samples.

Overall, results of energy consumption and the corresponding energy cost analyses along with the physico-mechanical characterization showed that LCNF 70% fines content can be considered as the optimal binder formulation for the particleboard manufacture, both from technical and economic standpoints.

CHAPTER 6

CONCLUSIONS AND FUTURE RESEARCH

6.1. Conclusions

In this work, the utilization of cellulose nanofibrils (CNF) as a replacement for the conventional resin-adhesives in the formulation of particleboard (PB) was proposed. PB panels with varying CNF contents and target densities were produced through a two-step (i.e. cold and hot) pressing process. Mechanical and physical properties of the produced panels were evaluated. The removal of a considerable amount of water from the wood particle (WP)-CNF (wet furnish) during processing, necessitated the study of the dewatering behavior, which was assessed through pressure filtration tests, centrifugation, and characterization of hard-to-remove (HR) water. Seeking a cost-effective alternative to the CNF 90% fines content for particleboard manufacture, lignin-containing CNF (LCNF) was produced at different fines fractions from old corrugated containers (OCC) recycling as a low-cost precursor. Comparisons of morphology, surface characteristics, turbidity, transparency, tensile and binding properties of produced LCNF with the CNF at different levels of fines% were made. To investigate the feasibility of producing PB panels with LCNF, a selection of fines contents (i.e. 50, 70, 80, and 90%) from the produced LCNF were used to make the PB panels with the same processing parameters employed to make CNF-bonded PB panels and the physico-mechanical properties of the resulting LCNF-bonded panels were evaluated. The following conclusions can be drawn from the results and discussions presented in the previous chapters of this dissertation:

1- The PB panels manufactured using CNF as the binder were shown to meet the industry requirements in terms of mechanical properties for low-density grades. The modulus of rupture (MOR) and modulus of elasticity (MOE) of the produced panels increased as the panel density increased. Water absorption decreased as the density of the panels increased, whereas increasing the density led to an increase in the thickness swelling of the panels. It was determined that moisture removal plays an important role in the strength development WP-CNF furnish. The surface roughness showed to have a significant effect on the strength of the WP-CNF bonding. The 400-grit sanded lap shear specimens had higher bonding strength values compared to the 150 grit sanded ones.

2- Study of the dewatering behavior of WP-CNF particulate system through the pressure filtration tests that the particle size had a significant effect on the mechanical dewatering of wet furnish. It was found that among WP-CNF mixtures in general, those with smaller particle size had higher levels of water removal during filtration experiments. The lowest level of dewatering and smallest change in the drainage rate occurred during the filtration of WP with the largest particle size and smallest specific surface area. Samples of pure CNF 3 wt.% and 10 wt.% generally showed lower rates of water removal, as compared to those of WP-CNF mixes, which could be attributed to the fact that most of the water in a WP-CNF mix is in the form of free water as a result of "contact dewatering" and can be easily removed from the system, while in pure CNF suspensions, adsorbed water predominantly exists, which is difficult to remove. The determination of the permeability coefficients of wet furnishes revealed that the

permeability of the wet furnish decreases over filtration time, regardless of the furnish formulation.

3- Results of the morphological analyses on the CNF and LCNF at different fines contents exhibited a reduction of about 86% in the average fiber diameters by refining from 50% to 100% fines levels for both CNF and LCNF, which is equivalent to a noticeable increase in the specific surface area of the fibers and can be extremely promising for a number of applications. Interfacial contact angle measurements of the films indicated that LCNF films were generally more hydrophobic than the CNF ones. It was also observed that the surface behavior of the CNF and LCNF films differently changes upon refining from 50 to 100 fines%. The CNF samples became less hydrophilic, while the LCNF ones showed lower levels of hydrophobicity by increasing the fines levels. Results of the mechanical tests revealed that the CNF films, in general, had higher tensile modulus and strength values compared to the LCNF films at the same fine%. It was concluded that in most cases either CNF with relatively lower fines% (70 and 80%) or LCNFs derived from an inexpensive source, i.e. OCC, can meet the technical requirements to be economical replacements for the regular 90% fines CNF in many applications.

4- Analysis of production cost in terms of energy consumption and the corresponding energy indicated that at the same level of fine%, the energy consumption and cost of CNF production is remarkably higher than those of LCNF. From 50 to 80 fines% the average difference between the energy consumption of CNF and LCNF at each fines

level is nearly 870 kWh (70 USD) per metric ton. The differences increased to 1450 kWh/MT (116 USD/MT) and 4270 kWh/MT (341 USD/MT) for 90 and 100% fines contents, respectively. Results of the lap-shear test indicated that the shear strength values of both CNF and LCNF samples at 50 and 60 % fines contents were not significantly different. However at fines contents above 60%, CNF samples generally had higher lap-shear strength. It was also revealed that the PB panels made with LCNF 50% had the lowest stiffness values. Going from 50 to 70% fines contents, a 40% increase was seen in the average stiffness of the LCNF-bonded panels. The average flexural strength values of the panels also showed a 57% raise when the fines contents increased from 50 to 70%. It was also observed that the LCNF 70% panels had the highest MOR values among all the formulations. Results of sorption properties evaluation confirmed an overall reduction in the water absorption and thickness swelling values of the LCNF panels when the fines% increased from 50 to 70%, whereas no significant change was seen in the water absorption of the panels, when going from 70 to 90% fines contents. Overall, LCNF 70% fines content was found to be the optimal binder formulation for the particleboard manufacture, both from technical and economical standpoints.

6.2. Future Research

1- The adhesion studies presented in this work were mainly assessed through the lap shear testing, which may not be representative of the bonding that occurs in an actual wood particle-CNF system. The study of adhesion mechanisms involved in a three dimensional network of binder-WP, where binder-binder interactions might actually play a more important role than binder-WP interactions is crucial to thoroughly understand the binding properties of CNF and LCNF for the composites applications.

2- The study of the dewatering properties of WP-CNF particulate system via pressure filtration tests showed to be one of the most effective way to quantify the effect of contact dewatering. However, further studies are required for highlighting the direct influence of particle surface area on contact dewatering. Furthermore, the effects of other particle characteristics such as absorptivity, bulk density, compaction, and porosity need to be clearly examined.

3- Study of the dewatering behavior of CNF (at the fines contents below 90%) and LCNF as low-cost replacements for regular CNF is highly encouraged to optimize the water removal processes during panel production.

BIBLIOGRAPHY

(1) Abdul Khalil, H. P. S.; Davoudpour, Y.; Islam, M. N.; Mustapha, A.; Sudesh, K.; Dungani, R.; Jawaid, M. Production and Modification of Nanofibrillated Cellulose Using Various Mechanical Processes: A Review. *Carbohydr. Polym.* **2014**, *99*, 649–665. https://doi.org/10.1016/j.carbpol.2013.08.069.

(2) Moon, R. J.; Martini, A.; Nairn, J.; Simonsen, J.; Youngblood, J. *Cellulose Nanomaterials Review: Structure, Properties and Nanocomposites*; 2011; Vol. 40. https://doi.org/10.1039/c0cs00108b.

(3) Klemm, D.; Kramer, F.; Moritz, S.; Lindström, T.; Ankerfors, M.; Gray, D.; Dorris, A. Nanocelluloses: A New Family of Nature-Based Materials. *Angew. Chemie - Int. Ed.* **2011**, *50* (24), 5438–5466. https://doi.org/10.1002/anie.201001273.

(4) Tayeb, A. H.; Amini, E.; Ghasemi, S.; Tajvidi, M. Cellulose Nanomaterials-Binding Properties and Applications: A Review. *Molecules* **2018**, *23* (10). https://doi.org/10.3390/molecules23102684.

(5) Zeng, J.; Xu, X.; Chen, X.; Liang, Q.; Bian, X.; Yang, L.; Jing, X. Biodegradable Electrospun Fibers for Drug Delivery. *J. Control. Release* **2003**, *92* (3), 227–231. https://doi.org/10.1016/S0168-3659(03)00372-9.

(6) Amini, E. N.; Tajvidi, M.; Bousfield, D. W.; Gardner, D. J.; Shaler, S. M. Dewatering Behavior of a Wood-Cellulose Nanofibril Particulate System. *Sci. Rep.* **2019**, *9* (1), 14584. https://doi.org/10.1038/s41598-019-51177-x.

(7) Amini, E.; Tajvidi, M.; Gardner, D. J.; Bousfield, D. W. Utilization of Cellulose Nanofibrils as a Binder for Particleboard Manufacture. *BioResources* **2017**, *12* (2). https://doi.org/10.15376/biores.12.2.4093-4110.

(8) Balea, A.; Sanchez-Salvador, J. L.; Monte, M. C.; Merayo, N.; Negro, C.; Blanco, A. In Situ Production and Application of Cellulose Nanofibers to Improve Recycled Paper Production. *Molecules* **2019**, *24* (9), 1–13. https://doi.org/10.3390/molecules24091800.

(9) Ghasemi, S.; Tajvidi, M.; Gardner, D. J.; Bousfield, D. W.; Shaler, S. M. Effect of Wettability and Surface Free Energy of Collection Substrates on the Structure and Morphology of Dry-Spun Cellulose Nanofibril Filaments. *Cellulose* **2018**, *25* (11), 6305–6317. https://doi.org/10.1007/s10570-018-2029-3.

(10) Sun, W.; Tajvidi, M.; Hunt, C. G.; McIntyre, G.; Gardner, D. J. Fully Bio-Based Hybrid Composites Made of Wood, Fungal Mycelium and Cellulose Nanofibrils. *Sci. Rep.* **2019**, *9* (1), 1–12. https://doi.org/10.1038/s41598-019-40442-8.

(11) Habibi, Y.; Lucia, L. A.; Rojas, O. J. Cellulose Nanocrystals: Chemistry, Self-Assembly, and Applications. *Chem. Rev.* **2010**, *110* (6), 3479–3500. https://doi.org/10.1021/cr900339w.

(12) Dufresne, A.; Cavaillé, J.; Vignon, M. R. Mechanical Behavior of Sheets Prepared from Sugar Beet Cellulose Microfibrils. *J. Appl. Polym. Sci.* **1997**, *64* (6), 1185–1194. https://doi.org/10.1002/(sici)1097-4628(19970509)64:6<1185::aid-app19>3.3.co;2-2.

(13) Klempner, D. *Handbook of Polymeric Foams and Foam Technology*; Vol. 404.

(14) Brandeis, C.; Guo, Z. Decline in the Pulp and Paper Industry: Effects on Backward-Linked Forest Industries and Local Economies. https://doi.org/10.13073/FPJ-D-14-00106.

(15) Dufresne, A. *Nanocellulose : From Nature to High Performance Tailored Materials*.

(16) Miller, J. Nanocellulose: Technology, Applications and Markets. 2015 TAPPI International Conference on Nanotechnology for Renewable Materials.

(17) *Particleboard Environmental Product Declaration*.

(18) Safety and Health Topics | Formaldehyde | Occupational Safety and Health Administration https://www.osha.gov/SLTC/formaldehyde/ (accessed Nov 23, 2019).

(19) Christensen, R.; Robitschek, P.; Stone, J. Formaldehydabgabe Aus Spanplatten. *Holz als Roh- und Werkst. Eur. J. Wood Wood Ind.* **1981**, *39* (6), 231–234. https://doi.org/10.1007/BF02606276.

(20) Amazio, P.; Avella, M.; Emanuela Errico, M.; Gentile, G.; Balducci, F.; Gnaccarini, A.; Moratalla, J.; Belanche, M. Low Formaldehyde Emission Particleboard Panels Realized through a New Acrylic Binder. *J. Appl. Polym. Sci.* **2011**, *122* (4), 2779–2788. https://doi.org/10.1002/app.34327.

(21) Prasittisopin, L.; Li, K. A New Method of Making Particleboard with a Formaldehyde-Free Soy-Based Adhesive. *Compos. Part A Appl. Sci. Manuf.* **2010**, *41* (10), 1447–1453. https://doi.org/10.1016/j.compositesa.2010.06.006.

(22) Kojima, Y.; Kawabata, A.; Kobori, H.; Suzuki, S.; Ito, H.; Makise, R.; Okamoto, M. Reinforcement of Fiberboard Containing Lingo-Cellulose Nanofiber Made from Wood Fibers. *J. Wood Sci.* **2016**, *62* (6), 518–525. https://doi.org/10.1007/s10086-016-1582-3.

(23) Diop, C. I. K.; Tajvidi, M.; Bilodeau, M. A.; Bousfield, D. W.; Hunt, J. F. Evaluation of the Incorporation of Lignocellulose Nanofibrils as Sustainable Adhesive Replacement in Medium Density Fiberboards. *Ind. Crops Prod.* **2017**, *109* (July), 27–36. https://doi.org/10.1016/j.indcrop.2017.08.004.

(24) Diop, C. I. K.; Tajvidi, M.; Bilodeau, M. A.; Bousfield, D. W.; Hunt, J. F. Isolation of Lignocellulose Nanofibrils (LCNF) and Application as Adhesive Replacement in Wood Composites: Example of Fiberboard. *Cellulose* **2017**, *24* (7), 3037–3050. https://doi.org/10.1007/s10570-017-1320-z.

(25) Tang, Y.; Shen, X.; Zhang, J.; Guo, D.; Kong, F.; Zhang, N. Extraction of Cellulose Nano-Crystals from Old Corrugated Container Fiber Using Phosphoric Acid and Enzymatic Hydrolysis Followed by Sonication. *Carbohydr. Polym.* **2015**, *125*, 360–366. https://doi.org/10.1016/j.carbpol.2015.02.063.

(26) Wan, J.; Yang, J.; Ma, Y.; Wang, Y. Effects of Pulp Preparation and Papermaking Processes on the Properties of OCC Fibers. *BioResources* **2011**, *6* (2), 1615–1630. https://doi.org/10.15376/biores.6.2.1615-1630.

(27) Yousefhashemi, S. M.; Khosravani, A.; Yousefi, H. Isolation of Lignocellulose Nanofiber from Recycled Old Corrugated Container and Its Interaction with Cationic Starch–Nanosilica Combination to Make Paperboard. *Cellulose* **2019**, *26* (12), 7207–7221. https://doi.org/10.1007/s10570-019-02562-2.

(28) Antonovi??, A.; Jambrekovi??, V.; Kljak, J.; ??pani??, N.; Medved, S. Influence of Urea-Formaldehyde Resin Modification with Liquefied Wood on Particleboard Roperties. *Drv. Ind.* **2010**, *61* (1), 5–14.

(29) Christensen, R.; Robitschek, P.; Stone, J. Formaldehyde Emission from Particleboard. *Holz als Roh- und Werkst.* **1981**, *39* (6), 231–234. https://doi.org/10.1007/BF02606276.

(30) Senyo, W.; Creamer, A.; … C. W.-F. products; 1996, undefined. The Use of Organosolv Lignin to Reduce Press Vent Formaldehyde Emissions in the Manufacture of Wood Composites. *search.proquest.com*.

(31) Elbert, A. A. Influence of Hardener Systems and Wood on the Formaldehyde Emission from Urea-Formaldehyde Resin and Particleboards. *Holzforschung* **1995**, *49* (4), 358–362. https://doi.org/10.1515/hfsg.1995.49.4.358.

(32) Amazio, P.; Avella, M.; Emanuela Errico, M.; Gentile, G.; Balducci, F.; Gnaccarini, A.; Moratalla, J.; Belanche, M. Low Formaldehyde Emission Particleboard Panels Realized through a New Acrylic Binder. *J. Appl. Polym. Sci.* **2011**, *122* (4), 2779–2788. https://doi.org/10.1002/app.34327.

(33) Xing, S.; Riedl, B.; Deng, J.; Nadji, H.; Koubaa, A. Potential of Pulp and Paper Secondary Sludge as Co-Adhesive and Formaldehyde Scavenger for Particleboard Manufacturing. *Eur. J. Wood Wood Prod.* **2013**, *71* (6), 705–716. https://doi.org/10.1007/s00107-013-0729-9.

(34) Sivasubramanian, S. Alternative Formaldehyde-Free Particleboard Compositions Based on Epoxidized Vegetable Oils. **2009**, 1–56.

(35) Tasooji, M.; Tabarsa, T.; Khazaeian, A.; Wool, R. P. Acrylated Epoxidized Soy Oil as an Alternative to Urea-Formaldehyde in Making Wheat Straw Particleboards. *Wood Adhes.* **2011**, *4243* (May), 341–352. https://doi.org/10.1163/016942410X507786.

(36) Prasittisopin, L.; Li, K. A New Method of Making Particleboard with a Formaldehyde-Free Soy-Based Adhesive. *Compos. Part A Appl. Sci. Manuf.* **2010**, *41* (10), 1447–1453. https://doi.org/10.1016/j.compositesa.2010.06.006.

(37) Bertaud, F.; Tapin-Lingua, S.; Pizzi, A.; Navarrete, P.; Petit-Conil, M. Development of Green Adhesives for Fibreboard Manufacturing, Using Tannins and Lignin from Pulp Mill Residues. *Cellul. Chem. Technol.* **2012**, *46* (7–8), 449–455.

(38) Tongboon, S.; Kiatkamjornwong, S.; Prasassarakich, P.; Oonjittichai, W. Particleboard from Rubber Wood Flakes with Polymeric MDI Binder. *Wood Fiber Sci.* **2002**, *34* (3), 391–397.

(39) Hubbe, M. A.; Rojas, O. J.; Lucia, L. A.; Sain, M. Cellulosic Nanocomposites: A Review. *Int. J. Interact. Mob. Technol.* **2018**, *12* (3), 929–980. https://doi.org/10.15376/biores.3.3.929-980.

(40) Siró, I.; Plackett, D. Microfibrillated Cellulose and New Nanocomposite Materials: A Review. *Cellulose*. Springer Netherlands 2010, pp 459–494. https://doi.org/10.1007/s10570-010-9405-y.

(41) Klemm, D.; Kramer, F.; Moritz, S.; Lindström, T.; Ankerfors, M.; Gray, D.; Dorris, A. Nanocelluloses: A New Family of Nature-Based Materials. *Angew. Chemie Int. Ed.* **2011**, *50* (24), 5438–5466. https://doi.org/10.1002/anie.201001273.

(42) Moon, R. J.; Martini, A.; Nairn, J.; Simonsen, J.; Youngblood, J. Cellulose Nanomaterials Review: Structure, Properties and Nanocomposites. *Chem. Soc. Rev.* **2011**, *40* (7), 3941. https://doi.org/10.1039/c0cs00108b.

(43) Charreau, H.; L. Foresti, M.; Vazquez, A. Nanocellulose Patents Trends: A Comprehensive Review on Patents on Cellulose Nanocrystals, Microfibrillated and Bacterial Cellulose. *Recent Pat. Nanotechnol.* **2012**, *7* (1), 56–80. https://doi.org/10.2174/18722105130106.

(44) Gardner, D. J.; Blumentritt, M.; Kiziltas, A.; Kiziltas, E. E.; Peng, Y.; Yildirim, N. Polymer Nanocomposites from the Surface Energy Perspective: A Critical Review. *Rev. Adhes. Adhes.* **2013**, *1* (2), 175–215. https://doi.org/10.7569/RAA.2013.097309.

(45) Chirayil, C. J.; Mathew, L.; Thomas, S. *REVIEW OF RECENT RESEARCH IN NANO CELLULOSE PREPARATION FROM DIFFERENT LIGNOCELLULOSIC FIBERS*; 2010.

(46) Oksman, K.; Aitomäki, Y.; Mathew, A. P.; Siqueira, G.; Zhou, Q.; Butylina, S.; Tanpichai, S.; Zhou, X.; Hooshmand, S. Review of the Recent Developments in Cellulose Nanocomposite Processing. *Compos. Part A Appl. Sci. Manuf.* **2016**, *83*, 2–18. https://doi.org/10.1016/j.compositesa.2015.10.041.

(47) Peter I N C E, B. J. *Global Cycle Changes the Rules for U.S. Pulp and Paper*.

(48) Pettersson, P.; Lundström, T. S.; Sundsvall, M. P. *A METHOD TO MEASURE THE PERMEABILITY OF DRY FIBER MATS Tomas Wikström*; 2006.

(49) Kojima, Y.; Minamino, J.; Isa, A.; Suzuki, S.; Ito, H.; Makise, R.; Okamoto, M. Binding Effect of Cellulose Nanofibers in Wood Flour Board. *J. Wood Sci.* **2013**, *59* (5), 396–401. https://doi.org/10.1007/s10086-013-1348-0.

(50) Kojima, Y.; Isa, A.; Kobori, H.; Suzuki, S.; Ito, H.; Makise, R.; Okamoto, M. Evaluation of Binding Effects in Wood Flour Board Containing Ligno-Cellulose Nanofibers. *Materials (Basel).* **2014**, *6* (9), 6853–6864. https://doi.org/10.3390/ma7096853.

(51) Veigel, S.; Rathke, J.; Weigl, M.; Gindl-Altmutter, W. Particle Board and Oriented Strand Board Prepared with Nanocellulose-Reinforced Adhesive. *J. Nanomater.* **2012**, *2012*. https://doi.org/10.1155/2012/158503.

(52) Theng, D.; Arbat, G.; … M. D.-A.-I. C. and; 2015, undefined. All-Lignocellulosic Fiberboard from Corn Biomass and Cellulose Nanofibers. *Elsevier*.

(53) Bilodeau, M. A.; Bousfield, D. W. Composite Building Products Bound with Cellulose Nanofibers, July 31, 2014.

(54) Tajvidi, M.; Gardner, D. J.; Bousfield, D. W. Cellulose Nanomaterials as Binders: Laminate and Particulate Systems. *J. Renew. Mater* **2016**, *4* (5). https://doi.org/10.7569/JRM.2016.634103.

(55) Zhang, Y.; Nypelö, T.; Salas, C.; Arboleda, J.; Hoeger, I. C.; Rojas, O. J. Cellulose Nanofibrils: From Strong Materials to Bioactive Surfaces. *J. Renew. Mater.* **2013**, *1* (3), 195–211. https://doi.org/10.7569/JRM.2013.634115.

(56) *Adopted by the Board of Governors of the Southern Pine Inspection Bureau Approved by the Board of Review of the American Lumber Standard Committee*; 2013; Vol. 6.

(57) Zhang, W.; Lu, C.; Deng, Y.; Zhang, Y. Aerogels from Crosslinked Cellulose Nano/Micro-Fibrils and Their Fast Shape Recovery Property in Water Super Biosorbent from Dendrimer Poly(Amidoamine)-Grafted Cellulose Nanofibril Aerogels for Effective Removal of Cr(VI) View Project Engineering View Project Aerogels from Crosslinked Cellulose Nano/Micro-Fibrils and Their Fast Shape Recovery Property in Water †. *Artic. J. Mater. Chem.* **2012**. https://doi.org/10.1039/C2JM30688C.

(58) Li, K.; Peshkova, S.; Geng, X. Investigation of Soy Protein-Kymene® Adhesive Systems for Wood Composites. *JAOCS, J. Am. Oil Chem. Soc.* **2004**, *81* (5), 487–491. https://doi.org/10.1007/s11746-004-0928-1.

(59) Wong, E. D.; Zhang, M.; Wang, Q.; Kawai, S. Formation of the Density Profile and Its Effects on the Properties of Particleboard. *Wood Sci. Technol.* **1999**, *33* (4), 327–340. https://doi.org/10.1007/s002260050119.

(60) Glass; Samuel V; Zelinka; Samuel L. *Wood Handbook, Chapter 04: Moisture Relations and Physical Properties of Wood*; 2010.

(61) Reising, A. B.; Moon, R. J.; Youngblood, J. P. *EFFECT OF PARTICLE ALIGNMENT ON MECHANICAL PROPERTIES OF NEAT CELLULOSE NANOCRYSTAL FILMS*; 2012; Vol. 2.

(62) Joseleau, J. P.; Chevalier-Billosta, V.; Ruel, K. Interaction between Microfibrillar Cellulose Fines and Fibers: Influence on Pulp Qualities and Paper Sheet Properties. *Cellulose* **2012**, *19* (3), 769–777. https://doi.org/10.1007/s10570-012-9693-5.

(63) Gardner, D. J.; Oporto, G. S.; Mills, R.; Samir, M. A. S. A. Adhesion and Surface Issues in Cellulose and Nanocellulose. *Journal of Adhesion Science and Technology*. January 1, 2008, pp 545–567. https://doi.org/10.1163/156856108X295509.

(64) Gardner, D.; Tajvidi, M. Hydrogen Bonding in Wood-Based Materials: An Update. *Wood Fiber Sci.* **2016**, *48* (4), 234–244.

(65) Amini, E.; Tajvidi, M.; Gardner, D. J.; Bousfield, D. W. Utilization of Cellulose Nanofibrils as a Binder for Particleboard Manufacture. *BioResources* **2017**, *12* (2), 4093–4110.

(66) Ghasemi, S.; Tajvidi, M.; Bousfield, D. W.; Gardner, D. J.; Gramlich, W. M. Dry-Spun Neat Cellulose Nanofibril Filaments: Influence of Drying Temperature and Nanofibril Structure on Filament Properties. https://doi.org/10.3390/polym9090392.

(67) Tayeb, A. H.; Amini, E.; Ghasemi, S.; Tajvidi, M. Molecules Cellulose Nanomaterials-Binding Properties and Applications: A Review. **2018**. https://doi.org/10.3390/molecules23102684.

(68) Purington, E.; Bousfield, D.; Gramlich, W. M. Fluorescent Dye Adsorption in Aqueous Suspension to Produce Tagged Cellulose Nanofibers for Visualization on Paper. *Cellulose* **2019**, *26* (8), 5117–5131. https://doi.org/10.1007/s10570-019-02439-4.

(69) Desmaisons, J.; Gustafsson, E.; Dufresne, A.; Bras, J. Hybrid Nanopaper of Cellulose Nanofibrils and PET Microfibers with High Tear and Crumpling Resistance. *Cellulose* **2018**, *25* (12), 7127–7142. https://doi.org/10.1007/s10570-018-2044-4.

(70) Zolin, L.; Destro, M.; Curtil, D.; Chaussy, D.; Penazzi, N.; Beneventi, D.; Gerbaldi, C. Flexible Cellulose-Based Electrodes: Towards Eco-Friendly All-Paper Batteries; 2014; Vol. 41. https://doi.org/10.3303/CET1441061.

(71) Zhang, X.; Lin, Z.; Chen, B.; Zhang, W.; … S. S.-J. of P.; 2014, undefined. Solid-State Flexible Polyaniline/Silver Cellulose Nanofibrils Aerogel Supercapacitors. *Elsevier*.

(72) Bhandari, J.; Mishra, H.; … P. M.-I. journal; 2017, undefined. Cellulose Nanofiber Aerogel as a Promising Biomaterial for Customized Oral Drug Delivery. *ncbi.nlm.nih.gov*.

(73) Kojima, Y.; Minamino, J.; Isa, A.; Suzuki, S.; Ito, H.; Makise, R.; Okamoto, M. Binding Effect of Cellulose Nanofibers in Wood Flour Board. *J. Wood Sci.* **2013**, *59* (5), 396–401. https://doi.org/10.1007/s10086-013-1348-0.

(74) Leng, W.; Hunt, J. F.; Tajvidi, M. Screw and Nail Withdrawal Strength and Water Soak Properties of Wet-Formed Cellulose Nanofibrils Bonded Particleboard. *BioResources* **2017**, *12* (4), 7692–7710.

(75) Leng, W.; Hunt, J. F.; Tajvidi, M. Effects of Density, Cellulose Nanofibrils Addition Ratio, Pressing Method, and Particle Size on the Bending Properties of Wet-Formed Particleboard. *BioResources* **2017**, *12* (3), 4986–5000.

(76) Diop, C.; Tajvidi, M.; Bilodeau, M.; … D. B.-I. crops and; 2017, undefined. Evaluation of the Incorporation of Lignocellulose Nanofibrils as Sustainable Adhesive Replacement in Medium Density Fiberboards. *Elsevier*.

(77) Yousefi Shivyari, N.; Tajvidi, M.; Bousfield, D. W.; Gardner, D. J. Production and Characterization of Laminates of Paper and Cellulose Nanofibrils. *ACS Appl. Mater. Interfaces* **2016**, *8* (38), 25520–25528. https://doi.org/10.1021/acsami.6b07655.

(78) Ghasemi, S.; Tajvidi, M.; … D. B.-I. crops and; 2018, undefined. Reinforcement of Natural Fiber Yarns by Cellulose Nanomaterials: A Multi-Scale Study. *Elsevier*.

(79) Ghasemi, S.; Tajvidi, M.; Gardner, D. J.; Bousfield, D. W.; Shaler, S. M. Effect of Wettability and Surface Free Energy of Collection Substrates on the Structure and Morphology of Dry-Spun Cellulose Nanofibril Filaments. *Cellulose* **2018**, *25* (11), 6305–6317. https://doi.org/10.1007/s10570-018-2029-3.

(80) Dimic-Misic, K.; Maloney, T.; Liu, G.; Gane, P. Micro Nanofibrillated Cellulose (MNFC) Gel Dewatering Induced at Ultralow-Shear in Presence of Added Colloidally-Unstable Particles. *Cellulose* **2017**, *24* (3), 1463–1481. https://doi.org/10.1007/s10570-016-1181-x.

(81) Dimic-Misic, K.; Puisto, A.; Gane, P.; Nieminen, K.; Alava, M.; Paltakari, J.; Maloney, T. The Role of MFC/NFC Swelling in the Rheological Behavior and Dewatering of High Consistency Furnishes. *Cellulose* **2013**, *20* (6), 2847–2861. https://doi.org/10.1007/s10570-013-0076-3.

(82) Paradis, M. A.; Genco, J. M.; Bousfield, D. W.; Hassler, J. C.; Wildfong, V. Determination of Drainage Resistance Coefficients under Conditions of Known Shear Rate. *Tappi Eng. Convert. Conf. Trade Fair* **2001**, No. January 2015, 341–355.

(83) Sim, K.; Lee, J.; Lee, H.; Youn, H. J. Flocculation Behavior of Cellulose Nanofibrils under Different Salt Conditions and Its Impact on Network Strength and Dewatering Ability. *Cellulose* **2015**, *22* (6), 3689–3700. https://doi.org/10.1007/s10570-015-0784-y.

(84) Rantanen, J.; Dimic-Misic, K.; Kuusisto, J.; Maloney, T. C. The Effect of Micro and Nanofibrillated Cellulose Water Uptake on High Filler Content Composite Paper Properties and Furnish Dewatering. *Cellulose* **2015**, *22* (6), 4003–4015. https://doi.org/10.1007/s10570-015-0777-x.

(85) Dimic-Misic, K.; Maloney, T.; Gane, P. Effect of Fibril Length, Aspect Ratio and Surface Charge on Ultralow Shear-Induced Structuring in Micro and Nanofibrillated Cellulose Aqueous Suspensions. *Cellulose* **2018**, *25* (1), 117–136. https://doi.org/10.1007/s10570-017-1584-3.

(86) Liu, G. ; Maloney, T. ; Dimic-Misic, K. ; Gane, P.; Liu, G.; Maloney, T.; Dimic-Misic, K. Acid Dissociation of Surface Bound Water on Cellulose Nanofibrils in Aqueous Micro Nanofibrillated Cellulose (MNFC) Gel Revealed by Adsorption of Calcium Carbonate Nanoparticles under the Application of Ultralow Shear Acid Dissociation of Surface Bound Water on Cellulose Nanofibrils in Aqueous Micro Nanofibrillated Cellulose (MNFC) Gel Revealed by Adsorption of Calcium Carbonate 2 Nanoparticles under the Application of Ultralow Shear. https://doi.org/10.1007/s10570-017-1371-1.

(87) Clayton, S. A.; Scholes, O. N.; Hoadley, A. F. A.; Wheeler, R. A.; McIntosh, M. J.; Huynh, D. Q. Dewatering of Biomaterials by Mechanical Thermal Expression. *Dry. Technol.* **2006**, *24* (7), 819–834. https://doi.org/10.1080/07373930600733093.

(88) Rainey, T. J.; Doherty, W. O. S.; Martinez, D.; Mark, R. J.; Kelson, N. A.; Mark Martinez, D.; Brown, R. J. Pressure Filtration of Australian Bagasse Pulp. **2010**. https://doi.org/10.1007/s11242-010-9649-x.

(89) Hakovirta, M.; Aksoy, B.; Nichols, O.; Farag, R.; Ashurst, W. R. Functionalized Cellulose Fibers for Dewatering and Energy Efficiency Improvement. *Dry. Technol.* **2014**, *32* (12), 1401–1408. https://doi.org/10.1080/07373937.2014.887576.

(90) Lavrykova-Marrain, N. S.; Ramarao, B. V. Permeability Parameters of Pulp Fibers from Filtration Resistance Data and Their Application to Pulp Dewatering. *Ind. Eng. Chem. Res.* **2013**, *52* (10), 3868–3876. https://doi.org/10.1021/ie302078w.

(91) Nilsson, L.; Stenström, S. A Study of the Permeability of Pulp and Paper. *Int. J. Multiph. Flow* **1997**, *23* (1), 131–153.

(92) Finley Richmond. Cellulose Nanofibers Use in Coated Paper, University of Maine, 2014.

(93) Park, S.; Venditti, R. A.; Jameel, H.; Pawlak, J. J. Hard to Remove Water in Cellulose Fibers Characterized by High Resolution Thermogravimetric Analysis - Methods Development. *Cellulose* **2006**, *13* (1), 23–30. https://doi.org/10.1007/s10570-005-9009-0.

(94) Sen, S. K.; Baheti, V. K.; Venditti, R. A.; Pawlak, J. J.; Park, S.; Bansal, M. C. Cellulose Microfibril-Water Interaction as Characterized by Isothermal Thermogravimetric Analysis and Scanning Electron Microscopy. *BioResources* **2012**, *7* (4), 4683–4703.

(95) Osong, S. H.; Norgren, S.; Engstrand, P. An Approach to Produce Nano-Ligno-Cellulose from Mechanical Pulp Fine Materials. *Nord. Pulp Pap. Res. J.* **2013**, *28* (4), 472–479. https://doi.org/10.3183/npprj-2013-28-04-p472-479.

(96) Wang, X.; Cui, X.; Zhang, L. Preparation and Characterization of Lignin-Containing Nanofibrillar Cellulose. *Procedia Environ. Sci.* **2012**, *16*, 125–130. https://doi.org/10.1016/j.proenv.2012.10.017.

(97) Bian, H.; Chen, L.; Dai, H.; Zhu, J. Y. Integrated Production of Lignin Containing Cellulose Nanocrystals (LCNC) and Nanofibrils (LCNF) Using an Easily Recyclable Di-Carboxylic Acid. *Carbohydr. Polym.* **2017**, *167*, 167–176. https://doi.org/10.1016/j.carbpol.2017.03.050.

(98) Delgado-Aguilar, M.; González, I.; Tarrés, Q.; Pèlach, M. À.; Alcalà, M.; Mutjé, P. The Key Role of Lignin in the Production of Low-Cost Lignocellulosic Nanofibres for Papermaking Applications. *Ind. Crops Prod.* **2016**, *86*, 295–300. https://doi.org/10.1016/j.indcrop.2016.04.010.

(99) Rojo, E.; Peresin, M. S.; Sampson, W. W.; Hoeger, I. C.; Vartiainen, J.; Laine, J.; Rojas, O. J. Comprehensive Elucidation of the Effect of Residual Lignin on the Physical, Barrier, Mechanical and Surface Properties of Nanocellulose Films. *Green Chem.* **2015**, *17* (3), 1853–1866. https://doi.org/10.1039/c4gc02398f.

(100) Horseman, T.; Tajvidi, M.; Diop, C. I. K.; Gardner, D. J. Preparation and Property Assessment of Neat Lignocellulose Nanofibrils (LCNF) and Their Composite Films. *Cellulose* **2017**, *24* (6), 2455–2468. https://doi.org/10.1007/s10570-017-1266-1.

(101) Faruk, O.; Sain, M.; Farnood, R.; Pan, Y.; Xiao, H. Development of Lignin and Nanocellulose Enhanced Bio PU Foams for Automotive Parts. *J. Polym. Environ.* **2014**, *22* (3), 279–288. https://doi.org/10.1007/s10924-013-0631-x.

(102) Ding, Z.; Liu, X.; Liu, Y.; Zhang, L. Enhancing the Compatibility, Hydrophilicity and Mechanical Properties of Polysulfone Ultrafiltration Membranes with Lignocellulose Nanofibrils. *Polymers (Basel).* **2016**, *8* (10). https://doi.org/10.3390/polym8100349.

(103) Ding, Z.; Zhong, L.; Wang, X.; Zhang, L. Effect of Lignin-Cellulose Nanofibrils on the Hydrophilicity and Mechanical Properties of Polyethersulfone Ultrafiltration Membranes. *High Perform. Polym.* **2016**, *28* (10), 1192–1200. https://doi.org/10.1177/0954008315621611.

(104) Desmaisons, J.; Boutonnet, E.; Rueff, M.; Dufresne, A.; Bras, J. A New Quality Index for Benchmarking of Different Cellulose Nanofibrils. *Carbohydr. Polym.* **2017**, *174*, 318–329. https://doi.org/10.1016/j.carbpol.2017.06.032.

(105) Hubbe, M. A.; Lucia, L. A. The "Love-Hate" Relationship Present in Lignocellulosic Materials. *BioResources* **2007**, *2* (4), 534–535. https://doi.org/10.15376/biores.2.4.534-535.

(106) Erdtman, H. Lignins: Occurrence, Formation, Structure and Reactions, K. V. Sarkanen and C. H. Ludwig, Eds., John Wiley & Sons, Inc., New York, 1971. 916 Pp. $35.00. *J. Polym. Sci. Part B Polym. Lett.* **1972**, *10* (3), 228–230. https://doi.org/10.1002/pol.1972.110100315.

(107) Gibson, L. J. The Hierarchical Structure and Mechanics of Plant Materials. *J. R. Soc. Interface* **2012**, *9* (76), 2749–2766. https://doi.org/10.1098/rsif.2012.0341.

(108) Farooq, M.; Zou, T.; Riviere, G.; Sipponen, M. H.; Österberg, M. Strong, Ductile, and Waterproof Cellulose Nanofibril Composite Films with Colloidal Lignin Particles. *Biomacromolecules* **2019**, *20* (2), 693–704. https://doi.org/10.1021/acs.biomac.8b01364.

(109) Gharehkhani, S.; Sadeghinezhad, E.; Kazi, S. N.; Yarmand, H.; Badarudin, A.; Safaei, M. R.; Zubir, M. N. M. Basic Effects of Pulp Refining on Fiber Properties - A Review. *Carbohydr. Polym.* **2015**, *115*, 785–803. https://doi.org/10.1016/j.carbpol.2014.08.047.

(110) Ghasemi, S.; Tajvidi, M.; Bousfield, D. W.; Gardner, D. J. Reinforcement of Natural Fiber Yarns by Cellulose Nanomaterials: A Multi-Scale Study. *Ind. Crops Prod.* **2018**, *111*, 471–481. https://doi.org/10.1016/j.indcrop.2017.11.016.

(111) Peng, Y.; Han, Y.; Gardner, D. J. Spray-Drying Cellulose Nanofibrils: Effect of Drying Process Parameters on Particle Morphology and Size Distribution. *Wood Fiber Sci.* **2012**, *44* (4), 448–461.

(112) Leng, W.; Hunt, J. F.; Tajvidi, M. Effects of Density, Cellulose Nanofibrils Addition Ratio, Pressing Method, and Particle Size on the Bending Properties of Wet-Formed Particleboard. *BioResources* **2017**, *12* (3), 4986–5000. https://doi.org/10.15376/biores.12.3.4986-5000.

(113) Hunt, J. F.; Leng, W.; Tajvidi, M. Vertical Density Profile and Internal Bond Strength of Wet-Formed Particleboard Bonded with Cellulose Nanofibrils. *Wood Fiber Sci.* **2017**, *49* (4), 413–423.

(114) Diop, C. I. K.; Tajvidi, M.; Bilodeau, M. A.; Bousfield, D. W.; Hunt, J. F. Isolation of Lignocellulose Nanofibrils (LCNF) and Application as Adhesive Replacement in Wood Composites: Example of Fiberboard. *Cellulose* **2017**, *24* (7), 3037–3050. https://doi.org/10.1007/s10570-017-1320-z.

(115) Maine Electricity Rates | Electricity Local https://www.electricitylocal.com/states/maine/ (accessed Nov 19, 2019).

(116) Current lumber, pulp and panel prices | Natural Resources Canada https://www.nrcan.gc.ca/our-natural-resources/domestic-international-markets/current-lumber-pulp-panel-prices/13309 (accessed Nov 22, 2019).

(117) Occ Waste Paper Cardboard & Kraft Paper Scraps 100% - Buy Occ 11 Waste Paper,Occ Grade Waste Paper,Price Occ Waste Paper Product on Alibaba.com https://www.alibaba.com/product-detail/OCC-Waste-Paper-Cardboard-Kraft-Paper_62002849034.html?spm=a2700.7724838.2017115.28.4efb575dvrI28O (accessed Nov 22, 2019).

BIOGRAPHY OF THE AUTHOR

Ezatollah (Nima) Amini was born and raised in Tehran, Iran. He graduated from Moallem High School in 2005 and attended Amirkabir University of Technology (Tehran Polytechnic). Nima received his B.S. (2011) and M.S. (2014) in Textile Engineering from Amirkabir University of Technology, Tehran, Iran, and started his PhD in the Bioproducts Engineering at the School of Forest Resources, University of Maine in June, 2015. In March 2019, Nima Received the George F. Dow Graduate Research Award as well as the Blumenstock Family Forest Products Student of the Year Award. Nima is a candidate for the Doctor of Philosophy degree in Forest Resources: Bioproducts Engineering from the University of Maine in December 2019.